Institut für Hydrologie

der Albert-Ludwigs-Universität Freiburg i.Br.

Hydrological modelling in a small hyperarid catchment Nahal Yael, Israel

– runoff generation an transmission losses –

Anne-Christin Thormählen

Referent: Prof. Dr. Ch. Leibundgut

Koreferent: Dr. J. Lange

Diplomarbeit unter der Leitung von Prof. Dr. Ch. Leibundgut

Freiburg i.Br., Dezember 2003

Contents

List of figures in the text

List of tables in the text

Contents of the annex

Notations

A_s	[m²]	area of sub-catchments
B	[m]	width of water surface
$C_{1,2,3}$	[-]	auxiliary variables
$\bar{d}$	[m]	mean slope length
d_i	[m]	distance from the gauge i to point of estimation
K	[s]	storage constant
n	[$s/m^{1/3}$]	Manning roughness coefficient
p	[-]	weighting factor of the inverse distance
P	[mm]	mean annual precipitation
PET	[mm]	mean annual potential evaporation
Q	[m³/s]	peak discharge
Qi+1, j	[m³/s]	unknown discharge at the next node at the present time step
$Q_{i+1, j-1}$	[m³/s]	discharge at the next channel node at the last time step
$Q_{i, j}$	[m³/s]	discharge at the present node at the present time
$Q_{i, j-1}$	[m³/s]	discharge at the present channel node at the last time step
Q_{REF}	[m³/s]	reference discharge
R_{hy}	[m]	hydraulic radius
S_o	[-]	energy slope
t	[s]	hydrologic time-lag
$\triangle t$	[s]	computational time step
V	[m³]	total runoff volume
v_K	[m/s]	kinematic wave celerity
v_m	[m/s]	mean overland flow velocity
w_b	[m]	channel width at bankfull stage
w_i	[m]	channel width of inner channels
X	[-]	weighting factor (expressing the relative importance inflow and outflow have on the storage)
Δx	[m]	distance step, channel reach length
$Z(x_0)$	[-]	estimated value at point x_0
$Z(x_i)$	[-]	measured value at station x_i

Summary

The aim of this study was to apply and test the non-calibrated ZIN-Model in a small (0.5 km²) catchment in southern Israel.

The catchment of Nahal Yael in the Southern Negev Desert may be classified as a lower meso-scale catchment. It is characterised by hyperarid conditions with extreme dryness; mean annual rainfall amounts to 30 mm. Steep rocky slopes partly covered by colluvium drain into the main alluvial reach. Since 1968, a dense hydrologic network has been in operation collecting valuable data records on rainfall, runoff and sediment dynamics. So far, missing high quality data has prevented efficient tests of the ZIN-Model. Based on the unique database of Nahal Yael, existing components of this model are now to be applied and tested.

The ZIN-Model was especially developed for arid catchments. It accounts for the two main processes dominating flash flood generation in arid environments: (1) spatially heterogeneous runoff generation resulting from localised, high intensity rainfall and (2) transmission losses by infiltration into the dry river bed. The conceptual structure of the spatially distributed model includes sub-systems for runoff generation, runoff concentration and channel flow (including transmission losses). For the application in Nahal Yael, model input (rainfall grids of a spatial resolution of 2x2 meters) was derived from interpolating point data for every minute time-step. The runoff generation routine applies the grids of rainfall intensities over different surfaces that were classified during field surveys accounting for their infiltration properties (initial loss and temporal behaviour of infiltration). Hortonian overland flow was assumed to be the dominant process of runoff generation. Subsurface flow paths were neglected. Delineated by topography, the catchment wide pattern of rainfall excess was distributed over more than 500 small sub-catchments that served as model elements for runoff concentration. Runoff delivery from the model elements to the adjoining channels was delayed by a time-lag, which is depending on slope length. Throughout the channel network routing was accomplished using the Muskingum-Cunge procedure accounting for channel geometry and roughness of the channel bed. To quantify transmission losses a constant infiltration rate of the alluvial fill was assumed and discontinued, when the wetting front reached the bottom of the alluvial aquifer.

Model input data was partly collected by field surveys directly in Nahal Yael, other data have been available from previous studies and were prepared for model application. The rainfall-runoff database of Nahal Yael is unique for hyperarid catchments on a world scale. Despite this fact, data preparation was more difficult than expected. Correction of the rainfall data due to wind influence was not necessary as generally rainfall intensities during storm events were very high. Rainfall correction due to sloping ground was not possible as information on wind speed and direction were not available. Data records of rainfall recording stations were not synchronous and had to be synchronised ignoring

storm cell movement but assuming a uniform rainfall distribution all over the area. In one exceptional case, a storm trajectory from southwest to northeast could be recorded by multiple-channel recorders. For this event, two rainfall input scenarios could be compared (one accounting for storm trajectories, the other ignoring storm cell movement). The resulting simulated hydrographs were considerable different. Generally, catchment rainfall was derived by interpolating data records of the recording rainfall gauges by using the inverse-distance weighting (IDW) interpolation method. For some events decreasing rainfall amounts were measured with increasing elevation. Thus, for these events a rainfall-elevation regression was used as a second method to derive catchment rainfall. The two interpolation methods yielded different rainfall scenarios that were comparatively used as model input. Again, significant differences in simulated hydrographs for both rainfall scenarios resulted. In some cases, uncertainty of discharge measurements was relatively high. For one event, a well-defined measured hydrograph could not be determined from the water level records. A range defined by an upper and lower boundary was identified. Very high runoff coefficients sometimes greater 1 determined from measured rainfall and runoff data confirmed high data uncertainties. Comparing the runoff coefficients of nine single events, two of these events showed higher-than-average rainfall-runoff ratios that could not be explained. This data inconsistency was reflected by model simulations, which underestimated measured peak discharges and volumes significantly.

Despite the two events with conspicuous high runoff coefficients the non-calibrated simulations of runoff events showed generally good results within the uncertainty ranges of measured data. Model applications of this study emphasised the high influence of spatial and temporal distribution of rainfall input on model results since diverse rainfall scenarios yielded considerably different runoff simulations. Furthermore, the model results indicate that catchment rainfall in Nahal Yael is sufficiently represented by two rainfall recorders at representative sites, one close to the main channel the other located at a higher elevation close to the watershed. During events with rainfall data from 8 or more recording stations it seemed that the rain gauge set-up with many sites close to the watershed overvalued the influence of high elevations.

The application of the ZIN-Model in Nahal Yael yielded generally good model results at all measuring weirs and justified the existing non-calibrated model conception. In arid catchments without measured field data the model provides a good alternative to estimate extreme discharges and groundwater recharge to alluvial aquifers.

Key words: Nahal Yael – non-calibrated model – rainfall-runoff modelling – hyperarid – data- and model uncertainties

Zusammenfassung

Ziel der vorliegenden Arbeit war es, das für aride Gebiete entwickelte, nicht-kalibrierte ZIN-Modell in Nahal Yael, einem kleinen (0,5 km²) Einzugsgebiet im Süden Israels anzuwenden und zu testen.

Das Einzugsgebiet Nahal Yael im Süden der Negev Wüste, das der hydrologischen Mesoskale zugeordnet wird, zeichnet sich durch extreme Trockenheit mit einer mittleren jährlichen Niederschlagshöhe von 30 mm aus und kann zu den hyperariden Gebieten der Erde gezählt werden. Steile Hänge mit anstehendem Gestein, teilweise bedeckt von kolluvialem Hangschutt, prägen das Relief. Seit 1968 wird in Nahal Yael ein dichtes hydrologisches Messnetz betrieben, das seitdem lange Datenreihen von Niederschlag und Abfluss liefert. Basierend auf dieser hervorragenden Datengrundlage sollte das ZIN-Modell, das bisher aufgrund von mangelnder Datengüte noch nicht umfassend getestet werden konnte, angewendet werden.

Das ZIN-Modell wurde hauptsächlich für große aride Einzugsgebiete entwickelt. Es berücksichtigt die zwei wichtigsten Prozesse bei der Entstehung von Abflussereignissen in Trockengebieten: (1) die räumlich variable Bildung von Oberflächenabfluss, resultierend aus räumlich begrenzten Niederschlägen hoher Intensität und (2) Infiltrationsverluste (transmission losses) an das trockene Gerinnebett. Das flächendetaillierte Modell weist einen konzeptionellen Aufbau in Form einzelner Module für Abflussbildung, Abflusskonzentration und Wellenablauf (der die transmisison losses berücksichtig) auf. Bei der Anwendung in Nahal Yael diente als Eingangsgröße ein räumlich hoch aufgelöstes (2x2 Meter-Raster) Niederschlagsmuster im Minutenzeitschritt, dass aus Punktmessungen mittels des Inverse-Distance-Weighting-Verfahrens (IDW) ermittelt wurde. Dieses trifft im Rahmen der Abflussbildungskomponente auf unterschiedliche Oberflächen, welche hinsichtlich ihrer Neigung zur Abflussbildung (Anfangsverlust, Infiltrationseigenschaften) im Gelände klassifiziert wurden. Es wurde davon ausgegangen, dass der Horton´sche Oberflächenabfluss der dominierende Abflussbildungsprozess sei. Fließbewegungen im Untergrund wurden nicht betrachtet, sondern als Verlustanteil vom Niederschlag abgezogen. Durch die Topographie bestimmt, wurde der in den Teileinzugsgebieten gebildete Oberflächenabfluss den Gerinnen ohne Verluste, jedoch mit einer Zeitverzögerung in Abhängigkeit von der Hanglänge, zugeführt. Dort wurde der Wellenablauf unter Berücksichtigung der Gerinnegeometrie und der Rauhigkeit des Gerinnebettes mittels Verwendung des Muskingum-Cunge-Verfahrens berechnet. Um die Transmission losses zu quantifizieren, wurde außerdem für jeden Gerinneabschnitt eine konstante Infiltrationsrate angenommen, die auf null zurückgeht, sobald die Feuchtefront die unteren Grenze des Aquifers erreicht.

Die Erhebung der Modellleingangsdaten erfolgte durch eine umfangreiche Kartierung im Gelände sowie durch die Aufbereitung von Daten vorangegangener Studien. Trotz der für aride Gebiete außerordentlich guten Datenlage bereitete die Analyse und Aufbereitung der Niederschlags- und Abflussdaten einige Schwierigkeiten. Korrektur der Niederschlagsdaten bezüglich Windeinflusses waren wegen der generell sehr hohen Niederschlagsintensitäten nicht notwendig, wohingegen Niederschlagskorrekturen zum

Ausgleich der Hangneigung aufgrund fehlender Informationen über Windrichtungen nicht möglich waren. Die Aufzeichnungen der Niederschlagsstationen waren nicht synchron und mussten bis auf eine Ausnahme auf gleichmäßige Überregnung des Gebiets synchronisiert werden. Da in einem Ausnahmefall eine von Südwest nach Nordost verlaufende Niederschlagszugbahn messtechnisch erfasst worden war, konnten für dieses Ereignis Niederschlagsszenarien mit und ohne Berücksichtigung der Zugbahn verglichen werden. Die resultierenden simulierten Abflussganglinien unterschieden sich deutlich von einander. Die Niederschlagsaufzeichnungen an den einzelnen Messstationen wurden generell mit Hilfe des IDW-Verfahrens regionalisiert. Da bei einigen Ereignissen mit zunehmender topographischer Höhe abnehmende Niederschlagsmengen festgestellt worden waren, wurde als zweites Regionalisierungsverfahren eine negative Höhenregression für zwei Ereignisse angewendet. Die unterschiedlichen Niederschlagsszenarien wurden vergleichend als Modellinput verwendet. Auch hier ergaben sich signifikant unterschiedliche Simulationen der Abflussganglinie. Die Abflussmessungen wiesen zum Teil recht hohe Unsicherheitsbereiche auf. In einem Fall konnte keine eindeutige Abflussganglinie ermittelt werden, sondern nur ein Unsicherheitsbereich der den wahren Wert beinhaltet, durch eine obere und untere Grenze bestimmt werden. Sehr große Abflussbeiwerte, die aus den gemessen Daten ermittelt wurden und teilweise größer 1 waren, bestätigen die recht großen Datenunsicherheiten. Desweiteren wurden bei einem Vergleich der Abflussbeiwerte der einzelnen Ereignisse für zwei Abflussereignisse überdurchschnittlich hohe Werte festgestellt, die nicht erklärt werden konnten. Diese Inkonsistenzen in Form von überhöhten Abflussbeiwerten spiegelten sich bei der Modellierung in signifikanter Unterschätzung von Abflusspitzen und –volumina.

Abgesehen von den beiden Ereignissen mit auffällig hohen Abflussbeiwerten, bildeten die nicht-kalibrierten Simulation von neun Ereignissen die gemessen Ganglinien im Rahmen der Messungenauigkeit gut nach. Die Modellanwendung verdeutlichte den starken Einfluss der räumlichen und zeitlichen Niederschlagsverteilung auf die Modellergebnisse, da unterschiedliche Niederschlagsszenarien zum Teil sehr verschiedene simulierte Abflussganglinien zur Folge hatten. Desweiteren legen die Modellergebnisse nahe, dass der Gebietsniederschlag ausreichend durch zwei Niederschlagsstationen, eine in der Nähe des Hauptgerinnes und eine in erhöhter Lage, repräsentiert wird. Im Gegensatz dazu wurde während Ereignissen mit 8 oder mehr Niederschlagsstationen der Gebietsniederschlag überproportional stark durch viele Stationen in der Nähe der Wasserscheide beeinflusst, deren Standorte nicht repräsentativ für das Gesamtgebiet waren.

Die Anwendung des ZIN-Modells in Nahal Yael bestätigt mit meist guten Ergebnissen an den Pegeln der Teileinzugsgebiete und im Gesamtgebiet die vorhandene nicht-kalibrierte Modellkonzeption. Für aride Gebiete, in denen keine Geländemessungen vorliegen, ist es somit eine gute Alternative, Extremereignisse und Grundwasserneubildung abzuschätzen.

Stichworte: Nahal Yael – nicht kalibriertes Modell – hyperarid

Niederschlags-Abfluss-Modellierung – Daten- und Modellunsicherheiten

1 Introduction

This study was carried out in close cooperation between the Institute of Hydrology, University of Freiburg and Dr. Tamir Grodek and Dr. Judith Lekach from the Department of Physical Geography at the Hebrew University in Jerusalem and Dr. Noam Greenbaum from the University of Haifa. A scholarship of the DAAD (German Academic Exchange Service) provided the financial means for a two-month stay (June/July 2003) at the Hebrew University during which a ten-day period of field mapping in Nahal Yael was undertaken.

1.1 Aspects of hydrologic modelling in arid environments

Ephemeral streams in arid environments differ greatly from their perennial counterparts in more humid environments. The climatic and flow characteristics are so different that common flow models in perennial channels are unsuitable (SHANNON ET AL. 2002). The unpredictable nature of storm events in arid environments causes a great variability of rainfall both in space and time (e.g. BULL ET AL. 2000; SCHICK 1988; SHARON 1972B). The high spatial variability in rainfall intensities and amounts combined with variability in soil properties makes prediction of runoff generation very difficult. Antecedent conditions play a significant role in the response of a catchment on a storm as well as they influence both hillslope runoff and main channel hydrograph propagation. The variability in catchment response and the unpredictable nature of storm cells mean that hydrographs of ephemeral streams tend to be less predictable than those in perennial channels (HOOKE & MANT 2002).

In recent years there has been increasing emphasis on the development of physically based distributed models (e.g. TODINI 1988). Catchment models are being developed to gain more insight into the relevant water flow processes. For arid zone rainfall-runoff modelling it is essential that methods appropriate to special conditions are developed and applied (SIMMERS 2003).

Based on long data records and the research of many years, complex conceptual rainfall-runoff models depending on calibration were developed in humid areas, where they find widespread application. Scarce hydrometric stream flow data often prevents successful application of calibrated models in arid catchments. Nonetheless, until recently existing arid catchment modelling studies entirely depended on calibration with gauge stream flow data (e.g. SHANAN & SCHICK 1980, HUGHES & SAMI 1994, SHARMA & MURTHY 1998). Other techniques borrowed from the humid zone like empirical approaches are generally not very promising as well as they lump parameters over the whole catchment area (EL-HAMES & RICHARDS 1994). For example, typical flood

magnitude estimations are based on relating storm runoff to rainfall depth and catchment area (SORMAN & ABDULRAZZAK 1993). In arid regions with great heterogeneity this does not seem to be an appropriate tool. In the semi-arid watershed of Walnut Gulch, the long history of research provides good runoff records, which facilitated the successful application of calibrated models (GOODRICH ET AL. 1997; RENARD ET AL. 1993). The long history of research also allowed a non-calibrated model run of KINEROS, a complex distributed model developed for semi-arid catchments (SMITH ET AL. 1995). Because of limited field data usually available in arid catchments, the existing semi-arid parametrisation can hardly be transferred to other arid catchments.

This situation inspired LANGE ET AL. (1999) to develop a model not depending on calibration but accounting for the dominant processes of arid zone flood generation. This has been done for the 1400 km² Zin catchment in the Negev Desert, Israel. Compared to humid areas, runoff generation processes in the Negev are restricted to the surface with Hortonian overland flow being the dominant process of runoff generation. If the rainfall intensity exceeds the infiltration capacity, runoff accumulates on the ground surface, concentrates quickly and flows as an episodic flood event on dry channels beds. There, huge amounts of water may be lost by transmission losses recharging alluvial aquifers whereas contribution from indirect subsurface storages is negligible. Thus, only event water makes up desert floods and processes are limited to the surface, i.e. to two dimensions. Due to this fact modelling approaches of humid regions may be simplified and less processes need to be incorporated (e.g. evaporation and subsurface flow processes may be neglected).

The ZIN-Model has been developed especially for large arid catchments. Apart from the Zin catchment, it has been tested successfully in the semi-arid Nahal Natuf, Israel (250 km²) (LANGE ET AL. 2001) and in the Kuiseb catchment (15000 km²) in Nambia where only the routing component was applied (LANGE submitted). WAGNER (2002) modified the model for application at a much smaller scale (1.8 km²) in a humid environment with rapid surface flow processes (see also LANGE ET AL. 2003B).

Under hyperarid conditions, each event is an extreme event with unique rainfall and runoff characteristics. Data from different types of events are required to understand rainfall-runoff processes inside a specific catchment. Model simulation of different runoff hydrographs in arid catchments is a key to shed light on processes active during flash floods. They may provide answers to catchment scale patterns of runoff generation, to problems of flood prevention, groundwater recharge through channels, reservoir sedimentation and channel stability.

1.2 Previous studies in Nahal Yael

In 1965, the small watershed of Nahal Yael was established as a heavily instrumented research catchment. From then on it contributed to the understanding of geomorphologic and hydrologic processes in a hyperarid environment. During the first years, rainfall observations provided information on effects of wind and topography on rainfall distribution and the spottiness of desert rainfall (SHARON 1972A; SHARON 1972B; SHARON 1980). At the same time, some of the earliest measured discharge data provided information on the processes active during desert floods (SCHICK 2000). Attention was also paid to sediment transport, in the early years it mainly focused on bedload transport. Later on complete sediment budgets were published, the first in 1977 (SCHICK 1977). The second, more accurate sediment budget, was based on longer time series and on detailed analysis of flood deposits in an artificial reservoir downstream the basin outlet (SCHICK & LEKACH 1993). Many more interdisciplinary studies were reported by different authors:

- SCHWARTZ (1986) carried out process studies on transmission losses assessing the extent and water storage capacity of the alluvial fill.
- Detailed terrain based studies on infiltration properties of desert surfaces were undertaken by SALMON & SCHICK (1980) and GREENBAUM (1986).
- The impact of surface water on distribution, growth and mortality of acacia trees has been studied by BENDAVID-NOVAK & SCHICK (1997).
- A paleoflood analysis originating from Nahal Yael expanded to a full-scale study of paleofloods in the entire Negev desert (GREENBAUM ET AL. 2000).
- Quarternary geomorphology was assessed by cosmogenic dating methods which gave inside to climatic geomorphic history of Nahal Yael (BULL & SCHICK 1979; CLAPP ET AL. 2000).
- Evaluation on flood magnitudes and impacts of floods on urbanised alluvial fans (considering the town of Eilat and the surrounding mountains with Nahal Yael as an example) resulted in the formulation of a concept for flood protection for desert towns in general (GRODEK ET AL. 2000).
- Recently, the discovery of a fluvio-pedogenic unit at a few decimetres of depth in the alluvial fill and adjoining terraces gives reason to further research. The so-called “red layer” was subject of an investigation published by LEKACH ET AL. (1998).

The processes active during high magnitude low frequency events, especially runoff generation, sediment transport and channel transmission losses were emphasised throughout the operating period of Nahal Yael. First modelling attempts were undertaken by SHARON & SCHICK (1980) but not brought to determination until today.

1.3 Objectives

The main area of application of the ZIN-Model is the simulation of high magnitude events in arid environments with limited data. Until today missing high quality data has prevented efficient testing of this model. Contrariwise, despite the long-term research and field experience in Nahal Yael, no hydrologic model has been applied in this catchment so far. Because the measured field data provides an excellent framework for a field based model test, the aim of this study is

1) the application of the ZIN-Model in Nahal Yael
2) to validate model performance in the small hyperarid catchment with extraordinary data records on rainfall and runoff
3) to verify and complete existing process knowledge on catchment scale flood generation in hyperarid areas based on the analysis of model results

The processes to be investigated include runoff generation, i.e. the spatial pattern of runoff generation and slope losses as well as the temporal behaviour and spatial extent of runoff losses by infiltration into the river bed alluvium. The study targets to a better understanding of desert floods supported by the field-based simulation of high magnitude discharges of the ZIN-Model.

1.4 Procedure

Various steps were identified to reach the aim of this study. First, the rainfall input data was analysed and prepared for model application. During this procedure, rainfall correction methods and interpolation techniques were examined and data was transformed to rainfall input grids.

Because the model code of the ZIN-Model is essentially field-based, reconnaissance in the field was the first step for the evaluation of relevant field data as model input. Mapping of terrain types and channels as well as determination of model parameters was carried out inside Nahal Yael during the stay in Israel. Based on the results of the field mapping, model elements for runoff generation, runoff concentration and channel routing were defined and incorporated into the GIS environment. Before the application of the ZIN-Model it was necessary to adjust the model components to the small scale of Nahal Yael.

Because of long rainless periods, modelling was accomplished event based. The unique database allowed model application for several events. For this study nine events were chosen. By remise no model calibration was performed, but all model parameters were determined from existing and collected field information. Before comparison with

measured stream flow data was possible, the recorded water level data was converted to discharge data.

The model results were interpreted for each event independently. In a first step the selected events were analysed concerning quality of measured rainfall and runoff data. Afterwards, model performance was evaluated with respect to plausibility of runoff generation, runoff concentration, channel flow and transmission loss routine. Doing so, intermediate results as time till onset of runoff, amount of generated runoff spatial patterns of generated runoff were analysed in the first instance, before interpretation of the simulated and measured hydrographs was carried out by direct comparison.

2 Arid zone hydrology

Arid lands encompass a third of the earth's surface (MAINGUET 1999), and are characterised by a general lack of moisture. This essentially climatic phenomenon is based upon the average climate conditions over a region (AGNEW & ANDERSON 1992). The main feature of aridity is a net surface water deficit, which results from climatic, topographic and oceanographic factors. These factors prevent moisture bearing weather systems reaching the land surface (THOMAS 1997). The dryness is mainly caused by high evaporation rates exceeding low precipitation rates. Aridity was first defined by Albrecht Penck at the beginning of the 20th century (WEISCHET 1995) based on the long-term evaporation-rainfall ratio. Clear boundaries of the arid zone do not exist; however, a widely accepted definition today was published by UNESCO (1977) and modified by DEICHMANN & EKLUNDH (1991) (Figure 2.1). The global aridity index is based on a ratio of mean annual precipitation (P) and mean annual potential evaporation (PET), estimated by the Thornthwaite approach. It classifies the world into four aridity zones and one humid zone, defined as follows:

hyper-arid zone	P/PET < 0.05	(2.1)
arid zone	0.05 <= P/PET < 0.20	(2.2)
semi-arid zone	0.20 <= P/PET < 0.50	(2.3)
dry-subhumid zone	0.50 <= P/PET < 0.65	(2.4)
humid zone	0.65 <= P/PET	(2.5)

The main hydrological difference between more humid areas and arid zones is a high variability in space and time of all hydrologic parameters (e.g. rainfall intensity, infiltration rates, runoff rates). Floods, although infrequent and rare, appear in all arid areas and often cause a heavy price in loss of life and property (SCHICK ET AL. 1997).

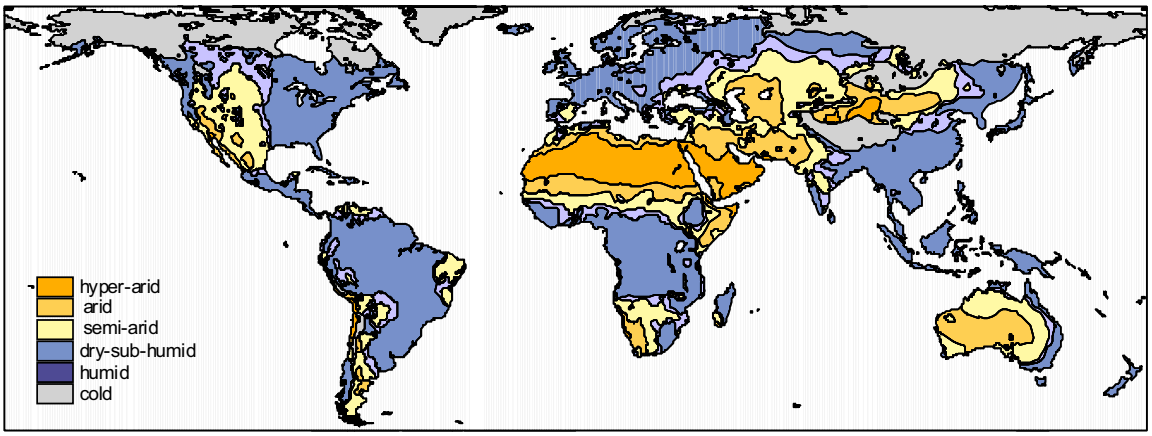

Fig 2.1: Arid regions around the world (after DEICHMANN & EKLUNDH 1991)

The main processes that dominate during flashy floods are the generation of Hortonian overland flow on dryland terrain and transmission losses into the dry alluvial beds of ephemeral channels.In dry environments, the hydrological regime is governed by missing base flow and single episodic flood events travelling on dry river beds, induced by localised, high intensity rainfall. Since vegetation is very sparse, interception losses are generally negligible for water balance calculations in arid zones.

2.1 Rainfall

The main climatological feature of arid areas is the ephemeral and often localised nature of precipitation usually associated with immense variations in space and time. Most dryland areas of the world are located beneath semi-permanent high pressure systems, where frontal activities with long-term rainfall or tropical storms are rare. Most frequently, rainfall occurs as thunderstorms which usually are the product of convection of heated air. Most thunderstorm cells are only a few kilometres in diameter, so they affect small basins of about the same size by inducing flash floods (GRAF 1988). As a result, arid regions suffer from very high rainfall variability with common coefficients of variation around 40%, and in extremely arid areas exceeding 100% (AGNEW & ANDERSON 1992). In extreme arid areas, annual precipitation may fall during very few events and a 24-hour rainfall may exceed the mean annual rainfall by a factor of 3 to 4 once in a 20 to 30 year period (SCHICK 1988). High temporal variability is associated with an enormous spatial variability. (SHARON 1972B) describes highly variable areal patterns of short term rainfall in southern Israel. In a climatically uniform area, on 21 separate days at three stations within 15 km of each other, the same order of magnitude was recorded on 4 days only. In a typical cloudburst of the extreme desert, the transition between total dryness and full blast rain is nearly instantaneous. Intensities of such storms can be very high, more than 330 mm/hour were documented by GOODRICH ET AL. (1997). The velocity of storm cells in the extreme desert varies from quasi stationary (velocity near zero) to several tens of kilometres per hour (SCHICK 1988).

2.2 Evaporation

Because of a lack of vegetation, transpiration plays a minor role in the water balance, especially in hyperarid catchments like Nahal Yael. In contrast to more humid areas this fact allows to discuss evaporation instead of evapotranspiration.

Evaporation is affected by several climatic elements (e.g. air temperature, relative humidity, net radiation). It is necessary to distinguish between actual rates of evaporation and potential rates. The concept of the potential evaporation assumes that water is not limited and is at all times sufficient to supply the requirements of the dry air

and the transpiring cover. Clearly, in arid environments, the value for actual evaporation seldom equals the potential evaporation, but is much lower.

Evaporation plays a decisive role in arid areas, as it dominates the long-term water balance. A study in Saudi-Arabia revealed, for example, that evapotranspiration losses make up 95% of the rainfall (ABDULRAZZAK ET AL. 1989). Daily values of potential evaporation, measured for example by class A pans, reach 10 mm and more (SCHICK 1988). For the short term water balance evaporation losses from the surface or open water tables are generally negligible, due to very short durations of the rainfall events. Furthermore, cloudiness, low air temperatures and relatively high humidity during storm events prevent high values of potential and actual evaporation. Transpiration plays a minor role, since considerable vegetation is restricted to stream channels. Apart from deep ground water recharge, the amount of annual evaporation should be of the same order of magnitude as the accumulated amount of infiltrated water, since shallow storages are quickly emptied by evaporation. Thus, evaporation minimises the effect of antecedent moisture, an important factor for flood generation in humid regions.

2.3 Runoff

The high variability of rainfall both in time and space, leads to very high variability of runoff. Due to an abundance of exposed bedrock and restricted soil and vegetation cover, a very rapid surface runoff response is typical for arid climates. However, runoff tends to be patchy and part of it may re-infiltrate before reaching a channel (BULL & KIRKBY 2002, YAIR 1992). The accentuated spatial heterogeneity makes it difficult to assess runoff response in catchment scale problems.

2.3.1 Runoff generation

In humid regions different runoff generation processes (e.g. runoff from saturated areas, piston-flow effects, macropore flow, slow outflow of large groundwater bodies) deliver more or less permanently water to perennial rivers. In contrast, in arid areas Hortonian overland flow, generated as infiltration excess runoff, is generally assumed to be the dominant mechanism of runoff generation (ABRAHAMS ET AL. 1994). Common definitions of overland flow describe it as water that flows over the ground surface heading for the next stream channel and as the initial phase of surface runoff in arid environments (LANGE 2003A). On plane surfaces a quasi laminar sheet flow may develop, but, more usually, flow is concentrated by topographic irregularities and water flows anastomosing in small gullies and minor rivulets downhill. The main cause of overland flow is the inability of water to infiltrate the surface as a result of high intensity of rainfall or a low value of infiltration capacity or both phenomena. The concept of Hortonian overland flow calculates runoff as the difference between rainfall rate and infiltration rate (HORTON

1933). If the infiltration capacity of the soil is exceeded, water accumulates on top, but before it runs downslope, surface depressions have to be filled up.

Ideal conditions for Hortonian runoff are found in most arid areas with moderate to steep slopes and sparse vegetation cover. In rocky deserts, underlying rocks are usually exposed or covered by a thin veneer of debris. At the base of most slopes colluvium accumulates. Only a minority of the world's deserts are covered by aeolian sediments with usually high infiltration rates. Rocky deserts generally have poor soil development and relatively little vegetation. The surface largely is the first point of contact by rainfall. Thus physical and chemical properties of superficial material play a primary role in runoff generation. In rocky deserts infiltration rates of bare rock surfaces are low (only a few millimetres per hour) and vary often only little due to differences in rock type or jointing. On rocky upslope areas, for example, large amounts of runoff may be generated immediately after the onset of rain. Infiltration rates of the colluvial base on the other hand are an order of magnitude higher and allow losses of large amounts of runoff originating from upslope areas. Hence, infiltration characteristics may differ significantly with slope position.

2.3.2 Channel flow

Because rainfall events are very rare, streams in the arid zone are usually ephemeral, hence flowing only occasionally and remaining dry for most of the year. Large through-flowing streams with their origin outside the arid zone (e.g. Nile River, Indus River or Colorado River) and small spring fed streams are the only exceptions. Floods in small dryland basins usually are of the flash flood type, either single peak floods or multiple peak events. Flash floods are almost always produced by convective rain storm cells and are typical for small scale catchments (< 100 km²), because most thunderstorm cells are relatively small in diameter (GRAF 1988). Flash floods are defined as stream flows that increase from zero to a maximum within a few minutes or at most a few hours. In the southern Negev region, less than one third of the events are caused by long-term, medium to low rainfall intensity patterns (SCHICK 1988). The advancing front of water in the channel (frequently observered as a "wall of water") is usually extremely turbulent, has large amounts of air creating foam and may push debris in front of its main mass. The hydrographs of such flash floods are characterised by a rapidly rising limb, a sharp peak and an equally sharp falling limb. Direct observations of these floods indicate supercritical flow, with surface velocity as determined by floats of about 5 m/s (SCHICK 1988). High magnitude events are highly efficient, modifying landscape by erosion and depositing huge amounts of debris.

2.4 Storages

In the arid realm, two types of surface flow losses occur, that fill temporal storages (LANGE 1999):

1) With Hortonian runoff, infiltration is a *direct loss* that governs the volume of storm runoff. Further direct losses occur when water is temporarily stored on route or in the stream system as detention loss or when depression storages retain water in depressions on the surface.

2) After surface flow has been generated and flows spatially concentrated, linear transmission losses into the riverbed alluvium of the stream channels reduce flood volume as *indirect losses.*

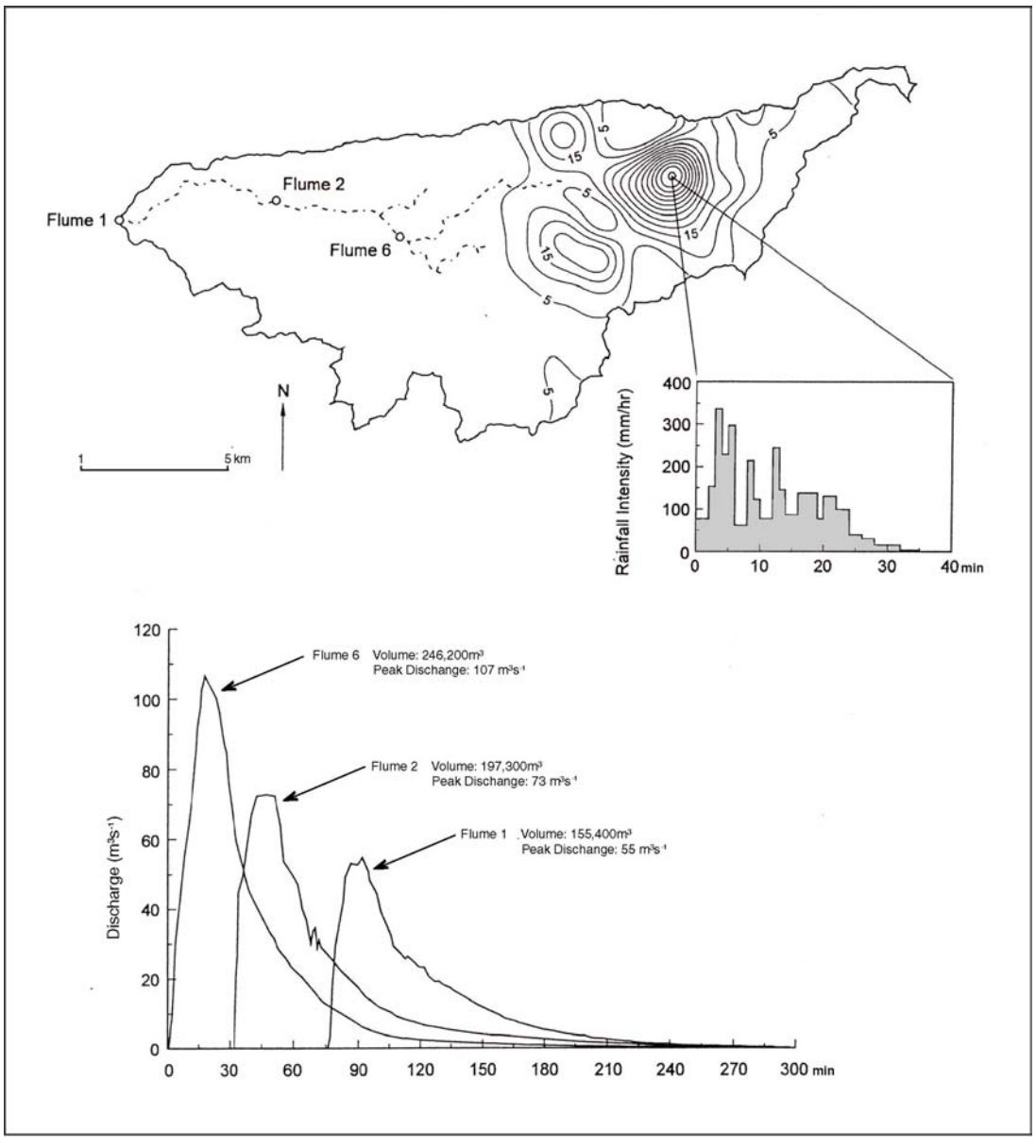

Fig 2.2: Transmission losses along an ephemeral channel (after GOODRICH ET AL. 1997)

The main water storage in dry environments is formed by coarse river bed alluvium. With rainfall events broadly separated in time, the alluvial fill has a large available volume for flood water infiltration practically at all times. The alluvial storages form an infiltration trap for water that flows into them either through the orderly tributary system or directly from adjoining slopes. Figure 2.2 shows a downstream decrease of water volume and peak discharge for an ephemeral stream, due to infiltration into the river bed, at Walnut Gulch experimental site, Arizona, USA. The alluvial bodies, filled by indirect losses may be relatively permanent and quite deep, serving as important water storage for vegetation or local population. Compared to alluvial fills, the second type of storage is shallower. It is recharged by direct losses and is quickly emptied by evaporation within a few days after the rainfall event. Percolation from rainfall to deep aquifers is generally very small.

2.5 Data collection

In the arid zone, problems of hydrometry are severe because the arid realm is not well endowed with hydrologic observations (AGNEW & ANDERSON 1992). Despite the great technical advance in precipitation measurement (e.g. rainfall radar) most data are based on ground stations. These are often close to settlements, and since population density is very low, huge areas are ungauged. Further reasons for meagre data availability are partly economic (in most arid zone countries, financial means are too short to install and maintain a hydrometric gauging network) and partly environmental, related to the extreme climate which results in mechanical breakdowns. Due to accentuated local variability of rainfall, coarse raingauge networks may not be able to mirror the distinct spatial patterns, and interpolation may cause substantial errors. For large catchments the interpretation of rainfall radar is the only possibility of deriving an accurate picture of catchment wide rainfall, even though adjustment with ground stations is still required.

Measurement problems during high magnitude desert floods reduce data quality of the discharge data. Runoff is mostly measured by standard runoff gauges, which measure water level by floats or pressure transducers. Under stable conditions, the stage-discharge relation can be plotted for each station to produce a rating curve. In arid environments, where cross-sectional geometry may permanently change during a flood event, such curves are far less accurate. Moreover, sedimentation in the cross-section is responsible for incorrect water-level measurements. It is also possible, that high magnitude events destroy gauging stations and wash them away or that the recorder pen sticks during the vital period as a result of inactivity. For catchments without permanent gauging stations, discharge must be estimated or calculated by indirect methods. For single channels, the slope-area method, which adapts a uniform-flow equation using measurements of cross-section area and water surface slope made in the field, is the most flexible.

Peak stages of historic and recent floods can be estimated by paleoflood methods. They use marks of flow, e.g. slackwater deposits or high water indicators as scour marks or driftwood, to reconstruct flood water tables. Slope-area calculations or hydraulic modelling are used to transform historic peak stages to paleodischarge estimates (KOCHEL & BAKER 1988).

2.6 Conclusion

The discussion above on the climate of arid areas points to rainfall variability in both space and time coupled with high potential evaporation. Nevertheless, arid zone catchment response is relatively simple compared to more humid regions, since indirect subsurface runoff components are negligible. Overland flow is the initial phase of surface runoff in dry regions. It is generated as Hortonian overland flow if rainfall intensity at any time during a storm exceeds the infiltration capacity of a soil surface, resulting in widespread surface ponding and overland flow. Ephemeral floods mostly travel on a dry river bed allowing significant infiltration losses into the channel alluvium on their way downstream. Hence, the occurrence of flash floods is dominated by the generation of Hortonian overland flow on dryland terrain and transmission losses into the dry alluvial beds of ephemeral channels. Data records (rainfall and runoff) of the episodic arid flow events are generally poor.

3 Study area

Following definitions of DYCK & PESCHKE (1995), Nahal Yael may be defined as a lower meso-scale catchment. Although relatively small, the spatial heterogeneity and spatial variability of parameters are responsible for complex mechanisms of action. In contrast, at microscale hydrologic systems elementary processes may be directly assessed by measurements and described by fundamental physical laws, which is not possible in Nahal Yael.

Nahal Yael (Nahal [hebr.]: stream) is a 2 km long ephemeral stream, draining 0.5 km² of bare rocky desert terrain in the Negev Desert, Israel. In 1965, the catchment of Nahal Yael in the Eilat Mountains was established as a field laboratory by A. P. Schick for studying climatic, hydrologic and geomorphologic processes in an extremely arid environment. Since then, measurements of precipitation, stream flow, erosion and deposition have been made by the Department of Geography at the Hebrew University of Jerusalem creating a database unique for arid catchments around the world.

3.1 Location and topography

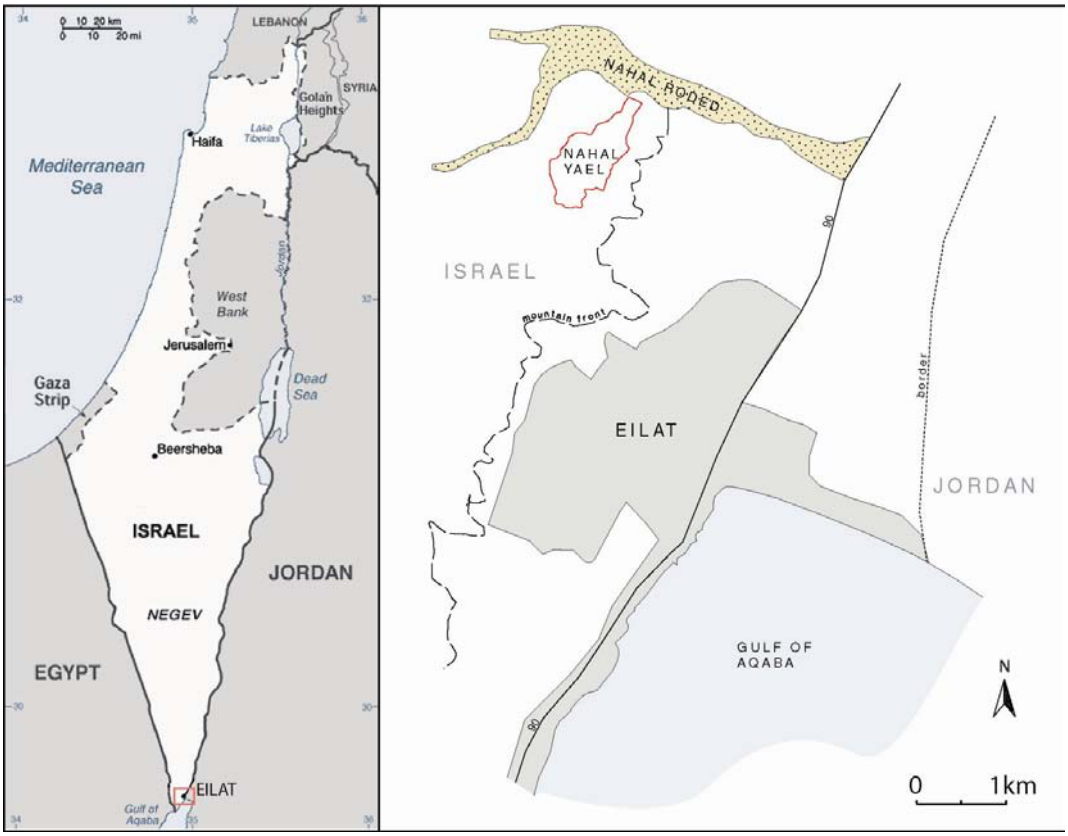

Fig 3.1: Location map

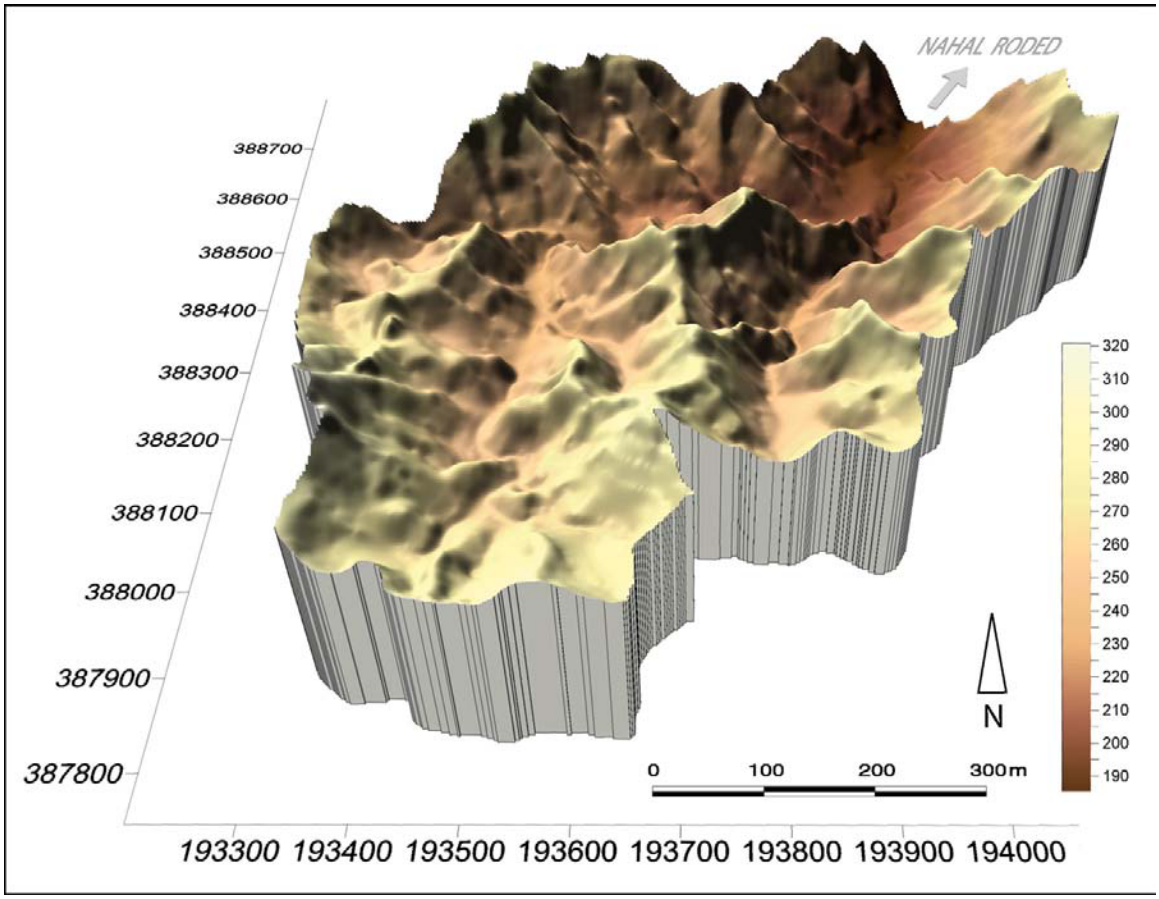

Fig 3.2: Nahal Yael watershed in 3D view

Drainage density in Nahal Yael is also high (19.5 km/km²). More than 100 first order channels drain into the 1 km long main alluvial valley, which forms the basic internal storage of the watershed. The alluvial reach with a mean channel slope of 0.05 is terminated at its downstream end by a 10 metres high waterfall. Here, the main gauging station of the project (station 02) has been in operation since 1966 (SCHICK & LEKACH 1993). An earth dam constructed in 1978, 200 meters downstream the waterfall, creates an ephemeral 100% trap efficiency reservoir (Figure 3.3).

Farther downstream the channel widens to form an alluvial fan whose toe borders on the wide braided channel of Nahal Roded, a relatively major tributary of the Southern Arava rift valley. The watershed has been subdivided into 4 instrumented units (Figure 3.3) for which precipitation, channel discharge and sediment yield data are available. The topography of Nahal Yael has been mapped very accurately in the 1960ies resulting in a map at a scale of 1:1250 with 1 metres contour interval.

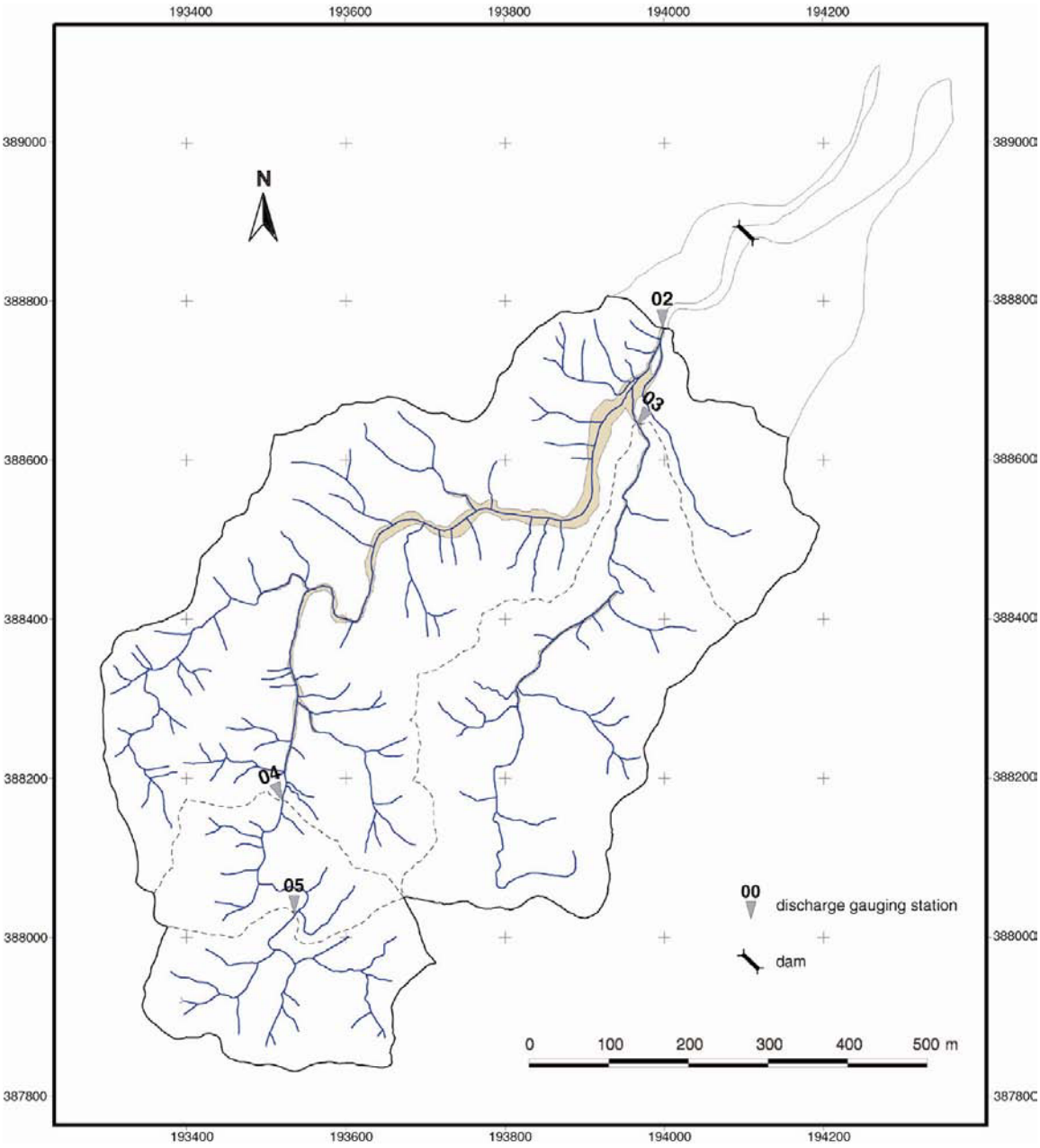

Fig 3.3: Nahal Yael with sub-catchments and discharge gauging stations

3.2 Climate

The climate in the southern Negev region is hyperarid, which is reflected in high air temperatures and meagre rainfall. Summer daytime air temperatures commonly exceed 40° C, expressed also in a high mean temperature maximum for August (38°C). The winter is mild, mean minimum temperature for January is 10°C, and mean annual humidity 39 % (GRODEK ET AL. 2000). WALTER & LIETH (1979) developed climatic charts that show annual characteristics of air temperature and rainfall. Mean monthly temperatures and rainfall amounts for Eilat are presented as such a chart in Figure 3.4.

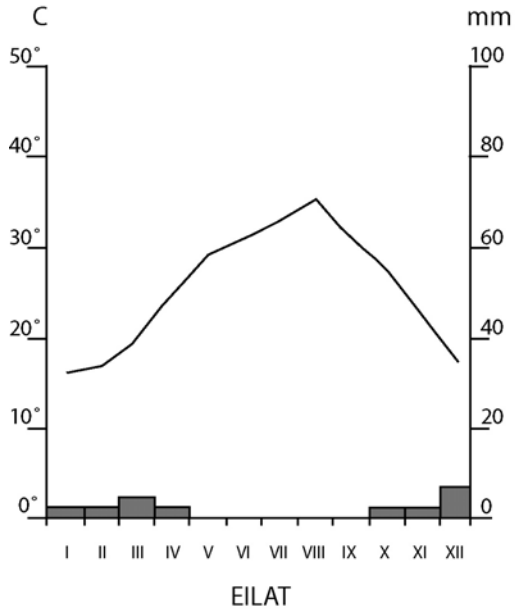

Fig 3.4: Climatic chart of Eilat (after ORNI & EFRAT 1966)

Rainfall is scarce and in some years rainfall is insufficient to cause stream flow in Nahal Yael (BULL & SCHICK 1979). The mean annual precipitation of about 30 mm over the last 50 years (measured at the first order station of the Israeli Weather Service in Eilat) falls mainly in winter, although high-intensity rains are more likely to occur in spring and autumn. When low level throughs of warm, dry air from the Red Sea are moving northwards and combine with high level throughs moving southwards, they produce

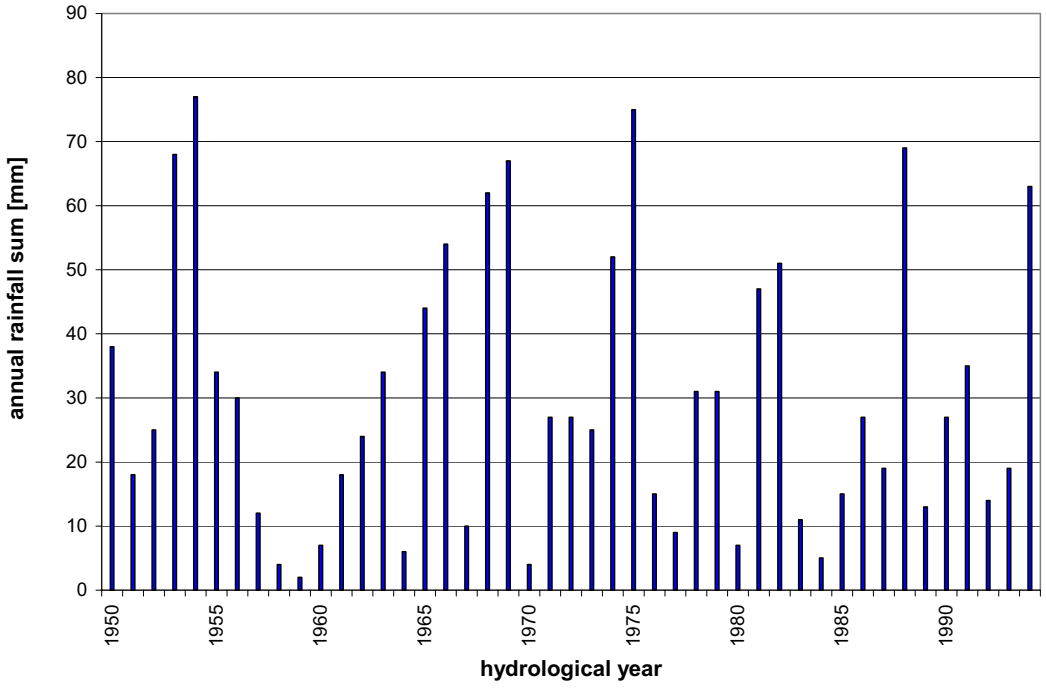

Fig 3.5: Annual rainfall amounts in Nahal Yael

instability in the whole troposphere which in turn produces convective rainfall over Nahal Yael especially in spring and autumn (WOHL & GRODEK 1994). The occurrence of a summer cloudburst is quite unlikely even though one took place in 1926 (SCHICK & SHARON 1974). Precipitation is characterized by a high variability at all time scales (SHARON 1972A). There are years with just a few millimetres of rainfall, e.g. in 1970 annual precipitation In Nahal Yael was not more than 2 mm. In contrast, in other years annual rainfall exceed the long term annual average by a factor of 2 or 3 (Figure 3.5). The coefficient of variation for the time series of annual rainfall sums from 1968 till 1989 is 0.72. The number of days with precipitation ranges between 0 and 10 per year (YAIR & KLEIN 1973). Similar to other hyperarid areas of the world, immense temporal variability finds its counterpart in the areal patterns for a given event. An extraordinarily large spatial variability of short-term rainfall has been documented by SHARON (1972B), although for much larger areas than Nahal Yael. Typical short duration cloudbursts of the extreme desert are characterised by a nearly instantaneous begin and high intensities. The transition between total dryness and full blast rain is registered as a sharp rise in the rain gauges. The maximum intensity measured in Nahal Yael in 1997 was 126 mm/h. In certain events, an amount equivalent to the mean annual rainfall may fall in less than an hour (SHARON 1972B).

3.3 Geology

Geologically, the catchment area is located within the Arabo-Nubean Shield of Precambrian rocks (SHIMRON 1974). All rocks form part of the Eilat Massif, a high grade regionally metamorphosed and complexly folded belt of metasedimentary and meta-igneous rocks. It forms a northern extension of the Sinaii Massive. The basin is underlain by E-W trending belts of folded pellitic schists and amphibolites with minor exposures of granite, granitic gneiss and porphyritic dikes. The southernmost portion of the area is occupied by schists, which is followed by a strip of amphibolitc rocks to the north. In the middle part of Nahal Yael schist is the dominant rock, whereas a post-metaphoric intrusion of granite outcrops is in the very northern part of Nahal Yael. This granite is of the coarse-grained, jointed and sheared pink porphyritic Eilat granite type. Several acid dikes directed N-S appear in the area. Common dike lithologies are feldspar porphyry, lamprophyre, quartz porphyry, and pegmatite. Furthermore, minor intercalated remnant portions of granitic gneiss outcrop in the amphibolite belt. The extent of all formations is shown in Figure 3.6. A detailed description of the mineralogy of metamorphic complexes (schists and amphibolites) and dikes can be found in SHIMRON (1974). The portions of underlying rock types are: 25% mafic (amphibolitic) rocks, 67% metasedimentary rocks (schist and granitc gneiss) and 8% granite.

In general the slopes are short but steep. Most of them are covered with mixed debris, which includes gneissic, amphibolitic and dyke elements. In the northern and middle sections exposed bedrock dominates the uplands. Significant colluvial cover is limited to

bedrock hollows and incised channels and to the lowermost parts of hillslopes. The amphibolite is the least resistent rock in the research area. It weathers easily, forming a coarse grained sand. This is why, in contrast to the northern, lower section hillslopes in the southern sections are relatively smooth (Figure 3.2). Bedrock is exposed on the top 10 to 20 metres and substantial colluvium covers the lower hillslopes consisting of a 5 to 20 centimetres thick rubbly layer of angular or platy stones. Fine particular matter that appears as suspended sediment in the floodwaters is not visibly exposed on the surface; it is derived from a sub-stone layer.

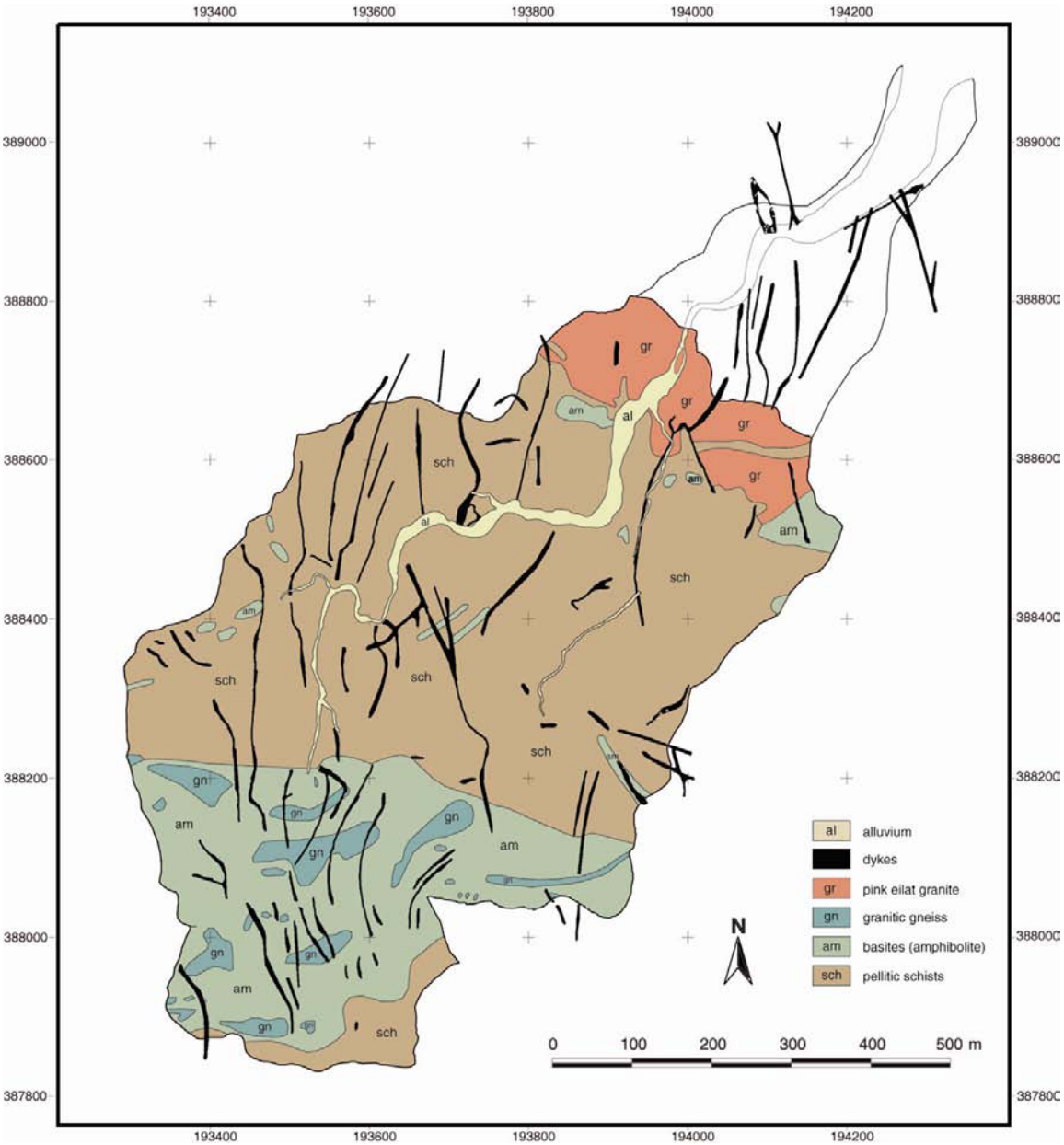

Fig 3.6: Geological overview of Nahal Yael (after SHIMRON 1974)

3.4 Soils and vegetation

The hill slopes are almost barren of vegetation and sparse growth of trees, bushes and grass is restricted to the main stream channel, where moisture conditions are more favourable. Except for few Acacia trees in the alluvial reach no trees are found inside Nahal Yael (Figure 3.7).

Fig 3.7: Photograph of alluvial reach of Nahal Yael

Typically for arid environments, the steep slopes are bare of any soil cover or vegetation and provide little protection from areal erosion. Most weathering products from the slopes are washed away and accumulate in the main channel forming the active river bed alluvium. The only place, where desert soils may be found, is on more gentle alluvial terraces. Their typical profile consists of a superficial varnished desert pavement underlain by a silty vesicular horizon and a gravely C horizon. BULL & SCHICK (1979) observed similar units in Holocene and Pleistocene terraces and alluvial fan surfaces in Nahal Yael. These units have some initial characteristics of desert soil development such as horizonation followed by calcium carbonate, gypsum and halit deposition, iron oxides release and accumulation of fine material.

3.5 Hydrology

The result of the high climatic variability is a great variability in flows, which last between 10 minutes and a few hours. Flooding processes are markedly different from those in humid environments. Like most small arid basins, Nahal Yael responds quickly to rainfall. Water level in completely dry channel beds rises within minutes to peak discharge, remaining at this level for some minutes, followed by abrupt recession that lasts only a few hours. Flow is characterised by unsteady, non-uniform and highly turbulent flow conditions and specific peak discharge of the high magnitude events is very high. The supercritical flow provides high values of stream power, which are responsible for movement of sediment and substantial reworking of the channel geometry throughout the event.

Roughly half of the flows are longitudinally interrupted events and terminate at various distances along the alluvial reach. The other half, defined as persistent events, activates the whole channel length, but not necessarily its entire width. At least one flow almost every year is recorded at the three upstream tributaries. In contrast, the recurrence interval of the persistent events that reach the basin outlet is 2.5 years (LEKACH & SCHICK 1982). The discrepancy caused by high transmission losses of the alluvial reach (SCHWARTZ 1986). The longest period between subsequent major events was over 81 months between events 12B and 13, and the two shortest periods were 4 and 8 hours for events 7A and 7B and 12A and 12B respectively. As threshold for the initiation of overland flow, a daily rainfall of 3 mm was determined by YAIR & KLEIN (1973) in sub-catchment 05, whereas the threshold for the initiation of channel flow amounts to 5 mm (YAIR & KLEIN 1973). The basin is subdivided into three small sub-catchments, whose runoff is being measured at stations 03, 04 and 05 (Figure 3.3) and the main alluvial reach, which terminates at station 02. All stations are built on stable bedrock cross sections to avoid runoff losses beneath the stations. The hydrometric stations consist of a broad crest concrete weir (station 05 is rectangular shaped, the other stations are of triangular shape), and an OTT type XX float-operated water level recorder. Photographs of all gauging stations are found in Annex A.1-A.4. The runoff data collected during 37 years of operation is summarised in Table 3.1. The main channel is roughly 1 kilometre long, with a mean slope of 0.05. In the sub-catchments the channels are basically rocky, with occasional patches of thin alluvium. In sub-catchment 05 the typical channel width is 2.5 metres with a few small waterfalls of 20 to 60 centimetres height, accompanied by steep rocky banks. The channel mostly flows on bedrock, with some shallow alluvial veneer sometimes more concentrated in pockets in the rock and in the form of strips along rocky depressions. Continuous alluvium, however shallow, covers the channel bed only over a 17 metres long reach immediately upstream of hydrometric station 05. Between stations 04 and 05 the channel is an alternation of rocky riffles and pools with waterfall heights between 0.5 and 1 metres. Here, the alluvial cover is still semi continuous and found in pools only. In sub-catchment 03 the situation is very similar with a bedrock channel in the upper parts and considerable alluvium in the lower parts, a few

hundreds of meters upstream of station 03. Sequences of riffles and pools are also found with waterfall heights up to 1.5 metres.

Tab 3.1: Runoff events between 1966 and 2001 (after GRODEK 2002)

		St. 02		St. 03		St. 04		St. 05	
date	event	V	Q	V	Q	V	Q	V	Q
01-01-1966	E 1	nd	1,50	nd	nd	nd	nd	nd	nd
13-03-1966	E 2	nd	2,10	nd	nd	nd	nd	nd	nd
25-04-1968	E 3	nd	1,10	510	0,64	321	0,71	nd	nd
24-05-1968	E 4	3977	2,10	nd	1,40	843	1,07	nd	0,34
24-11-1968	E 5	0	0,00	0	0,00	37	0,02	62	0,04
25-11-1968	E 6	213	0,03	187	0,13	406	0,22	445	0,13
21-01-1969	E 7a	3592	0,85	153	0,48	87	0,47	147	0,26
21-01-1969	E 7b	7466	1,90	443	1,37	405	0,79	105	0,62
25-03-1971	E 8	0	0,00	0	0,00	40	0,24	37	0,04
22-12-1971	E 9	0	0,00	0	0,00	1830	0,25	573	0,09
12-11-1973	E 10	nd	1,05	nd	1,90	nd	0,90	nd	0,83
04-12-1974	E 11	nd	0,22	nd	0,08	nd	nd	nd	0,18
20-02-1975	E 12a	4571	1,08	1540	0,24	3038	0,17	940	0,12
20-02-1975	E 12b	1312	2,05	nd	0,75	nd	0,50	nd	0,38
11-12-1978	E 13	0	0,00	0	0,00	110	0,02	53	0,04
09-02-1979	E 14	0	0,00	0	0,00	30	0,03	31	0,03
26-12-1980	E 15a	1853	2,90	nd	1,50	418	0,81	461	0,65
26-12-1980	E 15b	267	0,47	nd	0,63	75	0,34	239	0,25
31-10-1981	E 16	2411	2,35	1744	1,05	nd	nd	536	0,57
22-03-1985	E 17	nd	0,10	nd	0,18	nd	0,25	nd	0,17
28-11-1986	E 18	0	0,03	nd	nd	nd	nd	nd	nd
17-10-1987	E 19a	nd	nd	nd	nd	nd	nd	nd	nd
18-10-1987	E 19b	670	0,37	nd	nd	151	0,14	nd	nd
30-11-1989	E 20	nd	0,01	nd	nd	nd	nd	nd	nd
23-10-1990	E 21	910	0,78	nd	nd	nd	nd	nd	nd
22-03-1991	E 22	nd	0,38	nd	nd	nd	nd	nd	nd
18-10-1997	E 27	2910	3,70	nd	nd	677	2,00	253	0,49

V: total runoff volume [m³] Q: Peak discharge [m³/s] nd: no data

The main alluvial channel between stations 02 and 04 is mostly braided and of varying width. The channel widens from 3 in the upper parts to 25 metres further downstream and is flanked by a 1 to 5 metres high well-developed alluvial terrace. It consists of well-defined bars and inner sub-channels. The low bars are distinguished by smooth surfaces of well-sorted material. The high bars are characterised by surfaces composed of a poorly sorted mixture of cobbles, pebbles and fines. Of the total channel reach area 51% are sub-channels, 30% are low bars and 19% are high bars. The volume of the

alluvial body of Nahal Yael, which underlies the main reach between stations 04 and 02 is 12600 m³. At its lower bound it is confined by bare rock. During floods the alluvium acts as temporary water storage with depths ranging between a few decimetres and 3.2 metres (SCHWARTZ 1986). The alluvial material is chiefly coarse with only a small portion of the fine fraction (< 0.063) and has a porosity of 30% (SCHWARTZ 1986). Stratigraphic surveys conducted in the alluvial fill of Nahal Yael and other channels in the Southern Arava Valley, indicate the existence of a continuous unit characterised by pedogenic features at an average depths of 0.5 metres below surface. Because of its colour it has been named “red layer”.

3.6 Conclusion

The Nahal Yael drainage basin in the Negev Desert of southern Israel is located on one of the most arid spots worldwide. High variability of rainfall causes tremendous variability of runoff. During 37 years of research, 20 persistent flood events that reached the basin outlet at station 02, and 7 longitudinal interrupted events were recorded. The basin of the ephemeral stream is characterised by steep barren slopes, covered partly by colluvium. Geologically, Nahal Yael is underlain by Precambrian rocks of igneous and metamorphic origin. Vegetation is very sparse and restricted to the main alluvial reach. Slopes are drained by a dense network of first order streams converging into the main alluvial reach. Nahal Yael has been monitored for over 3 decades; hence an abundance of rainfall, runoff and sediment data replicated in few other arid basins worldwide is available.

4 Model structure

The spatially distributed rainfall-runoff model has been developed specifically to simulate high magnitude events in dry environments (LANGE 1999) and was successfully tested at various scales (LANGE 1999; LANGE submitted; LANGE ET AL. 1999; WAGNER 2002). It has been named after Nahal Zin, an ephemeral stream with a large arid catchment (1400km²) in the Negev Desert, for which the model was conceptualised.

Like all hydrological models the ZIN-Model is a simplified representation of natural systems and is used as a mathematical tool to simulate and interpret hydrological processes. In contrast to other deterministic rainfall runoff models, the ZIN-Model is not depending on calibration with measured runoff data, thus it is also applicable in catchments without stream flow data. As all parameters are determined in the field and not a single parameter is fitted by calibration, the model may be termed “field based” (LANGE ET AL. 1999). Because Hortonian overland flow is the dominant runoff generation process and runoff contribution from underground storages is negligible, flood generation is limited to the surface and the model may be restricted to 2 dimensions.

4.1 Model conception

Owing to long dry periods the model is event based. As input data the model uses a catchment wide pattern of rainfall intensities in a time step of 1 minute. In Nahal Yael this information is derived from a dense network of recording rain gauges (see Chapter 6.1) but it may be gained from other sources (e.g. rainfall radar, physically based rainfall models) as well. As output, the model chiefly yields a hydrograph of discharge at any user-defined point every 50 metres along the watercourse. For plausibility checks, it is also possible to define other parameters or intermediate results (e.g. water depths, transmission loss parameters, etc.) as output.

The ZIN-Model is subdivided into three sub-systems or routines, namely runoff generation, runoff concentration and channel routing. For each sub-system, spatial sub-units and their effective parameters are determined (LANGE 1999):

- Rainfall impinges as a spatially distributed grid of rainfall intensities upon hydrologically different surfaces. The lands surface is classified into characteristic terrain types, with their different infiltration properties as effective parameters. These terrain types determine the spatial sub-units for *runoff generation*.
- For *runoff concentration* the drainage network is disaggregated into channel segments. Adjacent basins of the channel segments represent the spatial sub-units of this model routine.

- For *channel routing and transmission loss* parameters the same channel segments as used in the runoff concentration sub-system, are the spatial sub-units.

The aggregation of spatially homogenous areas into model sub-units is carried out independently for each sub-system. Thus, the model is very flexible and allows maximum accuracy with minimum spatial resolution. For the transfer of data between the sub-systems a Geographic Information System (GIS) is used, in the present study an ArcInfo interface has been employed.

Mapping of the spatial sub-units has been done directly in the field during a recent field campaign with additional data from topographic maps and previous field campaigns. Figure 4.1 shows a schematic flow chart of the model including the different types of spatial subdivision in the sub-systems, which will be explained in detail below. In this chapter, model operation is summarised briefly, details on parameter determination inside Nahal Yael will be described in Chapter 5. In the following, model parameters are given in italic followed by their respective units in squared brackets.

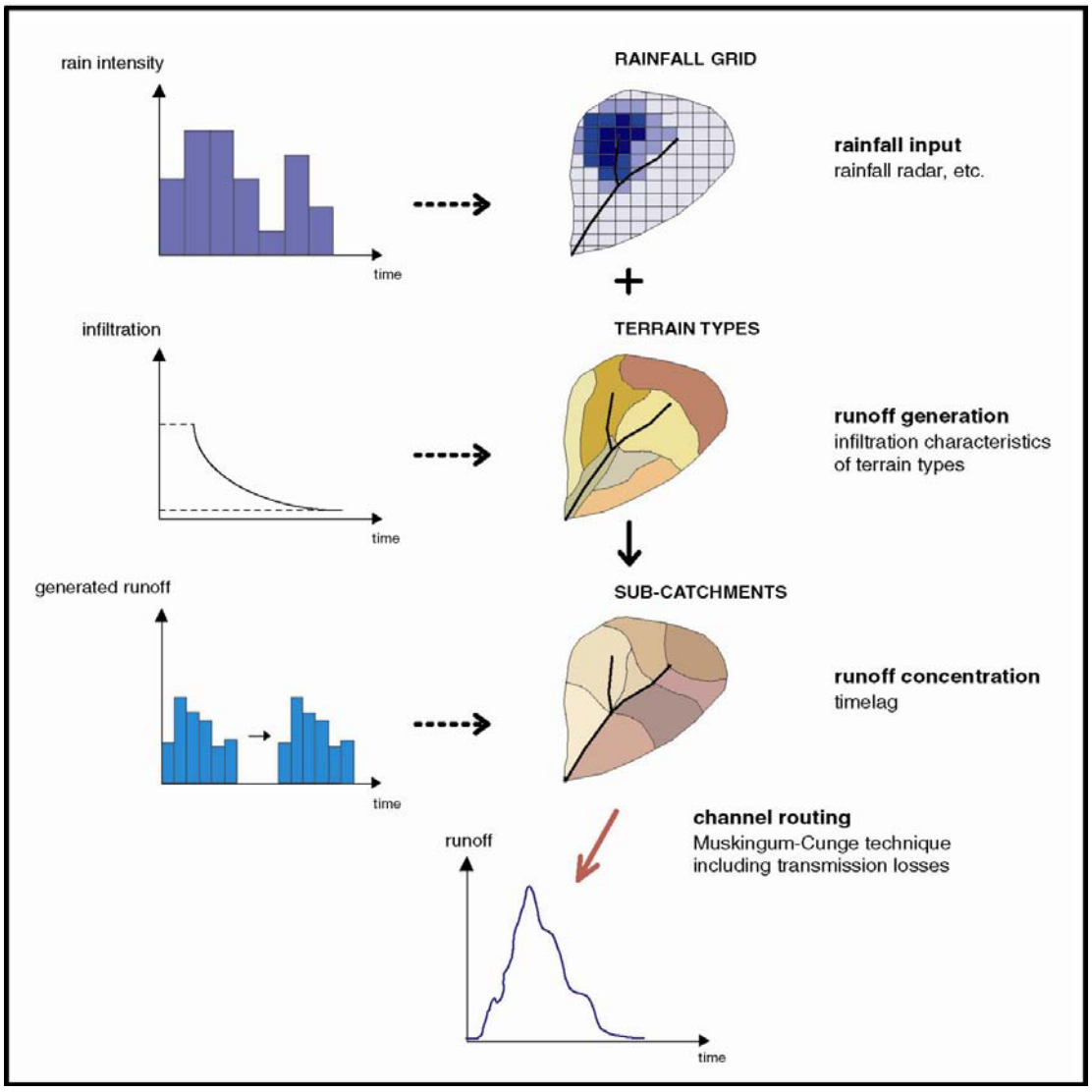

Fig 4.1: Schematic flow chart of the non-calibrated rainfall-runoff model (after LANGE 1999)

4.2 Runoff generation

The runoff generation process determines the portion of the rainfall that is transformed into direct runoff. Due to sparse vegetation cover, interception losses on plants play a minor role in arid environments and are not incorporated into the model. As described in Chapter 2.1.3, Hortonian overland flow is the dominant process of runoff generation in arid environments. After the concept of HORTON (1933), surface runoff is that part of the rainfall which is not absorbed by the soil by infiltration. The so-called rainfall excess generates runoff if the rainfall intensity exceeds the infiltration capacity of the surface. The infiltrated part of rainfall is lost for runoff generation, since subsurface flow paths may be neglected. With known rainfall intensities and neglected interception losses, only the temporal decay of the soil infiltration rate determines runoff generation. In the ZIN-Model Hortonian runoff generation is parameterised independently for each terrain type. The terrain types represent the sub-units for the model's runoff generation routine according to hydrologically relevant surface characteristics. After the accumulated rain has reached the initial loss, runoff is calculated as rain that falls in excess of the infiltration which drops down from initial infiltration rate to a finale rate (Figure 4.1 and Figure 5.4). In this study the values of *initial loss* [mm], *initial infiltration rate* [mm/h] and *final infiltration rate* [mm/h] and the *time dependent infiltration behaviour* [mm/h] have been determined directly in the field from rainfall simulator experiments undertaken by GREENBAUM (1986) and SALMON & SCHICK (1980). Thus, they account for all dominant processes in arid zone runoff generation (e.g. crust wetting, detention losses, etc).

4.3 Runoff concentration

For the determination of spatial sub-units, the channel network is divided into segments. The adjoining small sub-catchments, predetermined by topography are defined as model elements for runoff concentration. Runoff concentration describes the transformation of runoff generated at each model element to lateral inflow into the adjacent channel. The amount of Hortonian runoff as calculated by the runoff generation routine is summed up for each sub-catchment and each minute time step, respectively.

In large catchments, the runoff concentration often follows conceptualisations close to the Unit Hydrograph concept (SHERMAN 1932). In this style, the original ZIN-Model uses a mean response function of model elements, consisting of a hydrologic time-lag and a standardised shape. In Nahal Yael, slopes are very steep and short and channel segments are not longer than 50 metres, which implies relatively small model elements. Hence, the mean response function is replaced by a simple constant time delay as runoff concentration mechanism (Figure 4.1). After this concept, the shape of the runoff hydrograph does not change during runoff concentration but lateral inflow to the channel

is only delayed. The *time-lag* [s] is dependent on the mean slope length and separately determined for each model element.

4.4 Channel flow and transmission losses

The spatial sub-units for this part of the model are predefined by the channel segments used for runoff concentration. The resulting drainage network is subdivided into channel segments delimited by channel nodes. Each segment represents a cross-sectional homogenous section of the river network. Channel geometry is described by morphometric variables, such as *channel length* [m], *channel width* [m], *bankfull stage* [m] and *slope* [-].

The model takes into consideration that at the beginning of a flood only inner channels, covering just a small percentage of the channel width, are active. The full cross section is first inundated when the water level has reached bankfull stage. Hence, complex channel geometry consisting of inner channels and bars is simplified by interpolating linearly between the width covered by inner channels and the width at bankfull stage (Figure 4.2). The *percentage covered by inner channels* [-] has to be determined for each channel segment.

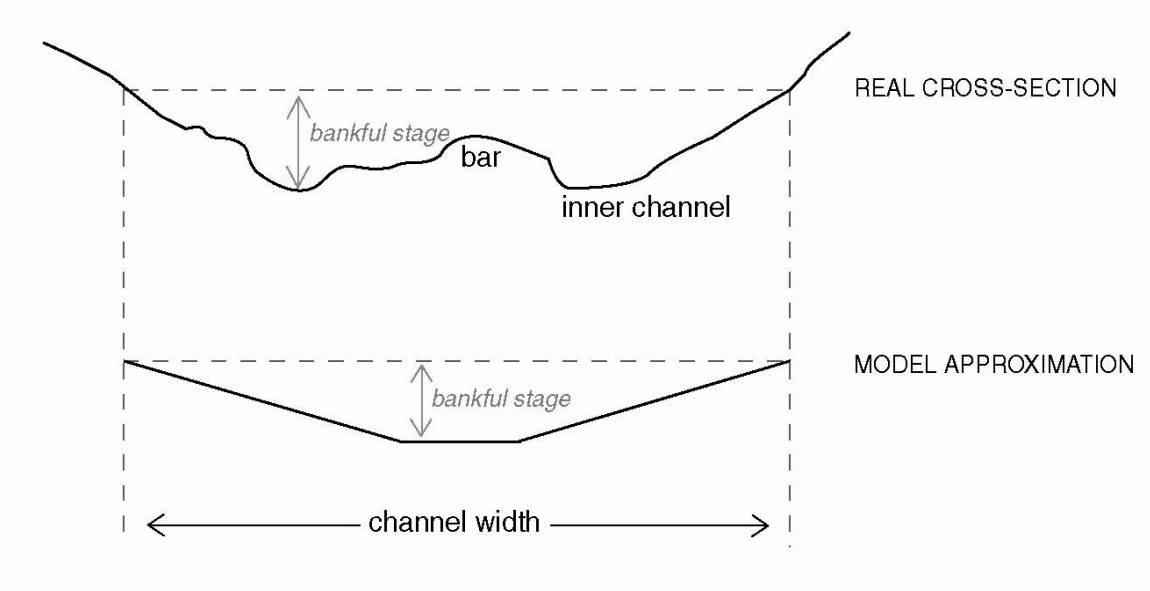

Fig 4.2: Simplified representation of cross-sectional geometry (after LANGE 1999)

In general, the resistance to flow in a watercourse may be parameterised by a friction coefficient, such as Manning n, Strickler k, Chezy c or Darcy-Weisbach f. These coefficients are usually determined by regressions and represent the effect of roughness elements of the channel banks and bed particles as well as form losses attributed to

dynamic alluvial bed forms and vegetation located along the banks. The ZIN-Model uses the *Manning n* [s/m$^{1/3}$] roughness coefficient, which is assigned as a constant value to each channel segment.

Channel flow is routed from one node to another, accounting for lateral inflow and transmission losses. Generally, flow routing procedures are mathematical tools for predicting the changing magnitude, speed and shape of a flood wave as a function of time. The result is a flow hydrograph at the respective stream section or at the basin outlet. Flow routing may be classified as either lumped or distributed. Lumped or hydrological routing procedures, compute the flow as a function of time at one location at the lower end of a channel reach. In contrast, for distributed or hydraulic routing the flow is calculated as a function of time simultaneously at several cross sections along the watercourse (FREAD 1993). Based on the Saint-Venant equations, the ZIN-Model uses a distributed routing procedure, which describes the flow process accounting for channel properties such as cross sectional geometry, slope, flow length and channel roughness. The differential Saint-Venant equations contain the fundamental laws of one-dimensional, unsteady flow and are based on the principles of conservation of energy and conservation of matter. They consist of two equations, one for the continuity part and another for the momentum part. The first describes mass conservation, while the latter contains terms for the physical processes governing the flow momentum, namely acceleration, pressure, gravity and friction forces. The continuity equation in its complete form is part of all distributed flow routing models, whereas different simplifications exist for the solution of the momentum equation. The simplest type of distributed routing models is the kinematic wave model. It assumes that accelerations are negligible and the friction slope equals the surface slope, i.e. acceleration and pressure terms in the momentum equation are assumed zero. Since this concept does not incorporate retention, the kinematic wave approach is not able to reproduce steep rising limbs (ANDERSON & BURT 1990). The diffusion wave model neglects acceleration but incorporates the pressure term, thus retention in the channel is accounted for. If the complete Saint-Venant equations are considered, the routing model is know as a dynamic routing model. The ZIN-Model uses a method based on the diffusion wave analogy which is capable of predicting hydrograph attenuation. It has been developed by (CUNGE 1969), modifying the hydrologic Muskingum procedure and has been effectively used as a distributed flow routing procedure (FREAD 1993). The Muskingum-Cunge method calculates the advancing flood wave from channel node to channel node at different time steps in a space and time discretised network using the following linear algebraic equations (LANGE 1999):

$$Q_{i+1,j} = C_1 \cdot Q_{i,j} + C_2 \cdot Q_{i,j-1} + C_3 \cdot Q_{i+1,j-1} \tag{4.1}$$

$$C_1 = \frac{\Delta t - 2 \cdot K \cdot X}{2 \cdot K \cdot (1 - X) + \Delta t} \tag{4.2}$$

$$C_2 = \frac{\Delta t + 2 \cdot K \cdot X}{2 \cdot K \cdot (1 - X) + \Delta t} \tag{4.3}$$

$$C_3 = \frac{2 \cdot K \cdot (1 - X) - \Delta t}{2 \cdot K \cdot (1 - X) + \Delta t} \tag{4.4}$$

$$K = \frac{\Delta x}{v_K} \tag{4.5}$$

$$X = 0.5 \cdot \left[1 - \left(\frac{Q_{REF}}{B \cdot v_K \cdot S_0 \cdot \Delta x} \right) \right] \tag{4.6}$$

where:

$Q_{i+1, j}$	unknown discharge at the next node at the present time step	[m³/s]
$Q_{i, j}$	discharge at the present node at the present time	[m³/s]
$Q_{i+1, j-1}$	discharge at the next channel node at the last time step	[m³/s]
$Q_{i, j-1}$	discharge at the present channel node at the last time step	[m³/s]
Δt	computational time step	[s]
K	storage constant	[s]
X	weighting factor (expressing the relative importance inflow and outflow have on the storage	[-]
$C_{1,2,3}$	auxiliary variables	[-]
Q_{REF}	reference discharge	[m³/s]
Δx	distance step, channel reach length	[m]
B	width of water surface	[m]
S_o	energy slope	[-]
v_K	kinematic wave celerity	[m/s]

For a wide channel where the hydraulic radius approaches the flow depth, the following approximation is valid:

$$v_K \approx \frac{5}{3} \cdot v \tag{4.7}$$

where v is the flow velocity [m/s], which may be calculated by solving a steady, uniform flow formula, e.g. Manning equation:

$$v = \left(R_{hy}^{2/3} \cdot S_0^{1/2}\right) / n \qquad (4.8)$$

where:

R_{hy}	hydraulic radius	[m]
n	Manning roughness coefficient	[s/m$^{1/3}$]

Admittedly, the problem of applying the Manning equation in an hyperarid environment, is that the formula is a regression rather than a deterministic function containing physical explanation. It was derived under conditions unlike those in dryland river channels (GRAF 1988).

For determination of the reference discharge mentioned in equation 4.6, different modes of the Muskingum-Cunge method exist, depending on the value chosen for Q_{REF}:

- If the value for Q_{REF} stays constant with time, meaning a constant value likewise for the parameters X and K for all time steps, a linear mode is used. It is not capable of predicting wave steepening.
- In the more accurate non-linear solution, an estimated value of the unknown flow Q_{REF} is determined each time step by extrapolation available Q-values from previously computed time and distance steps. The solution procedure is iterative and converges when computed and estimated values of Q agree within a suitably small tolerance. This procedure is capable of describing a steepening of a flood front, accounting for the fact that different discharges travel at different velocities.

The present ZIN-Model, applies the non-linear MVPMC3-method, using the maximum available information for Q_{REF}:

$$Q_{REF} = \frac{Q_{i,j} + Q_{i,j-1} + Q_{i+1,j-1}}{3} \qquad (4.9)$$

Little is known about the variation in time of channel transmission losses during flood events. Infiltrometer tests in alluvial channels provided information on infiltration characteristics (KÜLLS ET AL. 1995; LEKACH ET AL. 1998). During these tests a constant infiltration rate was reached very soon. On the other hand, tracer studies undertaken by LANGE & LEIBUNDGUT (1997) during a simulated flood event provided evidence that the infiltration rate at the very beginning of an event may be smaller than later on. However,

the present model uses a constant *infiltration rate* [mm/h] and the *porosity* [-] of the alluvium to parameterise channel transmission losses. Infiltration into the alluvial fill only starts after a *discharge threshold (qrobeg)* [l/s] is exceeded. This threshold was set in order to prevent the wetting front to advance during times of no flow while small amounts of water may be simulated by the model. The infiltrated amount of water (calculated as the wetted area multiplied by the infiltration rate) is subtracted from the flood volume for each time step. When the wetting front reaches the bottom of the alluvial fill, defined by the *alluvial depths* [m], the available storage volume has been satisfied and the calculation of transmission losses is stopped. Deep infiltration at the alluvium/bedrock boundary is probably negligible and was not incorporated into the present model.

4.5 Conclusion

This chapter summarises the performance of the ZIN-Model describing the model components “runoff generation”, “runoff concentration” and “channel flow and transmission losses”. The non-rigid spatial subdivision is very flexible as it is based on different spatial subunits for each model component. The dominant process of runoff generation in dryland areas is Hortonian overland flow, which is thus the only process of runoff production incorporated into the model. Runoff concentration is parameterised using a time-lag function. In the channel system, the advancing flood front is routed applying the hydrologic Muskingum-Cunge flow routing procedure. The model also accounts for transmission losses into the riverbed alluvium.

5 Parameter determination

Determination of the spatial pattern of model parameters took considerable time and effort. During a 10 day field campaign, the model elements and missing parameters were determined directly in Nahal Yael. Afterwards, field surveys and measurements had to be analysed and incorporated into the GIS framework.

5.1 Runoff generation

5.1.1 Spatial disaggregation

The spatial disaggregation for runoff generation is based on the results of sprinkler experiments inside Nahal Yael, undertaken by SALMON & SCHICK (1980) and GREENBAUM (1986). Their infiltration test provided the necessary information on infiltration properties on different surfaces. The spatial sub-units for runoff generation are represented by terrain types with the same temporal behaviour of infiltration.

During a field campaign of several days duration the different terrain types were mapped directly in the field. The rainfall simulator experiments of SALMON & SCHICK (1980) and GREENBAUM (1986) were carried out on different morphological units, e.g. on bare rocky surfaces of different lithology and on colluvial slopes of different slope angles. According to these morphological units, initially four terrain types (bare rock, steep colluvium, moderate colluvium and alluvium) were distinguished. Some parts of the catchment could neither be classified as bare rocky surface nor as colluvial slope. They were rather a mixture of both like e.g. bare rocky slopes partly covered with thin colluvium.

Tab 5.1: Summary of terrain types

	bare rock	steep colluvium	moderate colluvium	alluvium	bare rock + colluvial cover
granite	brG	sc	mc	al	bcG
granitic gneiss	brGg	sc	mc	al	bcGg
amphibolite	brA	sc	mc	al	bcA
pelltic schist	brS	sc	mc	al	bcS

Thus, it was decided to introduce a fifth category of terrain types accounting for these specific surface properties. The five terrain types were mapped independently from the lithological units for the entire catchment. A preliminary infiltration map resulted, which was subsequently combined with the geological information mapped by SHIMRON (1974) (Figure 3.6). The consolidation of both maps yielded eleven different terrain types (Table 5.1). The two maps were merged within the GIS framework using combination tools of ArcInfo (Figure 5.1). For colluvial slopes and alluvium, the underlying geology does not influence the infiltration properties, thus only one general type was assigned. A detailed description of all terrain types and their parametrisation follows in the next sub-chapter. Photographs, showing examples of the most important terrain types are given in Annex A.9-A.14.

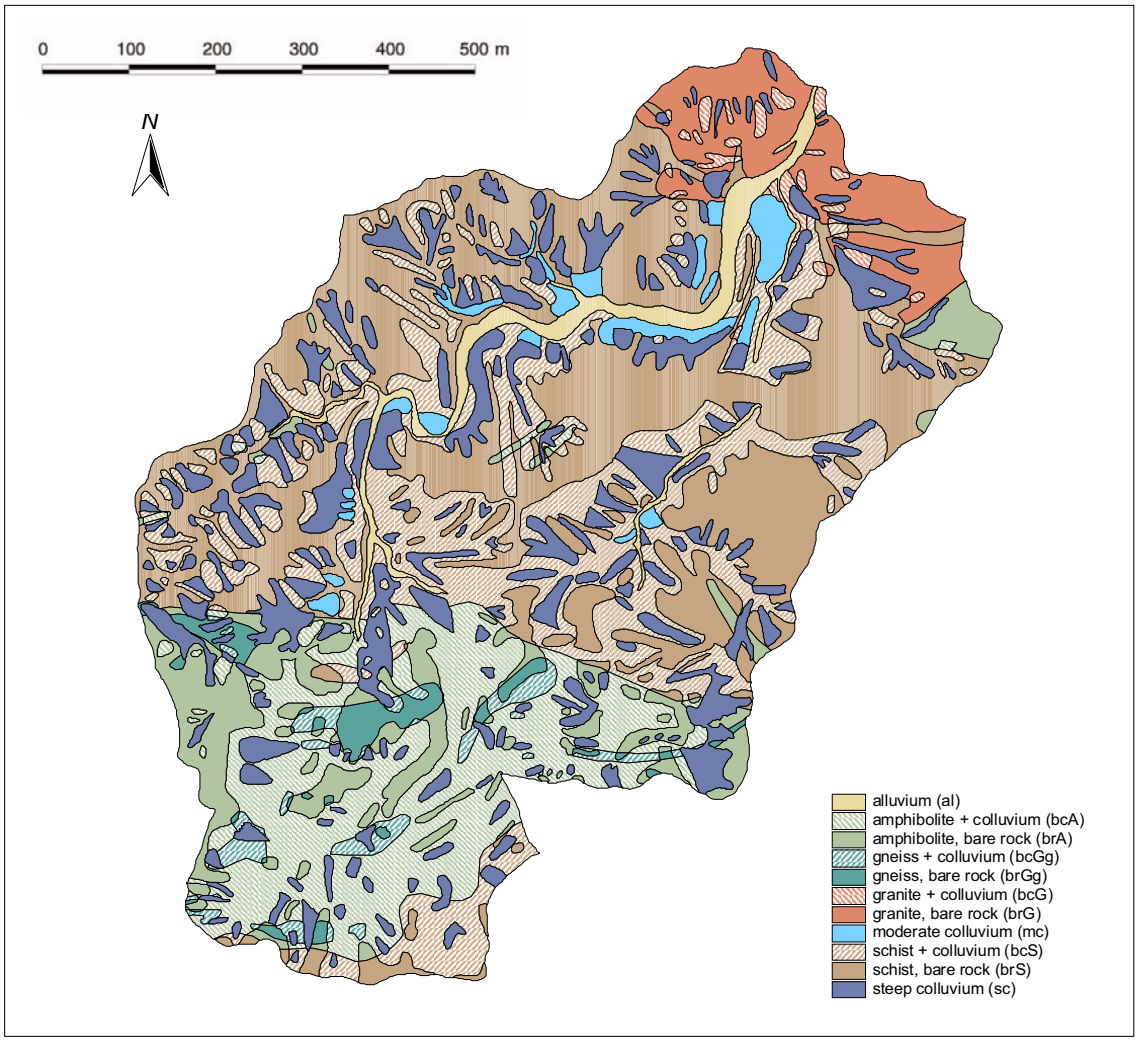

Fig 5.1: Terrain types inside Nahal Yael

5.1.2 Parametrisation

The necessary model parameters (temporal decay of infiltration with initial loss, initial and final infiltration rate) were provided by the experiments of GREENBAUM (1986) and SALMON & SCHICK (1980). For most terrain types, except for the category of bare rocky surfaces covered partly with colluvium (bcG, bcGg, bcA, bcS), results from sprinkling experiments were available. The experiments were conducted on small runoff plots (0.25 m²) (Figure 5.2), that were sprinkled by a rainfall simulator with a mean rainfall intensity of 70 mm/h. The experimental plots were chosen on representative sites, accounting for typical surface properties, such as jointing or the amount of debris cover. Parameters determined from measured values like rainfall intensity, time till onset of runoff, time till the final infiltration rate was reached and the discharge at the plot outlet were initial loss and infiltration rate at every minute time step. Both were already calculated by GREENBAUM (1986). Measuring the generated runoff at the outlet of the plot, the temporal behaviour of infiltration was derived by subtracting runoff rate from rainfall rate for any minute time step. The value of the initial loss reflects the amount of water that is lost mainly due to detention losses before Hortonian overland flow is generated. Discharge at the plot outlet first starts after the initial loss has been satisfied and runoff generation is initiated on the areas closest to the plot outlet. Thus, the initial loss was determined by multiplying the time till onset of runoff by the rainfall intensity.

Fig 5.2: Photograph of experimental runoff plot

Investigations in the field concentrated on the surficial cover governing infiltration characteristics, complementing the knowledge on infiltration characteristics. Table 5.2

provides an overview of the model parameters initial loss and final infiltration rate followed by a detailed description of all terrain types.

Tab 5.2: Infiltration characteristics of the different terrain types

Terrain type		portion in the entire catchment [%]	initial loss [mm]	final infiltration rate [mm/h]
bare rock surfaces		**44.6**		
granite	brG	5.4	0.7	2.5
granitic gneiss	brGg	1.6	0.6	1.0
basites (amphibolite)	brA	7.8	1.0	6.8
pellitic schist	brS	29.8	2.0	4.0
bare rock partly covered with colluvium		**34.1**		
granite	bcG	0.9	2.1	5.1
granitic gneiss	bcGg	1.7	2.0	4.5
basites (amphibolite)	bcA	13.5	1.8	6.8
pellitic schist	bcS	18.0	2.4	5.7
steep colluvium	sc	16.0	3.0	28.0
moderate colluvium	mc	2.3	2.0	15.0
alluvium	al	3.0	-	-

- Terrain types “brG”, “brGg”, “brA” and “brS” (bare rocks) consists of bare rocky surfaces which are mainly found on the upper parts of slopes. They are generally characterised by very low values of initial loss, fast decreasing infiltration rates and lowest final infiltration rate. Rock type and structure are the main factors affecting infiltration and runoff on rocky hillslope areas (GREENBAUM 1986). Thus, a subdivision according to lithology was necessary:
  - brG: Granitic slopes constitute only the lower part of Nahal Yael and are therefore of minor importance as runoff contributors. The slopes are partly smooth, partly jointed with a fairly sharp micro-relief. A mean initial loss of 0.7 mm and a final infiltration rate of 2.5 mm/h resulted.
  - brS: Most of the Nahal Yael catchment is schist. On slopes where the dip is parallel to the slope surface, schists produce smooth surfaces and generate runoff rapidly. Slopes with schist cleavage planes, that are inclined opposite to the slope, are very rough and densely jointed terrain surfaces. They are characterised by a higher depression storage and infiltration capacity. Since

the perpendicular schist is the dominant type, outcrops of parallel schists were neglected and infiltration characteristics of perpendicular dipped schists were assigned to all schist areas, resulting in a value of 2 mm for initial loss and 4 mm/h final infiltration rate.

  - brA: The *amphibolite* plays an important role for runoff generation in the upper parts of Nahal Yael (sub-catchments 04 and 05). The amphibolite weathers more readily than the other rocks in the catchment, leading to a continuous, relatively soft rock surface with a high degree of roughness and joints. Although its appearance is similar to that of a granite, its infiltration capacity is much higher. The values for initial loss and final infiltration rates are 1 mm and 6.8 mm/h respectively.
  - brGg: The *gneiss* surfaces cover only a small portion in the upper parts of the catchment. They react very soon to rainfall und generate runoff most quickly resulting in minimum values for initial loss (0.6 mm) and final infiltration rate (1 mm/h).

- Terrain type “sc” (steep colluvium) covers extensive areas in Nahal Yael. About 16% of the catchment size was mapped as steep colluvium. Colluvial slopes were mapped as “steep”, if the slope angle is above 10°. On steep colluvial slopes the type of rock, which makes up the colluvium, has no influence on the infiltration characteristics but infiltration is largely dependent on the size of the stone cover. Thus, no subdivision of the steep colluvial terrain type according to lithology was necessary. The steep colluvium is composed of fine sand with large amount of stones in size of 2 to 20 centimetres. The slope angle the most significant factor on colluvial slopes concerning infiltration properties, since it determines the characteristics of the stone cover. In contrast to rocky hillslopes, an increase in slope angle leads to a decrease in runoff on colluvial slopes (GREENBAUM 1986), because steeper slopes are covered by larger stones, which allow higher infiltration rates. Colluvium is mostly concentrated on lower parts of the slopes or sits above the beginning of small first order channels in a funnel shape. The values of initial loss are significantly higher than those for bare rocky surfaces, since larger surface areas of debris cause higher detention losses and the volume of depression storages is higher. Resulting parameters for steep colluvial surfaces assigned for initial loss and infiltration rates are 3 mm initial loss and 28 mm/h final infiltration rate.
- Terrain type “mc“ (moderate colluvium) is assigned to colluvial surfaces with a slope angle of less than 10°. It covers only a very small portion of the catchment area (2.3%). Due to a small slope angle, the stone cover consists of small stones up to 5 centimetres diameter and the amount of sand and silt is notably higher than on steep colluvial slopes. To some extent, initial stages of desert Reg soil

development, such as a vesicular A horizon, can be found on moderate colluvial slopes (Figure 5.3). Hence, infiltration rates are not as high as on steep colluvial slopes and values of 2 mm initial loss and 15 mm/h final infiltration rate were assigned.

Fig 5.3: Photograph of vesicular A horizon in a moderate colluvial surface (LANGE, unpublished)

- Terrain types “bcG”, “bcS”, “bcA” and “bcGg” represent bare rock surfaces that are partly covered by colluvium. This type is assigned to areas that are neither pure bare rock surfaces nor real colluvial slopes. In some parts the bare rock is covered by a thin debris mantle up to 0.5 metres depth with occasional outcrops of the underlying bare rock. In other parts, bare rock outcrops and colluvial surfaces alternate over very short distances, resulting in areas too small for the mapping scale. Thus, this category is a product of generalisation. An influence of lithology on runoff generation on these surfaces is very likely: runoff generated directly on bare rock outcrops is dependent on lithology as described above. Furthermore it is assumed that some of the water is flowing underneath the debris cover on top of the bare rock surface, where it is also influenced by lithology. The bare rock colluvial covered terrain types dominate the upper catchment area making up 34% of the whole catchment size. For this type, no information on infiltration behaviour from simulated rainfall experiments was available. Thus, the infiltration behaviour is not very well known, but is assumed to be intermediate of bare rock and colluvial infiltration. For the determination of the necessary model parameters, the infiltration curves of colluvium and each bare rock type were interpolated for every minute time step, resulting in synthetic infiltration curves. For the interpolation weighting factors of 0.6 for colluvium and 0.4 for bare rock were assigned based on field observations, where the colluvial influence appeared slightly stronger.

- Terrain type “al” (alluvium) was assigned to the main channel reach with recent, active alluvium. The channel alluvium consists of coarse fluvial deposits allowing very high infiltration rates that are decisive parameters for transmission losses. On these surfaces no runoff is generated because high infiltration rates do not allow rainfall excess. Thus, for runoff generation, the alluvium is assumed to be inactive.

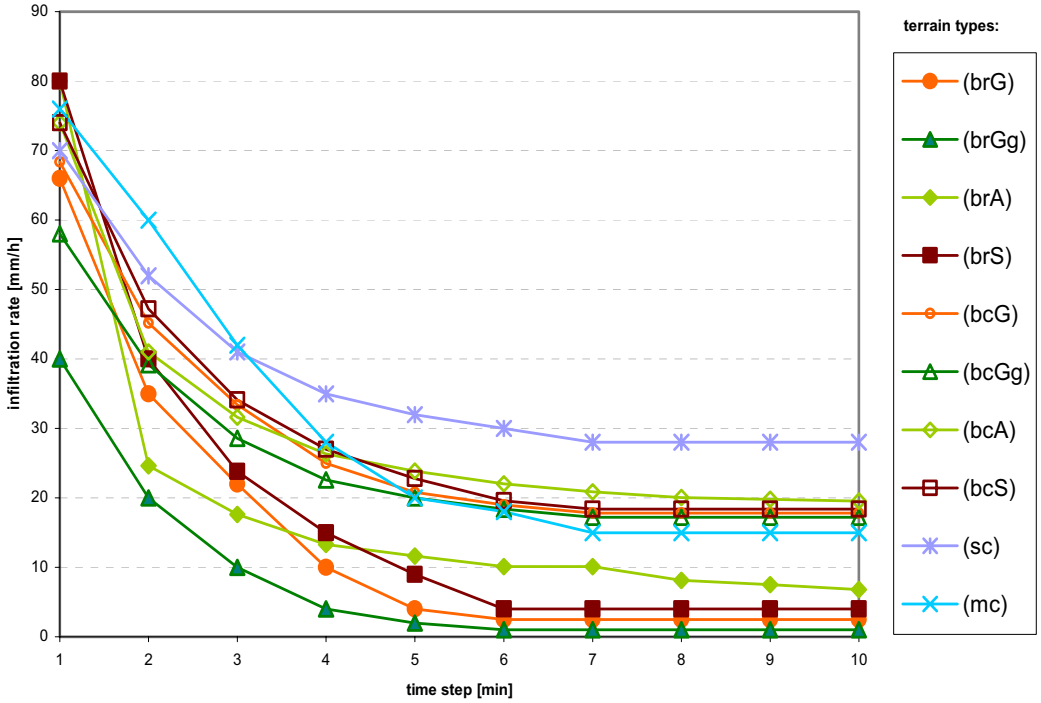

Fig 5.4: Infiltration curves of the different terrain types

The time functions of infiltration (infiltration curves, Figure 5.4) were directly derived from the experiments in a one minute time step and are not expressed as mathematical functions. Figure 5.4 shows, that infiltration rates on bare rock surfaces decrease stronger than those on colluvial surfaces. The synthetic infiltration curves of the covered bare rock surfaces lie in the same range as the curve for moderate colluvium.

All infiltration curves and the values for initial loss were attributed to the eleven terrain types yielding a catchment wide GIS-layer of infiltration characteristics. The infiltration characteristics in combination with the temporal behaviour of rainfall intensities govern the model’s Hortonian runoff generation. The temporal sequence of rainfall input in a one minute time step was applied onto the layer of infiltration properties. An Arc Macro Language (AML) routine was used to carry out the calculations for each minute time step on a cell-by-cell basis of the catchment wide 2 x 2 metres grid: After enough rain had fallen to meet the initial loss, runoff generation started, when rainfall intensities exceeded infiltration capacity. An example of the AML-routine is given in Annex A.46.

5.2 Runoff concentration

5.2.1 Spatial disaggregation

For the determination of sub-catchments, the channel network was subdivided into homogenous channel segments of 54 metres mean lengths that are also model elements for the channel routing procedure. Therefore, the subdivision of the channel network is explained in Chapter 5.3.1 in detail.

Starting from the channel segments small sub-catchments were defined according to topography. For this purpose, a detailed topographic map with a contour interval of 1 metres at a scale of 1:1250 was available. Furthermore, the delineation of sub-catchments was approved directly in the field during the field campaign mentioned above. The average area of the contributing sub-catchments, one on each side of the channel, was about 1000 m². Figure 5.5-d shows the subdivided channel network with adjacent polygons that represent spatial sub-units for runoff concentration.

5.2.2 Parametrisation

The small size of the sub-catchments, which is due to the small catchment size and the dense river network subdivided into 54 meter long segments, allowed the application of a simple time delay as mechanism of runoff concentration. Delayed by a time-lag generated runoff is translated without modification in shape from the slope to the adjoining channel. To account for different travel times along the various slopes, the time-lag was introduced separately to each sub-catchment. It is only depending on the mean slope length, which was calculated by dividing the sub-catchments size by the channel length (equation 5.1). It is believed, that most runoff flows downslope in small concentrations of flow directed by the relief of the slope. Hence, flow velocities are higher than for sheet flows. Different studies on overland flow hydraulics (ABRAHAMS ET AL. 1986A; ABRAHAMS ET AL. 1986B; EMMETT 1970; KIRKBY & CHORLEY 1967; ROELS 1984) report measured overland flow velocities on slopes of different slope angle with low to zero vegetation density. Generally, flow velocities increased with slope angle. ROELS (1984) found surface flow velocities between 0.2 m/s and 0.4 m/s on slopes of 13.7 and 17.8 % inclination respectively. EMMETT (1970) reports maximum velocities of 0.407 m/s on a slope of 33.15 % inclination. However, these velocities represent maximal surface velocities, that are markedly higher than mean flow velocities. ABRAHAMS ET AL. (1986a) state, that generally surface flow velocities have to be multiplied by a factor of 0.66 to derive estimates of mean flow velocity. Taking this into consideration and the very steep slopes of Nahal Yael with a mean slope inclination of 26° (48.8%), a mean flow velocity of 0.4 m/s was assumed. The hydrologic time-lag was calculated using equation 5.2.

$$\bar{d} = \frac{A_s}{\Delta x} \tag{5.1}$$

$$t = \frac{\bar{d}}{v_m} \tag{5.2}$$

where:

$\bar{d}$	mean slope length	[m]
A_s	area of sub-catchments	[m²]
Δx	channel reach length	[m]
t	hydrologic time-lag	[s]
v_m	mean overland flow velocity	[m/s]

The values for the time-lag ranged between 10 seconds and 3.5 minutes. A table of all channel segments with corresponding sub-catchments and the associated time-lag values is given in Annex A.51. The input values from runoff generation are passed over to the runoff concentration procedure in a one minute time step. For the channel routing, a time step of 5 seconds was required. Therefore, the runoff concentration procedure transforms the one minute input to 12 commensurate pulses that serve as input for the channel routing procedure.

5.3 Channel flow and transmission losses

5.3.1 Spatial disaggregation

The spatial subdivision for channel flow is the same as for runoff concentration and started at the channel network. The channel network as mapped on the topographical map was verified and partially modified during the field campaign (Figure 5.5-a). For model purposes, first-order channels had to be extended up to the watershed divide (Figure 5.5-b). Channel nodes were placed along the water course, firstly accounting for confluences. Secondly, the condition that generally applies is that the distance travelled by the wave or hydrograph in one time step $\triangle t$ must never exceed the distance between computational nodes. If the length of a sub-reach $\triangle x$ is too short, then computational instability may evolve, resulting e.g. in large non-physical oscillations. The condition to be satisfied here is known as the Courant condition for explicit numerical solution schemes of the Saint-Venant equations for open channel flow:

$$\Delta t \leq \frac{\Delta x}{v_K} \qquad (5.3)$$

where:

$\triangle t$	computational time step	[s]
$\triangle x$	distance step, channel reach length	[m]
v_k	kinematic wave celerity	[m/s]

The time step used for channel routing was 5 seconds. The maximum measured velocity of flood waves in a comparable environment of about 5 m/s (SCHICK 1988) was assumed as flow velocity. Combining equation 5.3 and 4.7, a minimum channel reach length of 41.66 metres for $\triangle x$ resulted. Having this length in mind, channel nodes were placed about every 50 metres between channel junctions (Figure 5.5b). Finally, the average length of the resulting 258 channel segments inside Nahal Yael was 54 metres, with minimum length of 42 metres and maximum length of 86 metres. For each model segment, 9 model parameters had to be determined (see Chapter 4.4) yielding 2322 different parameter values. To deal with the large amount of parameter values, LANGE (1999) applied a classification scheme for channel types. This scheme was transferred to Nahal Yael, grouping channel segments of similar morphology into channel types. Based upon a thorough field survey, 3 channel types were distinguished:

- *Channel type 1* represents the multitude of steep, narrow headwaters. This type is characterised by very high slope values up to 42° (89%). It consists of rocky reaches, often filled with colluvial deposits forming flow obstacles of different size. In some parts, the channel is obstructed over its entire width and length. Step-pool sequences in the first order channels of Nahal Yael were investigated by WOHL & GRODEK (1994). Well-developed bed steps are formed by clasts (with intermediate diameter exceeding the depths of the largest flows) or by the bedrock itself. Large boulders create waterfalls up to 0.8 metres height. Alluvial deposits are very rare and restricted to small pools of channel bed steps.
- *Channel type 2* is assigned to second order channels of 1 to 3 metres width. They are not as steep as the headwaters, but mean channel slope is still as high as 0.1. The rocky channel bed is rather smooth and partly covered by thin discontinuous alluvial cover. However, small channel bed-steps and boulders are present in the channel.
- *Channel type 3* represents the lower-gradient main channel along the alluvial reach. Channel width varies between 3 and 20 metres with alternating braid bars. The riverbed material is coarse alluvium. Sparse vegetation cover is restricted to this channel type, although it is limited to banks and high bars.

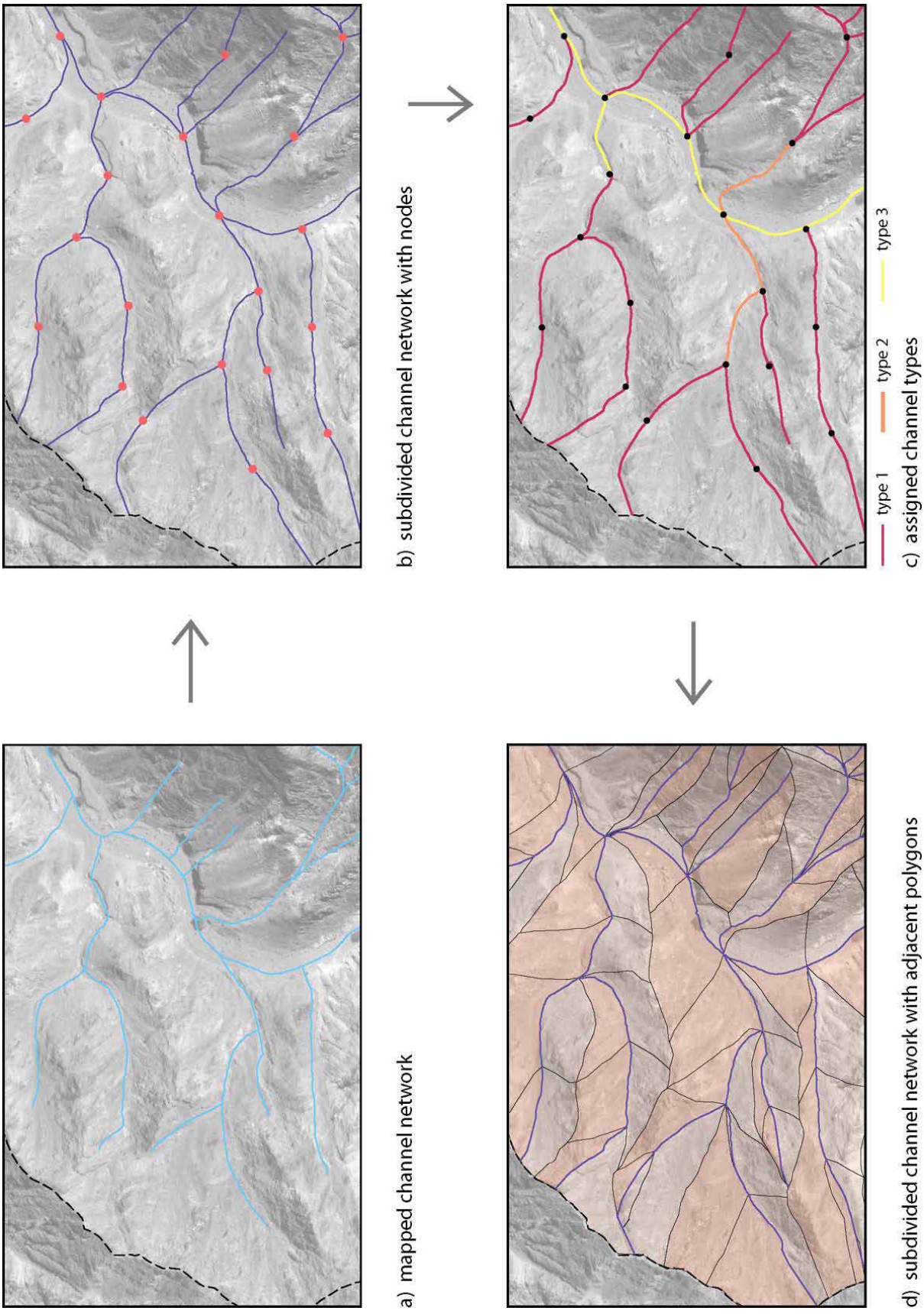

Fig 5.5: Spatial subdivision for runoff generation in Nahal Yael

Figure 5.5-c shows a part of the classified river network. Photographs as examples of the different channel types are found in Annex A.6-A8.

5.3.2 Parametrisation

For the determination of channel parameters, information from a topographic map and aerial photographs, as well as information from recent and previous field campaigns were available. All this information arranged inside the GIS environment to facilitate further analysis.

5.3.2.1 Channel flow parameter

From the topographic map, information on channel length and slope was extracted for each channel segment independently. As described in LANGE (1999), a representative channel width was derived from aerial photograph analysis: Channel width is calculated for each segment, dividing the segment's inundated area at bankfull stage by the respective channel length. The inundated area at the bankfull stage was determined by digitising the active river bed alluvium from the aerial photographs for each channel segment (Figure 5.6).

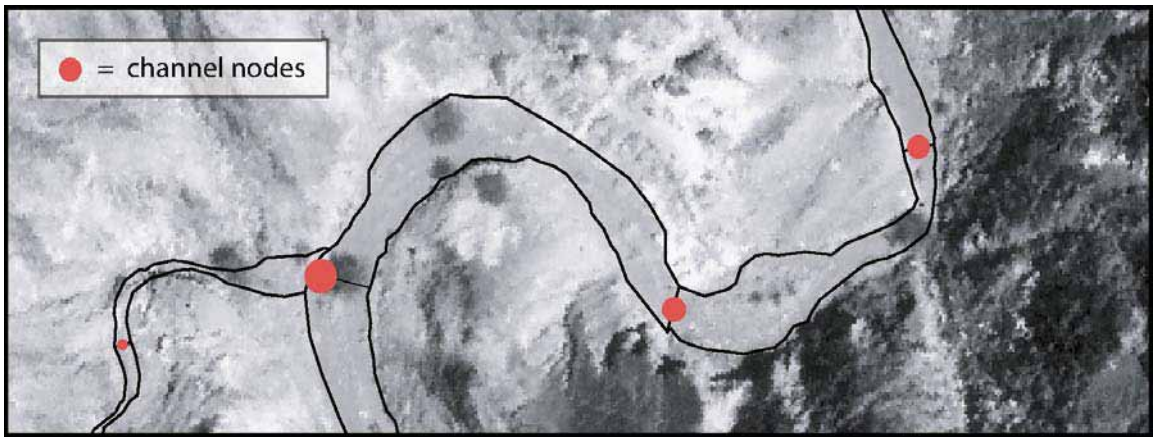

Fig 5.6: Determination of spatially averaged channel width

Information on the percentage covered by inner channels was available from previous field surveys undertaken by Y. TROSTLER (unpublished data). In that study, the main channel was subdivided into sections roughly 20 metres long, and a representative cross section was chosen for each section. Here, the channel width at bankfull stage (w_b) and the channel width of inner channels (w_i) were measured. The ratio w_i/w_b yielded a percentage covered by inner channels for each 20 metres section. To transfer these values to the model elements (channel segments) a weighted mean was calculated for each model segment accounting for the proportion of the 20 metres section in the

channel segment. Channel segments without alluvial fill cover the entire cross-section; the respective percentage covered by inner channels was set to 100%.

For the constant parameter roughness coefficient the channel classification scheme was applied, reducing the number of parameter values from 258 for each segment to 3 for each channel type. Important factors influencing the roughness coefficient are surface roughness of the bed material, obstructions to flow and type and density of vegetation. Quantitative estimates of Manning n values for channel type 3 were found in the literature (CHOW ET AL. 1988; JARRETT 1985; PHILLIPS & INGERSOLL 1998). Channels of this type are characterised by the lowest channel roughness. The channel bed surface is rather smooth, consisting of a mixture of gravels and fines. Though vegetation is only inundated at the highest water stages, it reduces flow velocities and leads to increased turbulence and roughness during high magnitude events. The assigned Manning n value is 0.04, taking channel variations and meandering into consideration as well. BWG (2001) and MARCUS ET AL. (1992) evaluated channel roughness in small mountain streams, some of which are comparable to channel type 2. Roughness is increased due to occasional flow obstacles and river bed steps. Following BWG (2001) and MARCUS ET AL. (1992) estimates, the resulting Manning n value is 0.1. For the very steep headwaters little information on roughness coefficients was available. Under extremely rough conditions in steep mountain channels, flow depths may be lower than median sediment diameter, increasing flow resistance heavily. MARCUS ET AL. (1992) state, that conventional techniques for estimating roughness in mountain streams underestimated values of Manning's n by a factor of 2 or more during large floods. BWG (2001) found a maximum value for Manning n of 0.33 in a natural mountain channel of 0.038 slope at low water level. Considering the very high channel slopes, the heavily obstructed channels and step-pool sequences into consideration, a Manning n of 1 was assigned to channel type 1. Channel roughness coefficients were kept constant in time and not varied according to water level in the channel segment.

Bankfull stage is a decisive parameter for the interpolation of cross sectional width. Thus, it is mainly important for channel segments where the percentage covered by inner channels is smaller 100%, i.e. basically the segments with alluvial fill (see also Chapter 4.4). For all other segments, bankfull stage is rather constant and a representative value of 0.8 metres was assigned.

5.3.2.2 Transmission loss parameter

River bed alluvium is found in all type 3 channels and in some type 2 channels. As model parameters the depths, porosity and infiltration rate of the alluvium had to be determined. Information on the extent of the alluvial fill was available from a geophysical survey by SCHICK (1980b) and the MSc-Thesis of SCHWARTZ (1986). Firstly depths of the alluvial fill were assessed by about 40 seismic soundings (SCHICK 1980B). SCHWARTZ (1986) gained additional information from pits that were dug into the alluvium to assess the alluvial depths directly. All data yielded depth in the range between

0.5 and 2.0 metres. Generally, alluvial depth increases downstream. For the upper parts a fill depth of around 0.6 to 1.2 metres is indicated, while for the middle and lower parts depths reached about 1.5 metres. Based on this field data, values of mean alluvial depths were assigned to each channel segment.

Porosity was also derived from SCHWARTZ (1986), who determined a mean porosity of 0.3 for the whole channel alluvium based on grain size distribution analysis.

Little is known about infiltration rates during flood events. Thus, infiltration rates are assessed by infiltrometer tests. These tests tend to overestimate infiltration rate due to lateral outflows. Unknown amounts of water may escape laterally when the wetting front advances deeper than the limiting infiltrometer ring. LEKACH ET AL. (1998) determined infiltration rates of the alluvium in Nahal Yael, which were corrected by GRODEK (2002) yielding a mean infiltration rate of 480 mm/h. For the model parameter infiltration rate, this value was assigned. It is of the same order of magnitude as values estimated by LANGE (1999): a value of 550 mm/h was determined during an experimental flash flood simulation with the aid of tracer techniques.

LEKACH ET AL. (1998) detected a continuous compacted red-coloured fluvio-pedogenic unit beneath the surficial grey alluvium in Nahal Yael. This so called “red-layer” unit appears at an average depth of 50 centimetres. It was identified as a partial buffer to floodwater infiltration, since infiltration rates of the red layer are much lower than those of the alluvial fill above (LEKACH ET AL. 1998). Generally, model applications did not account for the red layer. Nevertheless, for one event it was incorporated as a completely impermeable layer stopping transmission losses at a depth of 0.5 metres.

5.4 Conclusion

The spatial disaggregation of the ZIN-Model was carried out for each of the models sub-systems runoff generation, runoff concentration and channel routing independently.

For runoff generation spatial sub-units were mapped directly in the field according to relevant infiltration characteristics and combined with lithological information from a geological map (SHIMRON 1974). Basically, runoff generation sub-units are bare rock surfaces, steep and moderate colluvium, alluvium and a mixture category consisting of bare rocky surfaces partly covered by colluvium. A catchment wide layer of infiltration characteristics resulted. Model sub-units for runoff concentration are small tributary catchments delineated by topography, one on each side of each channel segment. They were determined from topographical maps and affirmed during field survey. For channel routing, 258 channel segments of about 50 metres lengths represent model elements. They are the same channel segments already used for runoff concentration.

Parameter determination for all sub-units is essentially field based:

Rainfall simulator experiments on experimental plots inside Nahal Yael yielded information on the infiltration behaviour of most terrain types. Only for the mixture category, infiltration curves were interpolated from measured bare rock and colluvium infiltration properties. Data interpretation of the rainfall simulator experiments yielded an absolute value for initial loss and an infiltration capacity for every one minute time step. On alluvial surfaces no runoff is generated. Infiltration rates of bare rocky surfaces show the lowest final infiltration rates and decrease much faster than those on all other terrain types. Steep colluvium is characterised by highest infiltration rates, those of moderate colluvium and the mixture category have intermediate values.

The mechanism of runoff concentration is a simple time delay. A time-lag was calculated depending on the mean slope length and determined for each of the 516 sub-catchments separately. Values for the time-lag range between 10 seconds and 3.5 minutes.

For channel routing, the segments with similar morphology were grouped into 3 channel types. This scheme was mainly applied for channel roughness coefficients that were assigned based on thorough field surveys and extensive literature studies. Other parameters were available from previous studies, from aerial photography and topographic maps or were determined in the field for each channel segment independently. Values for transmission loss parameters (depth, porosity and infiltration rate of the alluvial fill) were assessed based on data by SCHWARTZ (1986), assuming a constant infiltration rate and porosity for the alluvial fill.

6 Data analysis

6.1 Rainfall input

Accurate representation of rainfall in space and time is essential for rainfall-runoff modelling, as precipitation is the primary model input. The dominant impact of spatial and temporal variability for modelling small catchment response is relatively well known (OSBORN ET AL. 1972, WOOLHISER 1986, FAURES ET AL. 1995): Errors in the determination of rainfall input are propagated through the model and may be responsible for errors in the model output. Consequently, no satisfying results can be obtained. This is especially true for convective storm events with a great variability of rain in space and time.

In this study, catchment rainfall is obtained by interpolating point data from a dense network of recording rainfall stations, which are distributed evenly over the catchment. The model uses a spatially distributed pattern of rainfall intensities in a one minute time step.

The determination of catchment rainfall comprises two aspects: first, the point measurement of rainfall at a gauge and second, the interpolation of point data from a number of rainfall stations to estimate the spatial rainfall distribution.

6.1.1 Observational network and available data

The Nahal Yael watershed was instrumented in January 1968 with a dense network of rain gauges and recorders. A set of 13 recording stations (Hellman type recording rain gauge, Lambrecht, No. 1509 H) were uniformly spread all over the area (Figures 6.1, A.12). Four of these stations were located close to the channel in the lower part of the basin, while the other 9 stations were situated at relatively high elevations. The rain gauge density is with one station per 0.05 km² or 17.3 stations per km² extraordinarily high. This is also expressed by the maximum distance between two stations, which are not more than 300 meters apart from each other.

The network of rainfall recorders was reduced to 4 stations in the middle 1970ties. On the basis of data records for several years, it was concluded that two mountain top and two valley stations represent catchment rainfall satisfactorily (SCHICK 1980A). Also, at that time, the remaining Lambrecht type recorders were supplemented by new tipping bucket rain gauges at the same location. For some time both instruments were operated simultaneously before the Lambrecht recording gauges stopped operation in 1980. In 1990 the rainfall gauging network was reduced again. Since then only 2 stations, both located close to the main channel, were operated.

This dense network of recording rainfall stations was designed to study the spatial variations of rainfall. For this study, data records from the recording stations were available in a processed format, listing rainfall intensities [mm/h] in a time step of one minute.

To study the small scale topographic effect, a second set of 16 small-orifice collecting rain gauges (orifice diameter 29.2 mm) was installed along a 750 metres long east-west transect through the basin (Figure 6.1). These gauges yielded data of total rainfall amounts for several events. Results from the years 1968 and 69 are published in SHARON (1970a).

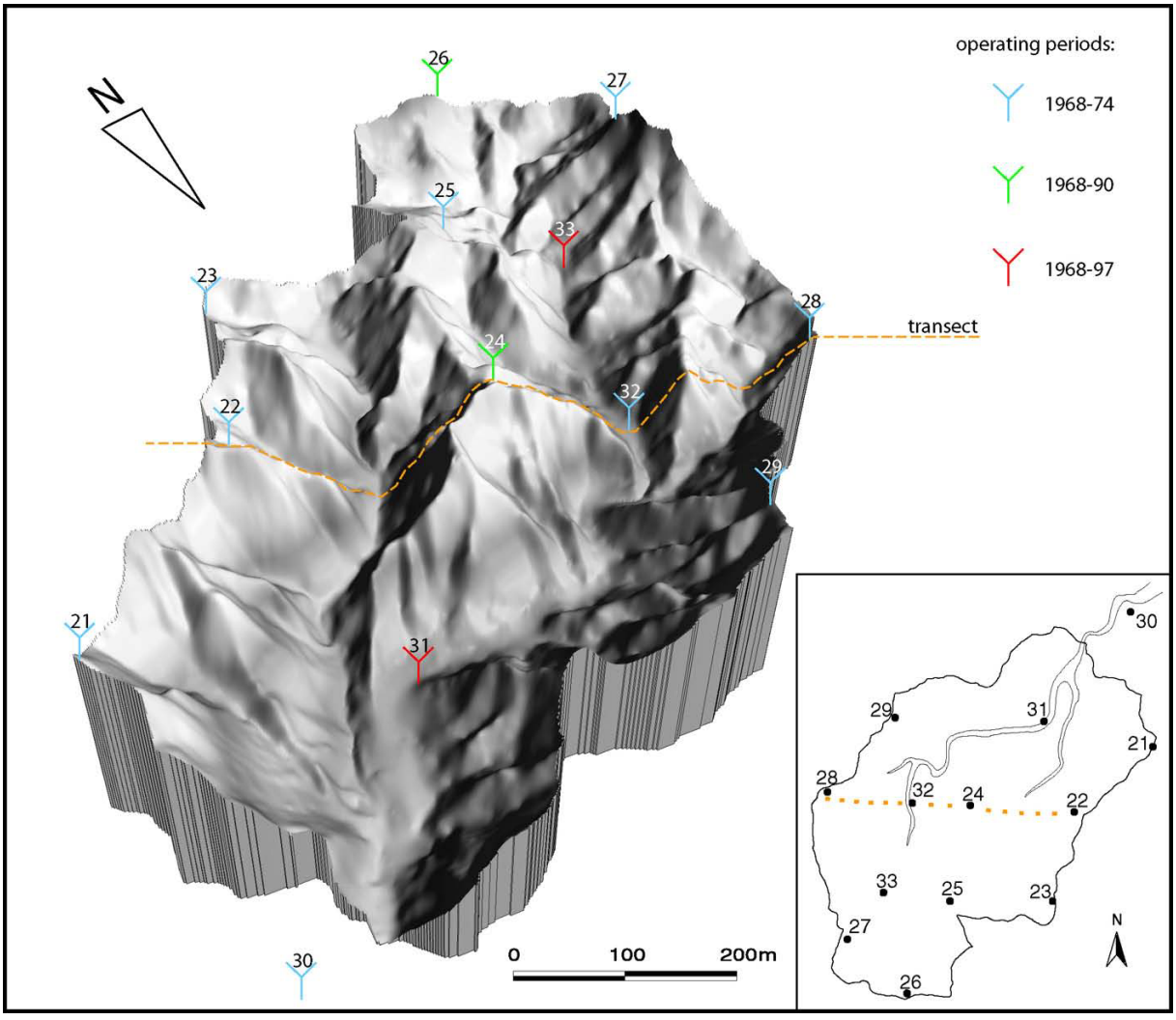

Fig 6.1: Rain gauge network in Nahal Yael

6.1.2 General error sources of precipitation measurement

In general, precipitation estimations are inaccurate since they are afflicted with various source errors. SEVRUK (1986) differentiates between *random errors* and *systematic errors*.

Random errors are mostly related to meter-reading mistakes or device failures. Additionally, random errors may occur during regionalisation of point data, owing to local irregularities of gauge surroundings and micro-climatical variations around the gauge site. A gauge site may thus no longer be representative for a larger area.

Systematic errors are believed to play the most important role when measurements of precipitation at a point are concerned. They are influenced by meteorological factors, such as rainfall characteristics, wind speed, etc. Furthermore, they vary according to the gauge type used and to the degree of protection of the gauge site against wind (SEVRUK 1986). Since most systematic errors occur as losses, the real amount of precipitation is usually underestimated by the measurement. Main components of the systematic error are losses due to the deformation of the wind field above the gauge orifice, losses from wetting of the walls of the collector and losses due to evaporation (SEVRUK 1982). The latter two play a minor role, especially during high intensity storms their effect is negligible (DVWK 1991). The systematic error for rain can range between 5 and 15% (SEVRUK 1982).

6.1.3 Uncertainty of precipitation measurement in Nahal Yael

On the steep slopes of Nahal Yael, rainfall occurs virtually exclusively as short-duration, high intensity cloudbursts. Under such conditions, the mere performance of the instruments, rather than systematic errors (i.e. mainly wind effects), may be the major problem (SEVRUK & GEIGER 1981). The excessive summer heat may cause additional mechanical problems with the measurement devices. The special problems of rainfall data collection that arise in an extremely arid environment are discussed below.

6.1.3.1 Wind influence

A generally accepted theory is that a large fraction of the total measurement error is a result of turbulence and increased wind speed in the vicinity of the gauge (LARSON 1986). The gauge causes an ascending air current over its rim with increased wind speed. It carries drops further downwind, which otherwise would have passed through the gauge orifice (Figure 6.2). The magnitude of the resulting gauge catch deficiency varies according to the type of gauge used and to the degree of wind protection. The systematic error also varies according to rainfall structure (falling velocity, i.e. drop size) and wind speed (SEVRUK 1983). If wind speed increases, errors due to wind field deformation enlage.

With increasing rainfall intensities, and therewith increasing drop size, the measurement deficit due to wind influence decreases. For short, heavy storms KREUELS & BREUER (1986) reported of deficits less than 3 %. For rainfall intensities above 1.8 mm/h, no influence of the wind on the amount of measured precipitation was found (BOGDANOVA 1966 cited in SEVRUK 1981).

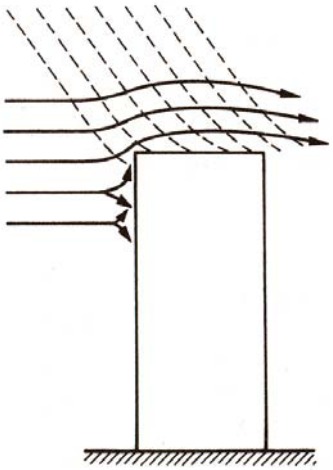

Fig 6.2: Impinging rainfall and flow path of wind causing gauge catch deficit

All events investigated in this study were convective storm events with very high rainfall intensity (maximum intensities reaching up to 120 mm/h), and the total amount of rainfall falling with intensities below 1.8 mm/h was smaller than 8%. Hence, it seemed reasonable to abandon rainfall correction due to wind influence.

6.1.3.2 Sloping ground

In very steep terrain, standard gauges with horizontal rim tend to underestimate precipitation in winds blowing upslope and overestimate precipitation in winds blowing downslope. Some authors suggest the use of ground level gauges with their rim inclined according to slope of the ground surface (SEVRUK 1974). A theoretical conversion from an inclined surface to a horizontal standard may be done by dividing the opening area of a gauge by the cosine of the slope angle.

SHARON (1980) reports great deviations between rainfall depths measured by inclined rain gauges compared to measurements of conventional gauging stations with horizontal orifice. The angle of the falling raindrops relative to the sloping surface and the slope orientation relative to wind direction, determine the magnitude of the deviation. Differences in hydrological rainfall on opposite facing slopes may reach a ratio of 1:2 or even exceed it in extreme cases (SHARON 1980). However, a great variability in time, space, and the size of drops characterise the angle of incidence during a rainfall event.

Only if the site storm vector can be specified within narrow limits, one may accurately estimate hydrological point-rainfall from conventional rain gage data by means of a trigonometrical model (SHARON 1980). Although a meteorological station was in operation inside Nahal Yael for some years, no data on wind direction and velocity were available. Thus, it was not possible to introduce any correction scheme due to sloping ground.

6.1.3.3 Instrumental problems

Two different types of recording rainfall gauges have been used in Nahal Yael:

The Lambrecht type recording stations register changing water levels on a chart. They operate based on the float and siphon principle (Figure 6.3): The gauge has a chamber containing a float which rises vertically as the water level in the chamber rises. Vertical movement of the float is translated to movement of a pen on a chart. A siphon is used to empty the chamber regularly after 10 mm of rainfall have accumulated. Possible sources of errors are early or slow siphoning, a stuck float, perturbance of the clockwork or a chart paper that was not accurately fixed (SEVRUK 1981).

The tipping bucket type rain gauges were installed to replace the Lambrecht type rain gauges but were operated for some time parallelly to the old gauges at a few locations. The measuring principle is a pair of buckets that are filled alternately. If one bucket is filled, it overbalances and directs the incoming rainfall to the second bucket. The flip-flop motion of the tipping buckets is transmitted to the recording device, which thus records increments of rain, typically 0.1 to 0.5 mm (WARD & ROBINSON 2000). In case of very intense rainfall events, tipping buckets are susceptible to negative systematic errors due to the dump interval (i.e. time required to complete the tip). Thus water is lost, while the bucket is being emptied. The same phenomenon may occur during the siphoning of the Lambrecht recorder, although this happens in much lager intervals than the tip of the bucket. The induced negative measurement error for the tipping bucket may be as high as 7% (ADAMI & DA DEPPO 1986). Besides the effect of rainfall intensity variations, errors due to poor upkeep, misalignments or inaccurate calibration are possible error sources.

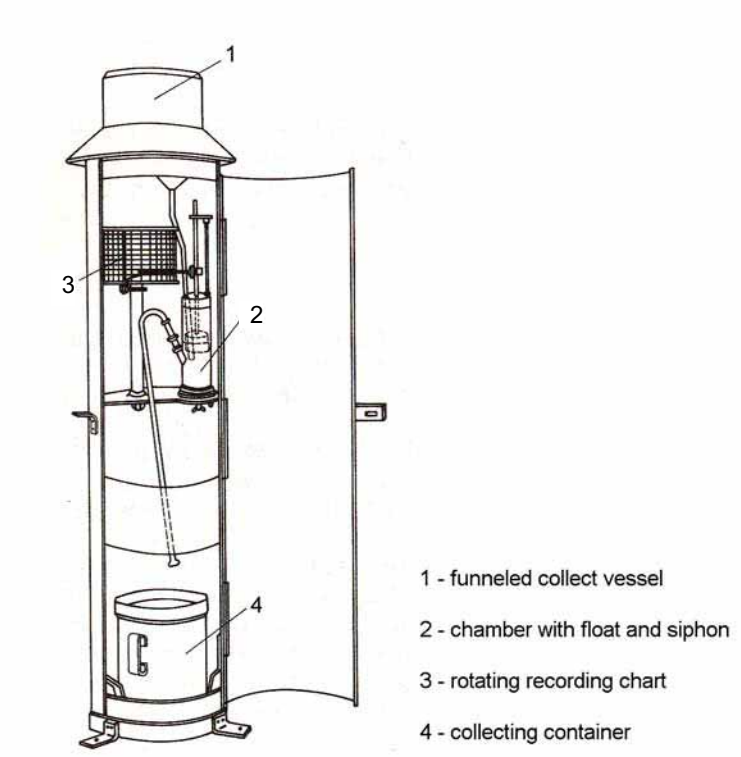

Fig 6.3: Function-drawing of Lambrecht-type recorder

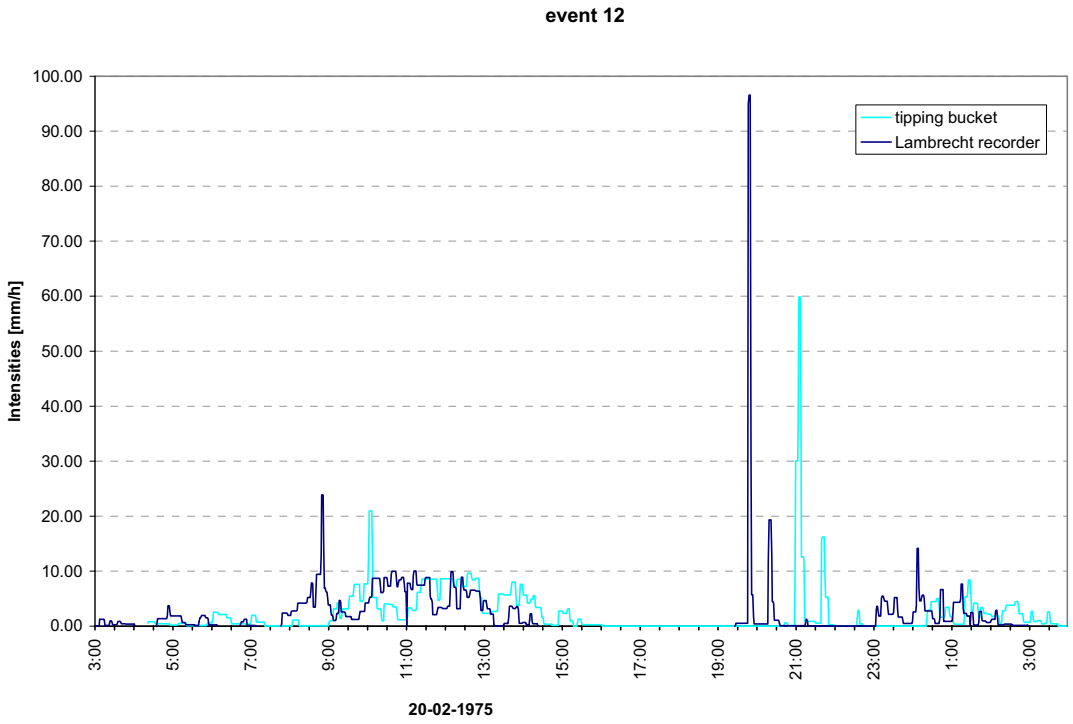

Fig 6.4: Measured rainfall intensities at stations 26 (Lambrecht recorder) and 26a (tipping bucket) located side by side during event 12

Figure 6.4 shows measured rainfall intensities at two recording stations, one Lambrecht type recorder and one tipping bucket at the same site. The time shift between the 2 stations will be discussed later (see Chapter 6.1.4.1). The measured amounts of water are within the same order of magnitude for both sub-storms (deviation: 1.7%) (Table 6.1). During event 12A only low intensities up to 23 mm/h were measured. For this event the tipping bucket records about 3% more rainfall, although the maximum intensity recorded by the tipping bucket is lower than that of the Lambrecht pluviograph. The maximum intensities during event 12B, which was much more intense, show large differences (61%), while the amounts are almost the same. A possible reason may be water losses during the dump period of the tipping bucket, although the discrepancy exceeds the value of 7% by far. During the 15 minute lasting high intensity spell around 8:00 pm the volume measured by the pluviograph exceeds the volume recorded by the tipping bucket by 3.5%, a fact supporting the thesis of lost volume at the tipping buckets. On the other hand, the pluviograph may overestimate rainfall intensities and volume during very high intensities if the temporal resolution of the chart is too low. Instrumental errors may vary from instrument to instrument and from event to event. The magnitude of the instrumental errors could not be determined from the available data.

Tab 6.1: Comparison of rainfall amounts and maximum intensities measured by a tipping bucket (station 26A) and a pluviograph at the same site (station 26) during event 12

		station no	12A	12B	12 total
rainfall amount	pluviograph	26	33.1	18.1	51.2
[mm]	tipping bucket	26a	34.2	17.9	52.0
	deviation		3.16%	-1.11%	1.69%
maximum intensity	pluviograph	26	23.8	96.5	
[mm/h]	tipping bucket	26a	20.9	59.9	
	deviation		-13.88%	-61.12%	

6.1.4 Data preparation

6.1.4.1 Synchronisation

At Lambrecht type rainfall recorders malfunctions of the clockwork often occur. Then, when a number of recording instruments are placed at relatively small distances from one another, the problem of synchronisation arises. This is especially true when difference caused by the movement of an event across a gauging network is in the same order of magnitude as the error of the recording clock. Large deviations in the onset of rain can be clearly related to errors in the clockwork. Some examples for that were found in the Nahal Yael data; in the most extreme case a station recorded the same pattern of rainfall intensities as the surrounding stations, but with a time shift of 8 hours. On the other hand, the reasons for deviations in the rainfall onset were difficult to assess. Except for one event in 1968 (event 3) where the advance of the storm cell was monitored by telemetry, the trajectories of the storm cells are unknown.

For event 3, the front of runoff generating rain was found to have proceeded over the 2 kilometre long Nahal Yael watershed in 18 minutes (equivalent cell velocity 111m/min) (PORATH & SCHICK 1974). During event 27, which occurred in October 1997, rainfall was recorded by two electronical data loggers with negligible errors in timing. Here, a time shift of 3 minutes was monitored between the two rainfall stations only 600 metres apart (equivalent cell velocity 200 m/min). These examples indicate a relatively slow velocity of moving storm cells compared to SHARON (1972B), who estimated typical velocities of storms moving over Nahal Yael to vary between 540 m/min and 1600 m/min. In the rainfall raw data the behaviour of rainfall intensities at the stations did not follow a certain pattern that might have revealed storm trajectories. The onset of rain was rather randomly distributed all over the catchment. Thus, high cell translation rates as indicated by SHARON (1972B) were assumed, producing a nearly instantaneous beginning of a

storm all over the basin. Under this assumption, which produces evenly distributed rainfall all over the catchment, synchronisation of all stations was accomplished. Figure 6.5 and Figure 6.6 show measured rainfall data during event 12 before and after synchronisation. Unfortunately it was not always possible to fix the “real” point in time of the rainfall data. For event 12 the tipping bucket (station 26a) with electronical time records was first assumed to be the most accurate station concerning timing. However, rainfall onset at this station and timing of measured runoff were in contradiction, as flow was recorded before the onset of rainfall at rainfall gauge 26a. Thus, rainfall records of stations 24, 26 and 30, which were more plausible compared to the discharge timing, were synchronised. Data records of station 26a were completely disregarded, since it is located at the same site as station 26. During synchronisation care was taken to shift rainfall data of all stations as little as possible. The possible error in timing was determined by calculating the mean of the absolute values of greatest positive and negative deviation from the assumed true point. Timing uncertainty varies significantly from event to event: for event 27 it is minimal with ± 1 minute whereas for event 12 the timing uncertainty is extraordinary high with ± 33 minutes. The mean timing uncertainty for all events investigated in this study reached a value of 13 minutes, and was not correlated with the age of the gauging stations.

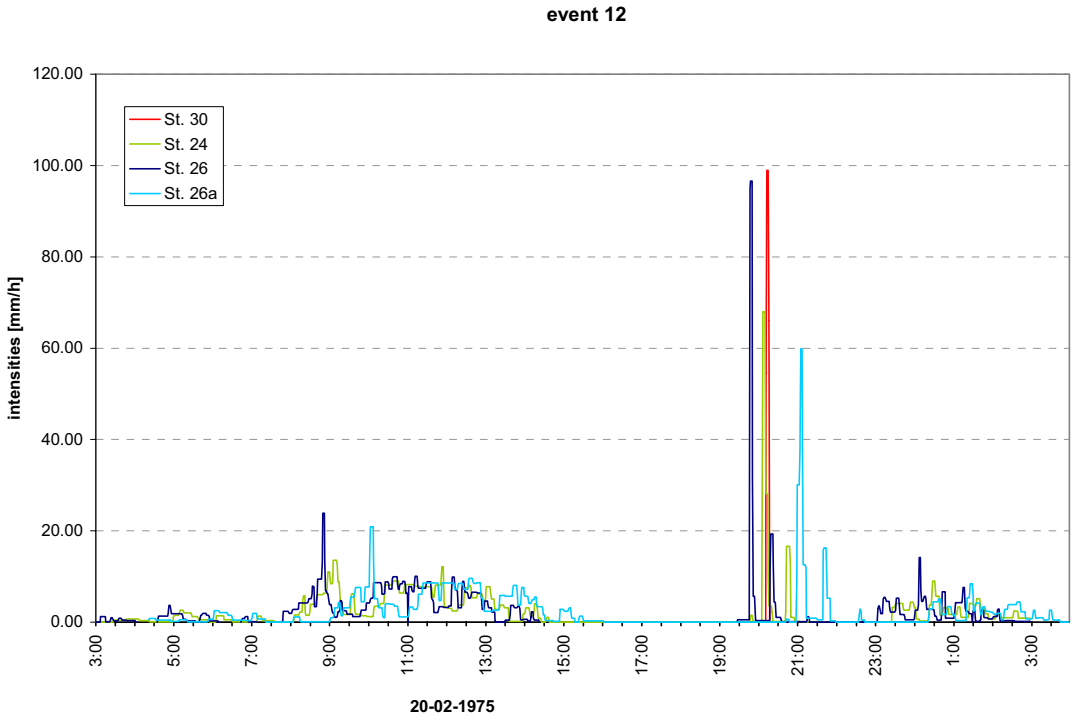

Fig 6.5: Rainfall intensities during event 12 at 4 stations before synchronisation

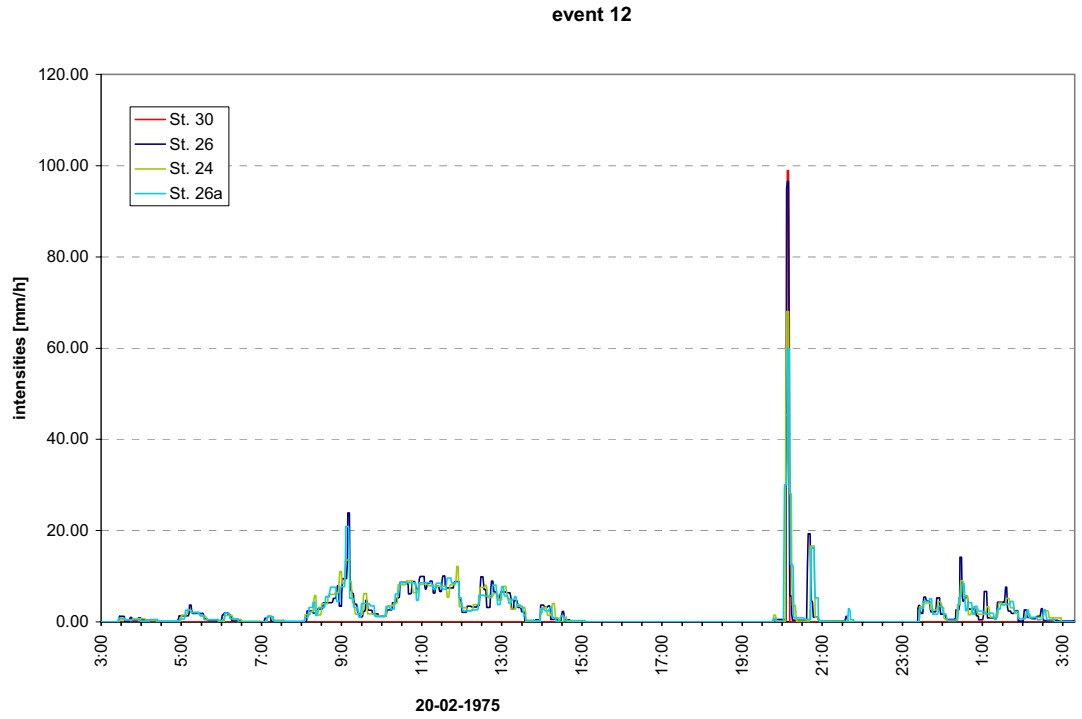

Fig 6.6: Rainfall intensities during event 12 at 4 stations after synchronisation

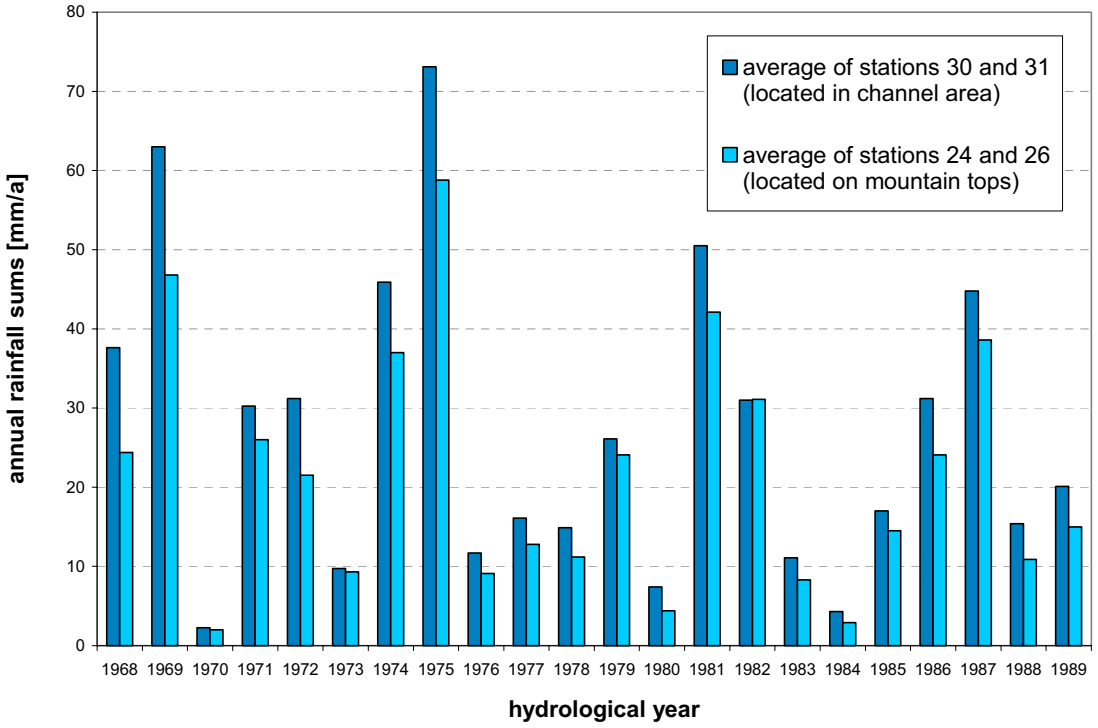

Fig 6.7: Mean annual rainfall amounts of two valley and two mountain top stations

6.1.4.2 Rainfall elevation gradient

In general, precipitation increases with altitude (orographic effect). In Nahal Yael the opposite was found by SHARON (1970A) and SHARON (1970B). Persistently an increase in the amount of rain reaching the channel area was observed, compared to the highest portions of the catchment. It was shown that these differences exceeded by far the possible errors in measurement due to the wind effect on raised rain gauges. The factors controlling these micro-scale variations, which are negatively correlated with altitude, have not been fully understood.

Tab 6.2: Analysis of rainfall events with data from 4 or more stations concerning rainfall-elevation gradient

	date	number of stations	gradient [mm/100m]	coefficient of determination
event 3	25.04.1968	9	-2,49	0,33
event 4	24.05.1968	11	-7,70	**0,63**
event 5	24.11.1968	10	-2,34	0,19
event 6	25.11.1968	10	-1,14	0,24
event 7	21.01.1969	9	-3,3	0,13
	22.03.1969	7	-0,45	0,08
	01.04.1969	10	-0,89	0,18
	15.04.1969	9	-0,5	0,33
	10.01.1971	9	-0,3	0,03
	10.01.1971	9	-0,81	0,23
	25.01.1971	7	-1,25	0,37
event 8	25.03.1971	10	-0,89	0,1
	15.04.1971	10	-1,22	**0,61**
	22.12.1971	4	-5,6	0,41
	23.11.1972	8	0,07	0,002
	24.11.1972	8	0,35	0,04
event 11	04.12.1974	5	-3,8	**0,74**
	07.02.1978	4	-1,42	**0,59**
event 13	11.12.1978	5	1,11	0,42
event 17	22.03.1985	4	-2,53	0,44
	16.10.1987	4	-1,64	0,25
	19.12.1987	4	0,26	0,05
	23.12.1987	4	-0,53	0,14
	01.04.1990	4	-2,39	**0,67**

It has been interpreted only in general terms as a combined wind-topography-conditioned effect (SHARON 1972A), where raindrops tend to be drifted away from over exposed parts and are subsequently deposited in the lower parts. The magnitude of the effect seemed to increase with wind speed. Indeed, SHARON's (1972A) analysis revealed this distinct pattern only for events in which the general wind direction was from the

west. Unfortunately, wind data from Nahal Yael was not available to be included in further analysis.

In an attempt to illustrate Sharon's pattern also by the long term data, rainfall records from 1968 to 1990 were analysed. Comparing the annual mean rainfall amounts averaged for two channel stations and two uphill stations, a clear general pattern could be observed (Figure 6.7). In a second step all events which showed complete data records from 4 or more stations, were included into an analysis of single events with total amounts exceeding 3 mm. Although a general trend following the pattern of a negative rainfall-elevation gradient was found in several events, a clear negative gradient with a coefficient of determination greater than 0.5 was determined only for 5 out of 24 events with total amounts exceeding 3 mm (marked in Table 6.2).

Hence, the pattern of stronger rainfall in the channel area was not applicable for all events. Because magnitude of the effect varies from event to event, calculation of the gradient had to be carried out separately for each event. From 9 events simulated, only two (event 4 and event 15) showed a rainfall-elevation gradient. A firmed gradient was found for event 4 from 11 recording gauges with a value of 7.7 mm/100m (coefficient of determination 0.63). For event 15 only two stations, one in the main channel and one on the hindmost mountain top were active. The resulting elevation gradient is 10.7mm/100m.

Implementation of the gradient was only possible based on total rainfall amounts per event and not for each time step independently. In the GIS, total rainfall amounts were calculated for each cell of the catchment-wide grid using cell distributed information on elevation and the values of elevation gradient. A uniform time response of rainfall all over the catchment was assumed and calculated as a standardised hyetograph in a one minute time step from synchronised rainfall records (Figure 6.8). This temporal behaviour of rainfall is then multiplied for each time step with the total rainfall amount for each cell yielding a spatially distributed pattern of rainfall that served as rainfall input scenario for model runs of event 4.

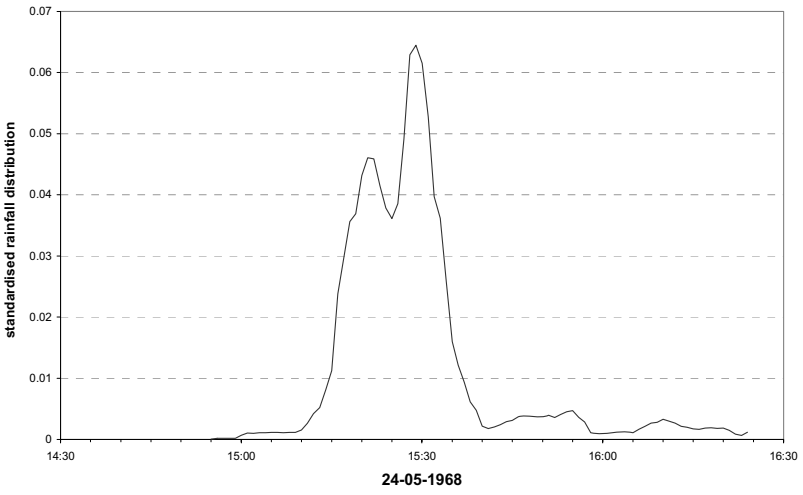

Fig 6.8: Standardised hyetograph (uniform temporal rainfall distribution) for event 4 in a time step of one minute

6.1.4.3 Spatial estimates of rainfall from rain gauge point data

FAURES ET AL. (1995) concluded that spatial variability of rainfall can lead to large variations in modelled runoff. Usually, for a 0.5 km² catchment, a single rain gauge would have been considered as representing catchment rainfall satisfactorily. The spatially non-uniform data from the dense network in Nahal Yael showed that calculating areal precipitation from one gauge with the standard uniform rainfall assumption can lead to large differences in rainfall input, depending on which station has been chosen.

For hydrological modelling it was necessary to compute a catchment wide rainfall distribution from the point values measured at the different stations. In this application the *inverse distance weighting* (IDW) method was used for spatial interpolation. It determines a value for any point based upon its distance from the stations, where measured data exist. The weight is a function of inverse distance. A continuous field estimate can be derived from irregularly spaced x-y-z data using the following equation:

$$z(x_0) = \frac{\sum \left(z(x_i) \cdot d_i^{-p} \right)}{\sum d_i^{-p}} \qquad 6.1$$

where:

$z(x_0)$	estimated value at point x_0	[-]
$z(x_i)$	measured value at station x_i	[-]
d_i	distance from the gauge i to point of estimation	[m]
p	weighting factor of the inverse distance (= 2)	[-]

This interpolation method was applied to the synchronised rainfall intensities in a one minute time step, resulting in a catchment-wide rainfall-intensity pattern for each time step.

6.2 Runoff measurement

6.2.1 General aspects

In rivers measurement of stream flow requires continuous water level records and an established relationship between water level and discharge (the stage-discharge-relation or *rating curve*). Stream flow is then deduced by transforming the record of stage into a record of discharge. The stage-discharge relation should not change over time. However, scouring of the stream bed or deposition of sediment in the stream can cause

a change of the rating curve over time. In the bed of arid ephemeral streams, scour and fill may change cross-sectional geometry even during a flood event. By constructing a special flow control device in the stream such as a sharp crested weir or flume this problem can be minimised. Still, errors due to sedimentation in the stilling basins may occur as well as during extremely low flows through imprecise levelling of the invert of the structure. If the rating curve is extended beyond the calibration range, further uncertainty in flood discharge may result.

Usually a rating curve is developed by contemporaneous set of measurements of discharge and gauge height at the station. In ephemeral streams like Nahal Yael, where flow rarely occurs during the presence of researchers, direct assessment of the rating curve is not feasible. Hence, discharge is computed indirectly using the slope-area method. Channel cross sections and longitudinal water surface profile are measured by field-surveys. Estimating Manning's roughness coefficients the Manning equation can be solved for the rate of flow in the channel (MAIDMENT 1992). Calculations with plausible values of measurement errors suggest that errors in the order of 25 % may be expected for this method (KIRBY 1985).

In Nahal Yael four gauging stations are operated (Figure 3.3). All stations consist of a broad crest concrete weir (station 05 is rectangular shaped, the other stations are of triangular shape) built on bare rock (Photographs of all stations are found in Annex A.1-A.4). Water level is measured by a float-operated water level recorder. A fifth gauging station is located at the foot of the alluvial fan near Nahal Roded confluence, where the dam was build in 1977. After the construction of the dam this station has been used as a reservoir water level gauge (Figure A.5). The hydraulic controls (weirs) associated with the gauging stations have gradually silted up. On several occasions, sediment from the immediate vicinity of the connecting intake pipes was cleared (SCHICK 1980A), but the continued piling up of sediment in the large area behind the weirs posed severe problems. For accurate level measurements, the original stilling basin properties had to be restored. Despite the inaccessibility of all four stations for vehicles, sediment clearing was accomplished in 1978 before event 13 occurred in Dezember 1978. Thereby 50 cubic meters of sediment were excavated and the gauging stations have been restored to their original level of accuracy for the next coming events.

6.2.2 Analysis of raw data

For almost all events, processed discharge data was available in irregular time steps. Thus, data preparation could be confined to plausibility checks and disaggregation of the data to a time step of 5 seconds. However, for event 7 a discharge rating existed only at stations 02 and 01. For this event, raw data analysis of stations 02 and 03 will be discussed below as an attempt to quantify measurement uncertainty. The main problem arises from sedimentation whereby the level of the gauge intake is lowered beneath the level of the channel. From the charts, the real ground level, i.e. the actual level of the channel, has to be determined. With additional information (e.g. from field surveys

during or shortly after the flood) about sedimentation or water marks, the original “true” water level may be reconstructed. After the reservoir had been build in 1978, accurate additional data on the flood volume could be derived from the recording station 01 monitoring the water level of the reservoir. This data was used for discharge rating at station 02 as well. Without this additional information only ranges of possible discharge may be defined by a lower and an upper boundary. Figure 6.9(a) shows water level data as it was recorded on the original chart at gauging station 02. Based on this, water level was reconstructed using additional information including water level marks in the field and values for the initial offset (23 centimetres from the previous event measured at time t_1) and final offset (42 centimetres due to sediment deposited on the connecting pipe after the whole event reached at time t_2). A virtual channel ground level (indicated by the black line in Figure 6.9(a)) was calculated and subtracted from the measured water level values yielding the corrected water levels shown in Figure 6.9(b). Finally, the rating curve was applied to the corrected water level.

Without additional information for stations 03, 04 and 05 minimum and maximum scenarios were constructed only from the level charts to assess the uncertainty range of discharge rating. Figure 6.10(a) shows the original water levels as measured at station 03 during event 7. Black lines indicate again the assumed ground level. Under the supposition that no sediment has accumulated, the first point of the hydrograph (t_1, lower water level) defines the level of the channel for the maximum scenario. For this scenario, flow did not decline to zero between the two peaks. Base level was reached again at the transition point of the falling limb to a linear curve (t_4). After this point, the linear recession is assumed to be caused by water remaining in the funnel of the gauging station after the event, infiltrating slowly into the alluvium.

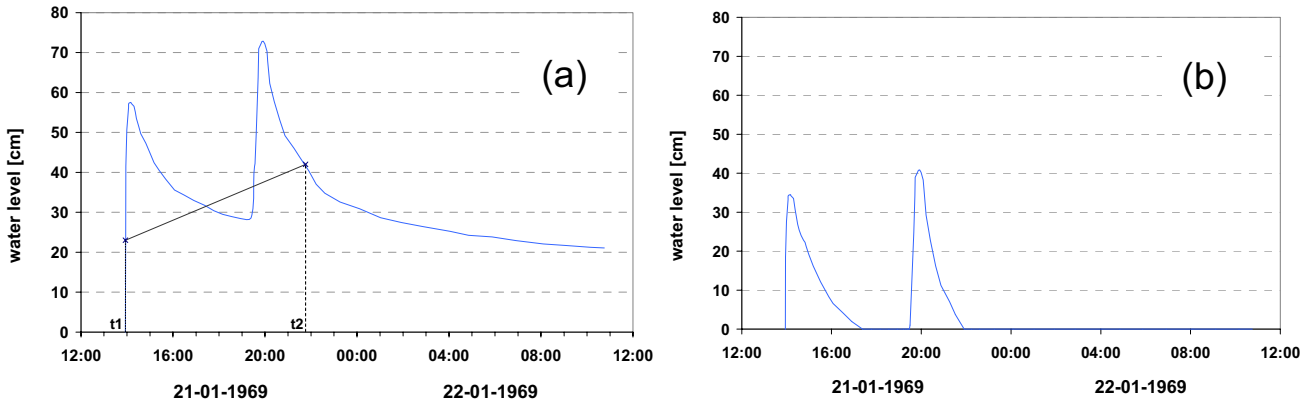

Fig 6.9: Station 02, event 7: (a) measured water level (b) corrected water level

The base level for the minimum scenario was determined from a point of inflection in the falling limb of the hydrograph (t_3). The breaking point in the curves was interpreted as an indicator for the transition of water level records from water flowing in the channel to water level records due to slow exfiltration from the accumulated sediment above. The corrected water levels for both scenarios are shown in Figure 6.10(b). Due to the

logarithmic scale of the rating curve, the differences between minimum and maximum scenario are much higher for the discharge than for water level (Figure 6.11).

The difference in peak discharge amounts to a factor of 3 for the first peak and to a factor of 2 for the second peak. Volumes of the two scenarios differ by a factor of 6 and 3.4 for the first and the second peak respectively. The same procedure was carried out for stations 04 and 05 as well. Figures describing the analysis of raw data for these stations are found in the Annex (Figure A.47-A.50). At station 04, the largest difference

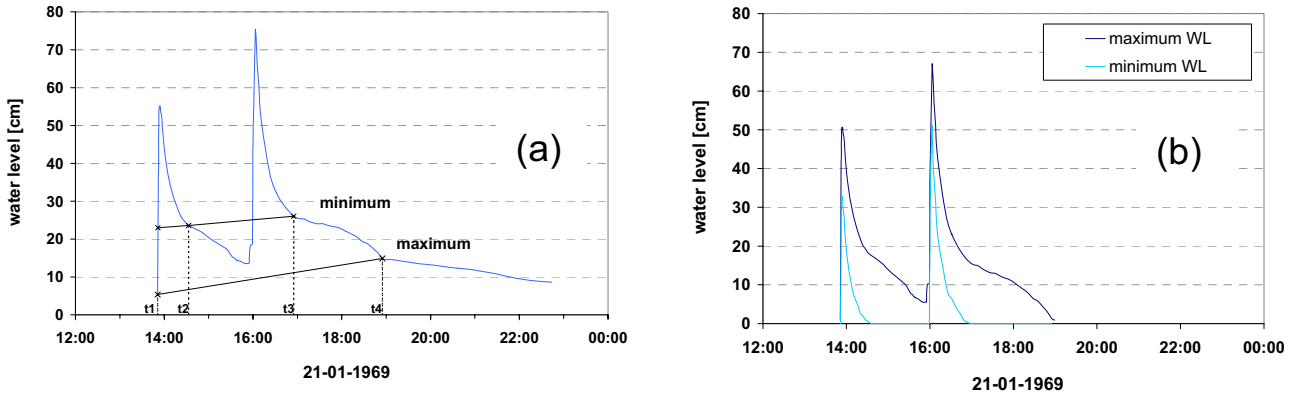

Fig 6.10: Station 03, event 7: (a) measured water level (b) corrected water level

between minimum and maximum scenario is derived. Discharge for the maximum peak scenario exceeds minimum peak discharge by a factor of 5.8 for the first peak and by a factor of 3.5 for the second peak. The volumes for this station differ by a factor of 18 (7) for the first (second) peak. At station 05 the differences between the scenarios are similar to those at station 03.

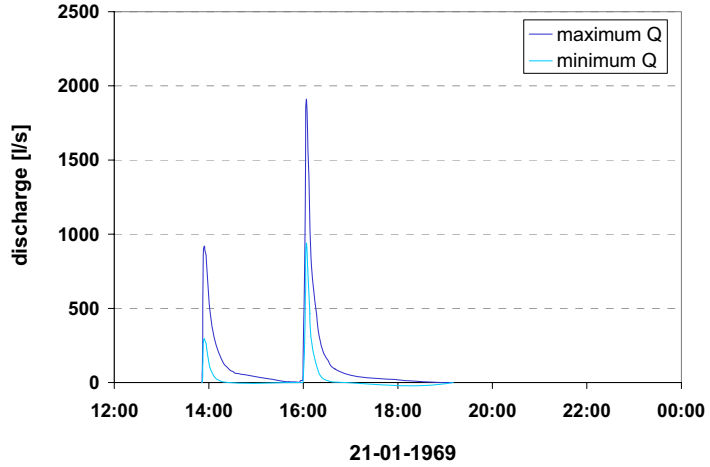

Fig 6.11: Determined range of discharge raging at station 03, event 7

6.3 Conclusion

6.3.1 Rainfall input

The need to accurately describe spatial and temporal rainfall variability for modelling small catchment response is well known (FAURES ET AL. 1995). In Nahal Yael an exceptionally dense rain gauge network was in operation for many years. From this network, catchment rainfall is derived by regionalisation of point data after the data had been checked for errors. This chapter first describes possible error sources of precipitation measurement in general. Usually, the systematic error due to wind influence plays a primary role. Secondly, the specific conditions prevailing in Nahal Yael are investigated. In contrast to low to medium intensities, the wind influence is rather negligible under high intensity rainfall conditions. Instead, other error sources prevail, e.g. as instrumental problems or inaccuracy due to sloping ground. Further problems arose from inaccurate timing of the different rainfall stations. Because of large deviations in the onset of rain, whole time series of rainfall intensities had to be shifted to synchronise the records.

A distinct areal pattern of variation in rain amount has been noted by SHARON (1970A) and SHARON (1970B), showing a relative abundance of rain in low-lying parts of the catchment. At higher elevations, the amount generally decreases. However, this local rainfall pattern was evident for not more than five events. Thus, rainfall-elevation gradient was considered only for events with a clear gradient (coefficient of determination > 0.6).

Generally, catchment-wide rainfall distribution was calculated from the point measurements using the IDW (inverse distance weighting) method. For events that showed a clear rainfall-elevation gradient, different rainfall scenarios were applied for model input.

6.3.2 Runoff measurement

Like in most arid and semi-arid streams, the extraordinary hydrometric stream flow data in Nahal Yael is inherent with unavoidable uncertainty. For events without accumulated sediment in the stilling pools beyond the gauging stations (the first events and events after sediment clearing), uncertainty is relatively low with an estimated error of 25% due to inaccuracy of the slope-area method (KIRBY 1985). The errors of discharge measurement are much higher if sediment has accumulated. Thereby, cross sectional geometry on which the slope-area calculations are based has changed resulting in inaccuracy of the rating curve. If evidence on real water level is given from field surveys, corrections of the measured water level are possible, although afflicted with much higher uncertainty. Without additional information on the height of sediment above the intake pipes, only estimates of a range can be given using the shape of the curves on the

original charts. For event 7 scenarios for minimal and maximal values were compared. Values of peak discharge show differences up to a factor of 5.8 and values for runoff volume differ by a factor of 18.

7 Uncertainty assessment

The accuracy of the model results is a function of the accuracy of the input data and the degree to which the model structure correctly represents hydrologic processes (DEVRIES & HROMADKA 1993). CHOW ET AL. (1988) distinguishes three categories of uncertainty in hydrologic modelling:

- *Natural uncertainty,* which arises from the random variability inherent in hydrologic systems.
- *Model uncertainty*, which describes how accurately the natural processes are represented by equations in the mathematical model.
- *Parameter uncertainties*, which are dependent on how accurately the values of model parameters may be determined.

MELCHING (1995) describes a fouth source of model uncertainty:

- *Data uncertainties*, which include systematic and random errors inherent in the input data.

Natural uncertainties influence all aspects of hydrologic modelling since they affect the input data, model parameters and model structure (MELCHING 1995). In the following, natural uncertainty is treated as a part of model, parameter and data uncertainty in the respective sub-sections.

7.1 Data uncertainties

As most computer models, the ZIN-Model requires input data on precipitation and watershed morphology. Stream flow data is only needed to evaluate model results. As model input for watershed morphology, characteristic terrain types were mapped directly in the field and sub-basins were determined from a topographic map (scale 1:1250). Doing so, unavoidable generalisation was adapted to the modelling scale. The inaccuracy of this data is of irrelevant magnitude compared to other uncertainty ranges, e.g. that of rainfall input.

The dominant source of data uncertainty influencing the reliability of model outputs is precipitation data (MELCHING 1995).

As already mentioned in Chapter 6.1, considerable data uncertainties in rainfall input may stem from:

- measurement errors
- synchronisation of rainfall data

- interpolation of catchment precipitation from point data

Factors influencing the quality of runoff data are described in Chapter 6.2. Uncertainties in runoff measurements are of different magnitude, mainly depending on the degree of sedimentation at the measuring weirs, which differs from event to event. The accuracy of measured discharge in Nahal Yael is relatively high for events 3, 4, 15 and 16, and relatively low for events 6, 8, 12 and 27. Lowest quality was found for event 7, where for gauged discharge data at stations 03, 04 and 05 only a lower and upper boundary defining a possible range of measured discharge data could be determined. A maximum limit of discharge measurement could be easily established but the uncertainty of the boundary for the minimum scenario was very high. This upper limit was determined from breaks in the hydrographs, which were not always well-defined. Partially measured discharge data are non-reliable, especially if runoff coefficients are close or above 1. This is the case for event 6 at stations 04 and 05, during event 7B at station 02, and during event 12A at station 04.

7.2 Parameter uncertainties

Parameters of the ZIN-Model are determined directly in the field through physical measurements or from topographic maps, aerial photographs or from information in the literature. LANGE (1999) and WAGNER (2002) assessed parameter uncertainty and carried out sensitivity analysis by determining the uncertainty ranges of each parameter. Parameter values were varied over their maximum range of uncertainty while the other parameters were kept constant (LANGE 1999). Subsequently, the effects of parameter variation on the simulated flood were analysed. Due to time limitations, a thorough sensitivity analysis and determination of uncertainty could not be carried out within the framework of this study.

7.3 Model uncertainties

Simplified description of complex hydrological processes is the cause for model uncertainty. Model uncertainty may be assessed comparing simulated model output, e.g. simulated peak discharge, with measured data.

In the *runoff generation* routine of the model the scaling problem (DEVRIES & HROMADKA 1993) is the most critical point. Infiltration properties were derived by field measurements at the point scale (0.25 m²) while the model is applied at the larger scale of sub-catchments (mean size ~1000 m²). At the transition from the plot scale to sub-catchments, additional processes may occur that may cause runoff losses. These processes include e.g. slope losses that may be found at the interface between a rocky

upslope area and its colluvial base. At the transition to colluvium, runoff that was generated on the upper, rocky part may infiltrate into the loose heterogeneous rock fragments. YAIR (1992) describes this phenomenon in detail. Additional losses may occur as channel losses when, at the beginning of an event, water flowing on dry channels disappears. This is especially true for some type-1 channels that are filled with considerable amounts of debris (Figure A.8).

For *runoff concentration*, the time-lag function simplifies natural processes markedly. The total amount of runoff generated on one model element during one time step arrives simultaneously at the channel only delayed by the time-lag. For the relatively small model elements as used in the present application and small time-lags due to steep slopes, the errors in neglecting different travel-time distributions seem reasonable.

Model structure uncertainties in the *channel routing and transmission loss* routine may originate from different sources simplifying the complex nature of hydrologic process. They were summarised by LANGE (1999) as model uncertainties due to:

- the simplified representation of the flow process as one-dimensional
- the approximations inherent in the Muskingum-Cunge technique
- the assumption of homogenous channel segments
- the simplified description of cross-sectional geometry
- categorisation of channels with a constant, stage-independent channel roughness
- the assumption of a constant infiltration rate for transmission losses, which are completely stopped when the wetting front reaches the base of the active alluvium

7.4 Conclusions

Uncertainty in hydrologic modelling arises due to the fact that no rainfall-runoff model provides a true reflection of all processes involved (BEVEN 2001). Constraints in model structure as well as in the available information on parameters and input data complicate the application of any hydrologic model. Thus, uncertainty assessment plays an important role as it provides the information needed to make preliminary estimations of the reliability of model output.

To simplify uncertainty assessment, four sources of model uncertainties are distinguished (natural, data, parameter and model uncertainties). The four problem areas are strongly interrelated, e.g. natural uncertainties influence all hydrologic processes. Additionally, e.g. estimations of parameter uncertainty assumes that the model structure has reasonably been examined.

8 Model application - results and analysis

From all events registered in Nahal Yael, nine were chosen for model application. These include eight events that reached station 02, among them were three double peak events and one event that infiltrated completely into the alluvial fill on its way downstream to station 02. All major events listed in Table 3.1 were analysed except for events 1 and 2 which took place before the construction of concrete weirs and event 10, when the watershed remained partially ungauged due to the Yom-Kippur-War. In general, rainfall input was derived from interpolating synchronised rain gauge data by inverse distance weighting (IDW). For single events, different precipitation scenarios were applied additionally.

In most arid catchments, gauged stream flow data are not available to compare simulated and measured runoff. Because Nahal Yael has been used as a research catchment for many years, the extensive database allowed comparisons of simulated and gauged runoff data. Model performance was interpreted visually depending on how accurately the simulation matches the measured hydrograph within its uncertainty ranges. In the following, results of the simulations and possible interpretations are presented in chronological order of the events. Because of the event based character of the model, this section comprises event characteristics and model results, as well as discussion of model performance for each event. With the discussion of events it was inevitable to mention possible error sources in model performance. These are not illustrated in detail here, but only in the following chapter.

Despite of few exceptions, graphics of model results are generally presented for station 02 at the basin outlet only. Figures showing hydrographs at the remaining stations are given in Annex A.17-A.45. Table 8.1 gives an overview of simulated events and their model results.

Tab 8.1: Summary of model results

event	specification	total amount	mean max. intensity	station 02	station 03	station 04*	station 05
E3	scenario 1 **	9.2	34.5	<<<	<	<<	-
	scenario 2 (instanteous rainfall onset)	9.2	34.5	<<<	<<<	<	-
E4	scenario 1 (rainfall-elevation gradient)	14.0	49.5	=	-	<<	-
	scenario 2 (IDW)	13.4	49.6	<	-	<<<	-
E6		4.7	31.6	=	<	=	=
E7	A ***	8.2	27.1	<<<	<<	=	<
	B ***	9.2	41.6	<	<	<	<<
E8		4.5	42.0	=	=	>>	>>>
E12	A	33.3	18.7	<<<	-	<<<	-
	B (standard initial loss)	18.3	87.8	=	-	-	-
	B (initial loss = 0)	18.3	87.8		-	-	-
E15	scenario 1 (mean)	33.9	47.3	=	-	=	<
	scenario 2 (IDW)	33.9	47.3	=	-	=	<
	scenario 3 (grad)	33.9	47.3	=	-	=	<
E16		20.0	51.7	=	=	-	=
E27		25.4					
	peak 1	8.1	81	>>	-	>>	>>>
	peak 2	11.9	117	>>	-	>>	>>>
	peak 3	3.2	42	>>	-	>>	>>>
	peak 4	2.2	48	>	-	-	>>>

>>> overestimated by factor three or more
>> overestimated by factor two to three
> significant overestimation
= within the uncertainty range
< significant underestimation
<< underestimated by factor two to three
<<< underestimated by factor three or more

* for event 27 the indication refers to station 08
** moving stormcell after Porath & Schick (1974)
*** for station 03, 04, 05 comparison with gauged minimum scenario

\- no data

8.1 Event 3, 25-4-1968

8.1.1 Event characteristics and available data

The rainstorm that was responsible for event 3 lasted about 30 minutes and yielded about 9 mm of rainfall. The concentration of water in the main channel and the rise of water were very fast. At station 04 the flow reached its peak within only 2 min. Peak discharge was 0.71 m³/s at station 04, 0.64 m³/s at station 03 and 1.1 m³/s at station 02.

At nine rain gauges, complete data sets were recorded. PORATH & SCHICK (1974) monitored the advance of the storm cell for this event by telemetry. Two synchronised multiple-channel recorders registered the values measured by the different recorders on a single composite chart paper. The system yielded an accurately time-correlated output of rainfall data, which is shown in Figure 8.1. The track of the storm that caused event 3 could be illustrated by isochrones. With this method problems of synchronisation due to inaccurate clockworks of the recording stations etc. were avoided.

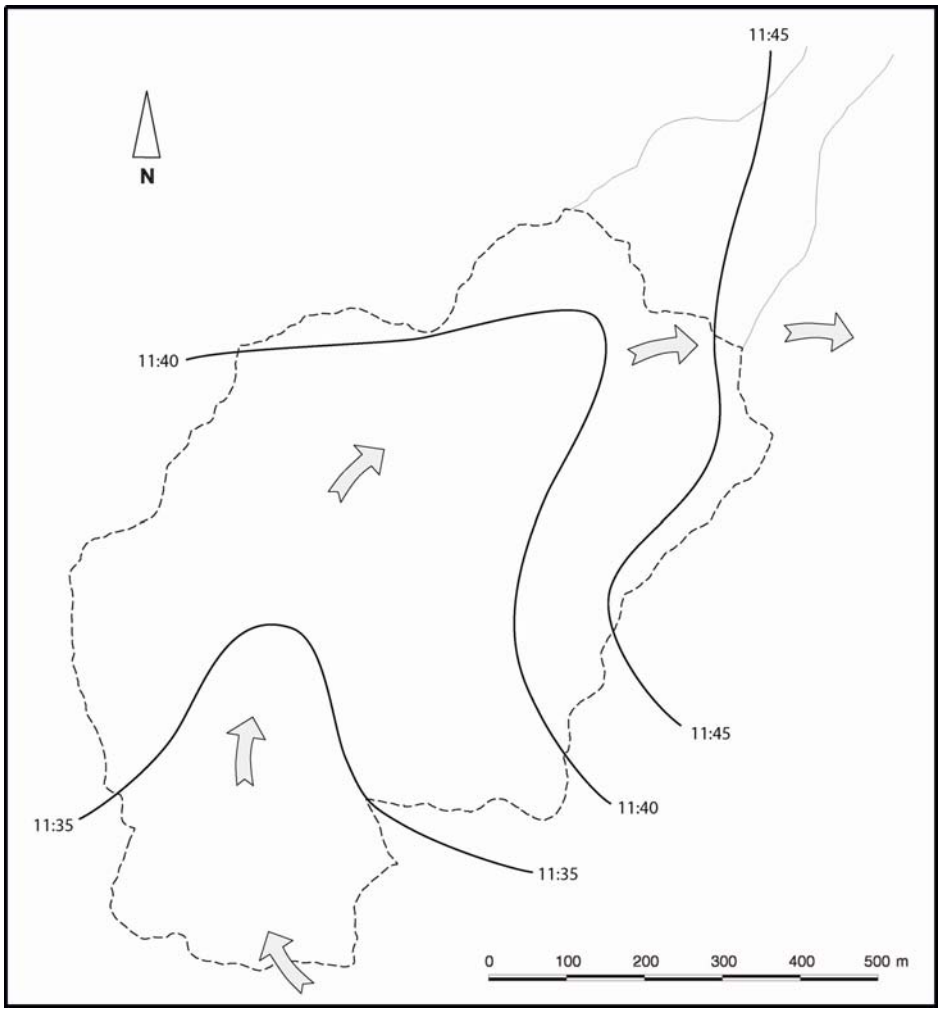

Fig 8.1: Isochrones of event 3, 25-04-1968 (after PORATH & SCHICK 1974)

Two rainfall scenarios were used as model input. The first scenario was derived from the storm trajectory by PORATH & SCHICK (1974) with accurate time records. The second scenario was calculated under the assumption of an instantaneous onset of the storm all over the area. For this scenario rainfall data from all stations was synchronised to the same point in time, as it was carried out for all other events. For both scenarios rainfall distribution was subsequently calculated for each minute time step using the IDW interpolation method (see Chapter 6.1.4.3).

The unique data record of PORATH & SCHICK (1974) allows analysing the possible impact of different temporal rainfall distributions. Figure 8.2 shows the time series of rainfall input for scenario 1 (according for storm trajectory) and Figure 8.3 for scenario 2 (synchronised to instantaneous onset). The spatially distributed pattern of total rainfall amounts is not different for both scenarios as only the temporal behaviour concerning the onset of rainfall is varying (Figure 8.4). Runoff data was available for stations 03 and 04. For station 02, only the value for peak discharge was registered. Because this was the first event after the construction of the measuring weirs, the accuracy of the discharge measurement is relatively high, only suffering form uncertainties of the slope-area method (25%) (KIRBY 1985).

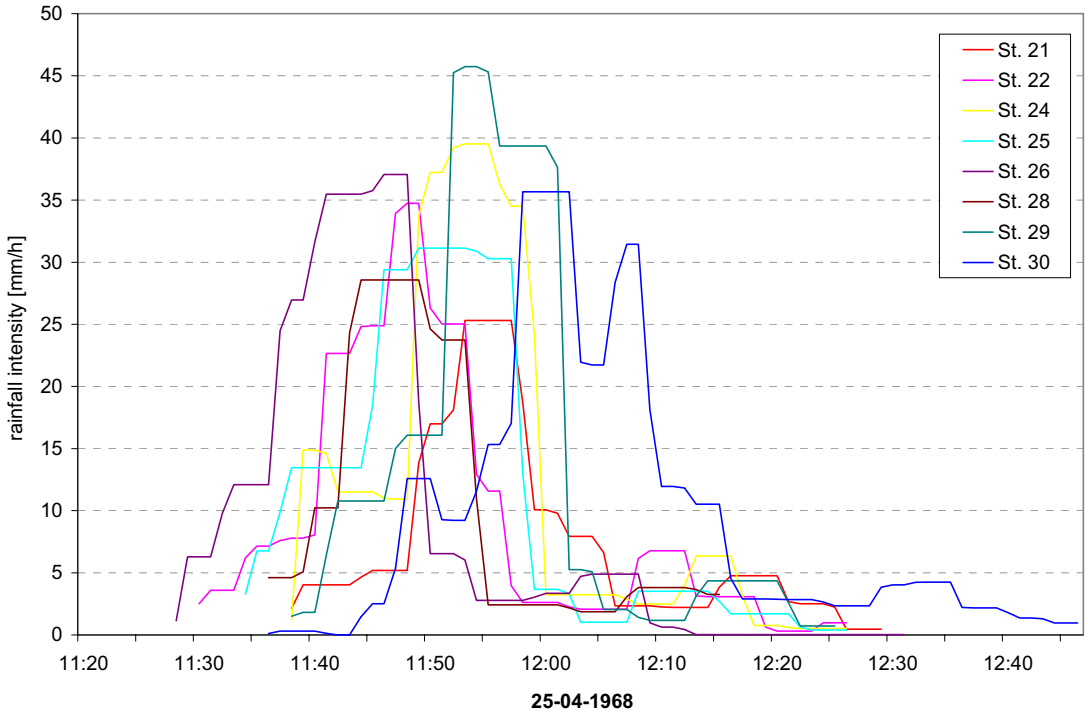

Fig 8.2: Temporal distribution of rainfall input for scenario 1 accounting for storm trajectory

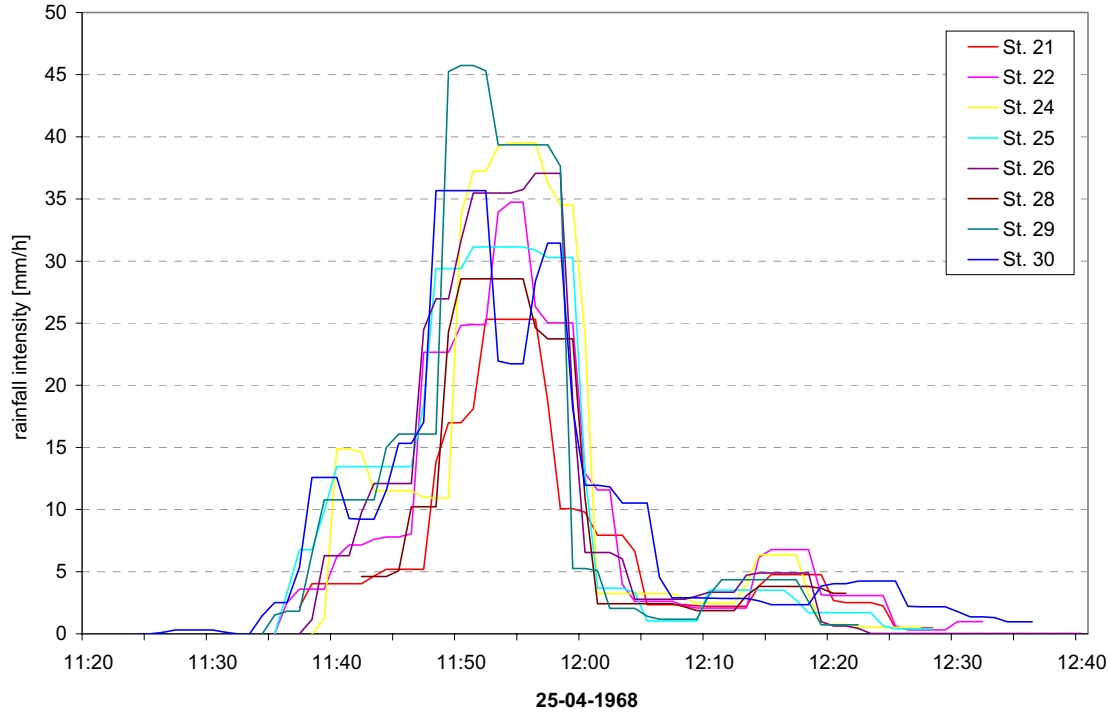

Fig 8.3: Temporal distribution of rainfall input for scenario 2 (synchronised to instantaneous onset)

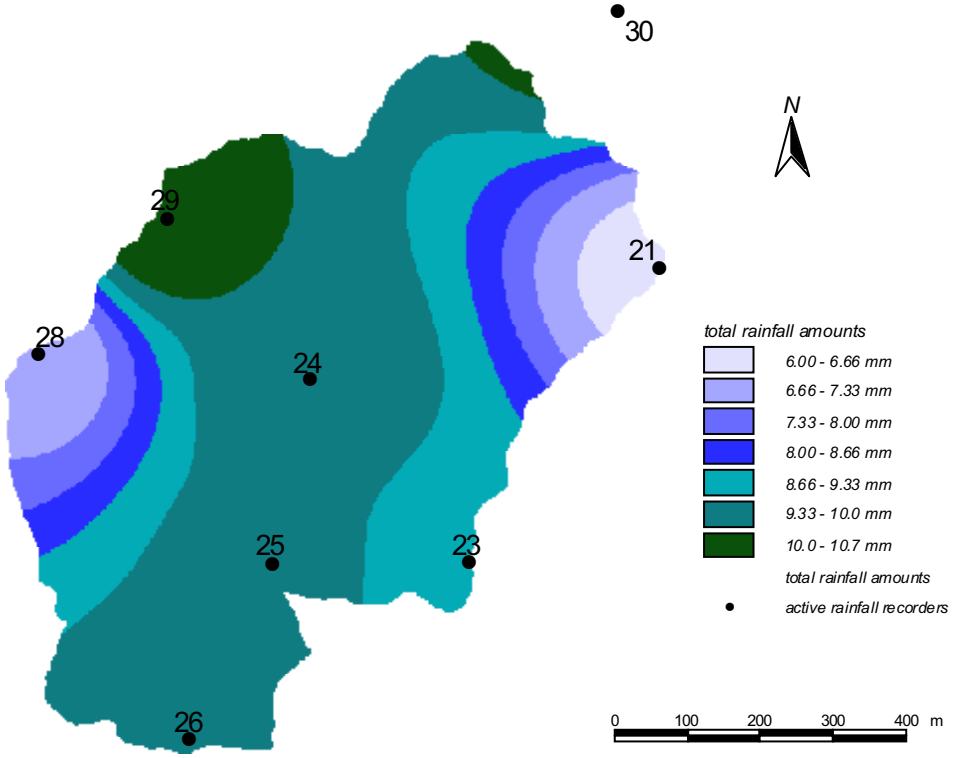

Fig 8.4: Total rainfall amount, event 3

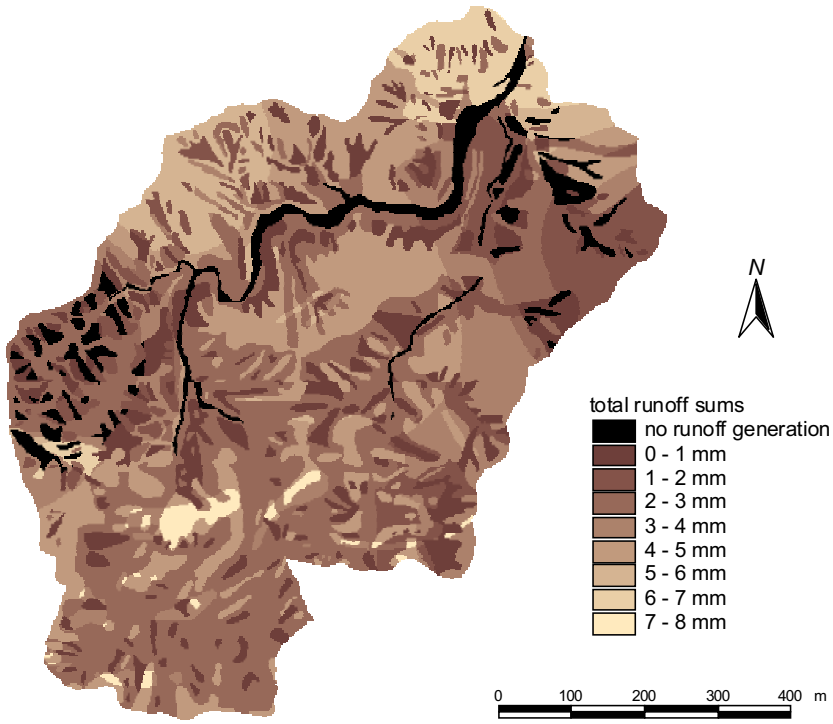

Fig 8.5: Total amount of generated runoff during event 3

8.1.2 Model results

After the model's runoff generation routine was passed, the model yielded (besides the generated runoff for each minute time step) a catchment wide pattern of total generated runoff (Figure 8.5). This pattern mainly reflects the terrain types with their different infiltration properties slightly modified by the pattern of total rainfall amounts. Subsequently, runoff concentration and channel routing routine yielded simulated hydrographs at all measuring weirs.

For this event, two simulated hydrographs could be obtained, one for each rainfall input scenario. Peak discharge at the basin outlet (station 02) was dramatically underestimated (Figure 8.6). Scenario 1 yielded peak discharge just below 200 l/s whereas scenario 2 simulates a peak of about 100 l/s. Both scenarios underestimated measured peak discharge by one order of magnitude. Differences in the temporal behaviour of runoff reflected the varying rainfall distribution of the two scenarios. Also at two other stations (03 and 04) with measured data for validation, the model underestimated peak discharge and runoff volumes significantly. The runoff response of scenario 1 is timed very well at station 04 although the shape differs from the measured runoff response.

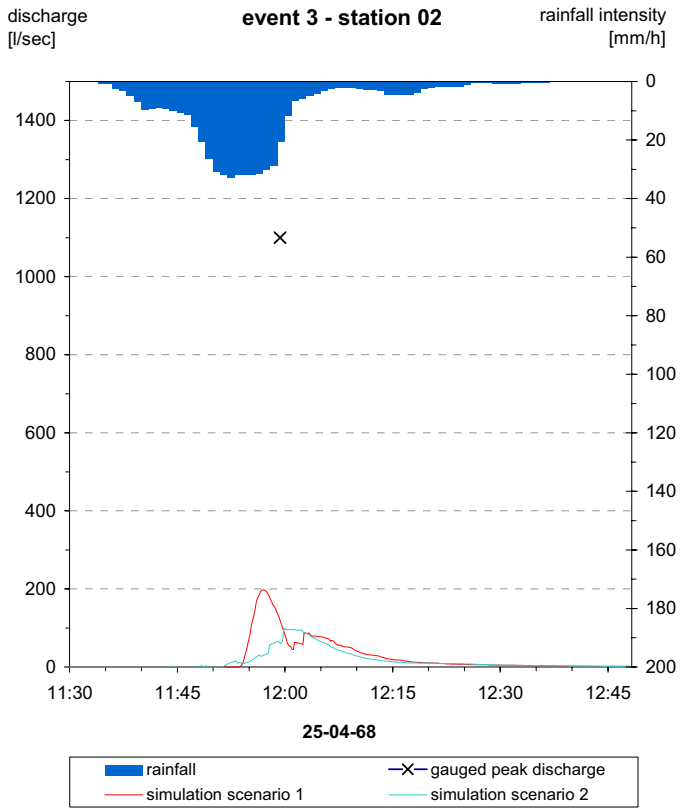

Fig 8.6: Model results event 3, station 02

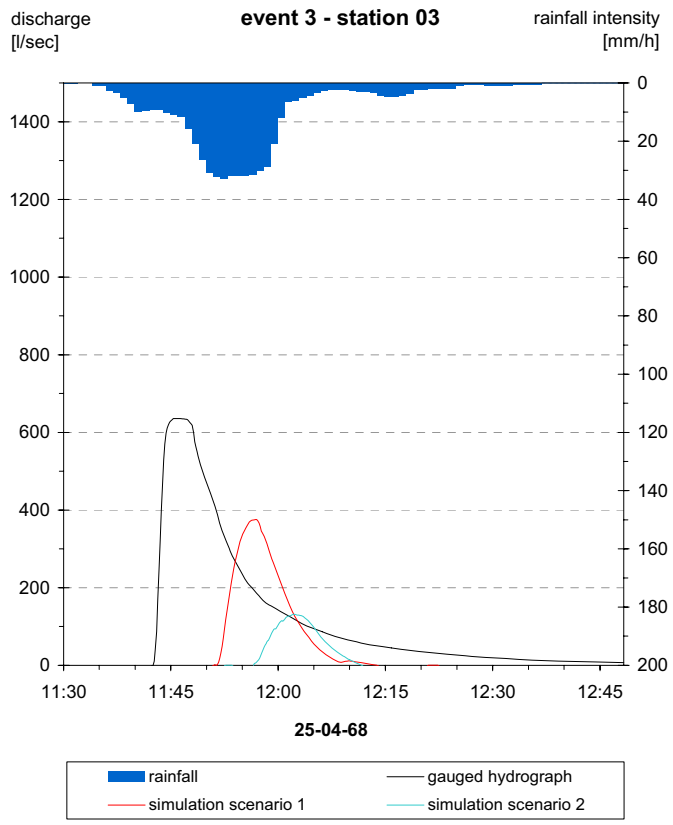

Fig 8.7: Model results event 3, station 03

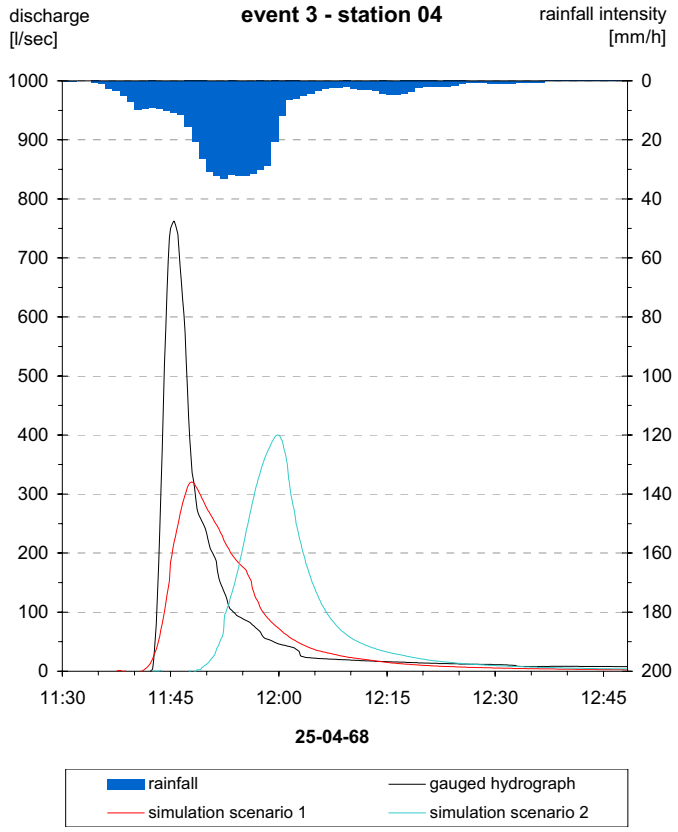

Fig 8.8: Model results event 3, station 04

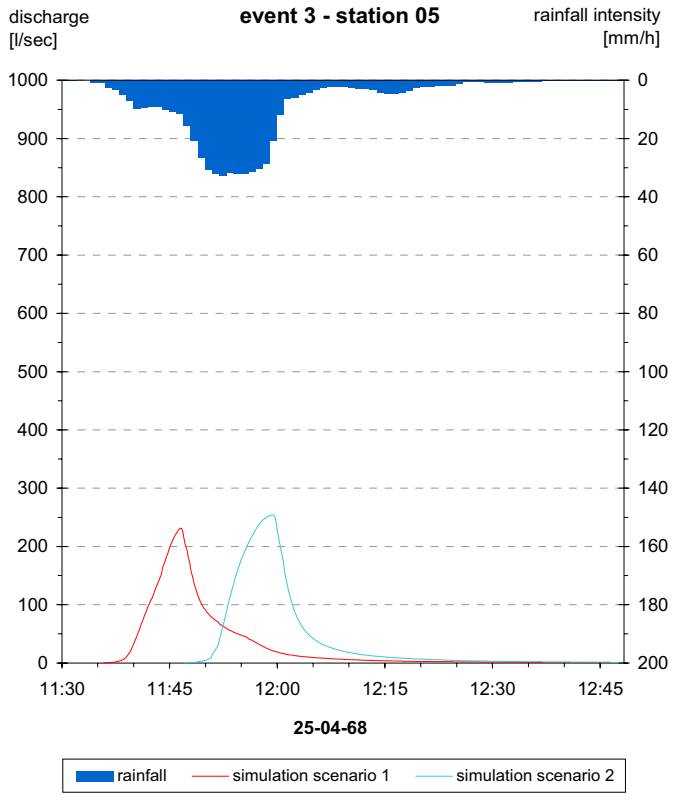

Fig 8.9: Model results event 3, station 05

8.1.3 Discussion

Model application with different rainfall scenarios representing the same amount of rainfall differing only by the temporal distribution emphasises the great influence of storm cell movement on model output.

Both scenarios underestimated peak discharge and volumes significantly. Because sub-catchment 05 is small and of rather compact shape, here the simulations yielded similar results for both scenarios except for a 15 minutes delay of scenario 2. In fact, this time shift is not relevant as timing uncertainty of the synchronised rainfall amounts to 18 minutes. At station 04, the simulated peak of scenario 1 was mainly caused by water flowing along the main channel arriving from station 05. Due to the slow southwards moving storm cell, the nearby slopes of station 04 responded some minutes later resulting in a secondary peak forming a shoulder in the recession of the hydrograph. At station 03, the scenario accounting for storm trajectories (scenario 1), yielded considerably better results in timing, peak discharge and flow volume than scenario 2. The stretched shape of this sub-catchment might be responsible for differences of simulated hydrographs. For station 02, a value of peak discharge was the only available data. It was underestimated dramatically by simulation of both rainfall scenarios. Scenario 1 was able to produce a sharper peak than scenario 2.

Assuming correct rainfall measurements, the underestimation of discharge at all stations can be explained either by a deficit in the amount of generated runoff or by a model error in describing channel transmission losses. Because underestimation occurs at station 04 as well (which is not affected by transmission losses due to a lack of alluvium), it was concluded that underestimation of rainfall input or runoff generation is more likely. It was expected, that errors in the runoff generation routine are rather due to the scaling problem (see Chapter 7.3) resulting in overestimations of generated runoff. A possible explanation may be provided by unrecorded pre-events that moisture the surface and consequently reduce initial losses. On the preceding day of event 3 a pre-rain was recorded in the late afternoon. As this rainfall amounted to less than 2 mm and event 3 occurred only around noon time the following day, it was assumed that this small pre-rain had already evaporated. However, the assumption that event 3 impinges on a dry surface (and the initial loss has to be satisfied before runoff is generated) might be wrong.

8.2 Event 4, 24-05-1968

8.2.1 Event characteristics and available data

Event 4 took place in May 1968, one month after event 3. A rainstorm that yielded a mean amount of 13 mm rainfall caused a flood in the entire watershed right down to

station 01. Effectively, rainfall lasted less than 30 minutes with maximum intensity of 83.5 mm/h measured at station 31. At station 04 the rise of water was again very fast. At this station, peak discharge yielded 1007 l/s and total runoff volume was calculated at 844 m³. The measured peak at station 02 was not as sharp but rose to 2100 l/s.

Measured rainfall data was available from 11 stations. For this event a distinct rainfall-elevation-gradient was noticed (Chapter 6.1.4.2, SHARON 1970A). Thus, different rainfall scenarios were applied again: Scenario 1 is derived from the elevation gradient and scenario 2 is calculated from synchronised data using IDW.

8.2.2 Model results

Model results were considerably different for the two rainfall scenarios. At station 02, peak discharge of scenario 2 (rainfall input derived from IDW) amounted to only half of the measured peak discharge, whereas scenario 1 also underestimates runoff but lies within the uncertainty range of the measured data (Figure 8.10). Simulated volumes differ by a factor of 2 at station 02 and underestimate measured volume largely. This is due to the long measured recession which could not be reconstructed by the model. At the other stations similar patterns are observed. Scenario 1 usually yields higher peak discharges and volumes. Measured peak at station 04 was considerably underestimated by both scenarios, while a better fit of the falling limb of the hydrograph was reached (Figure A.18).

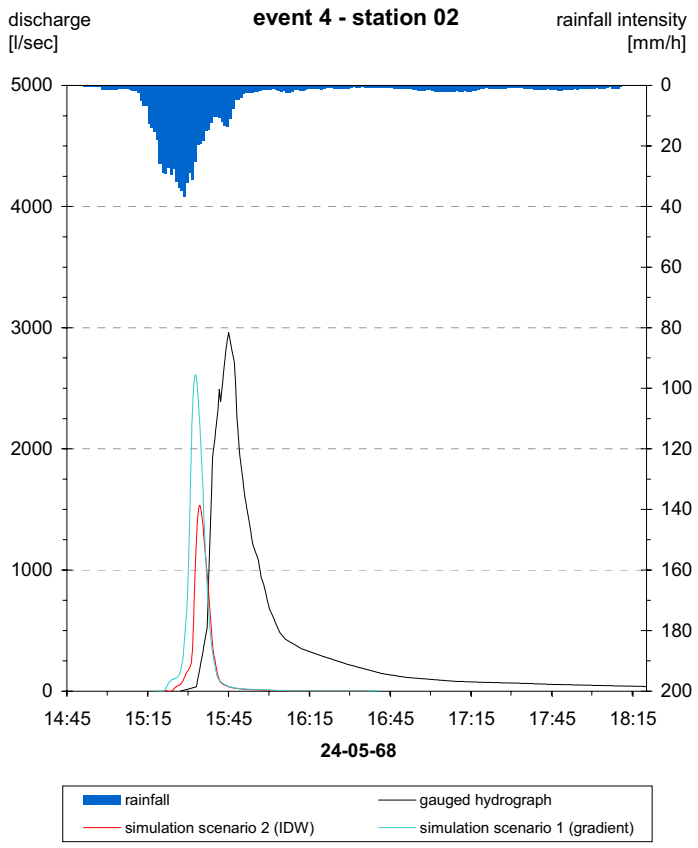

Fig 8.10: Model results event 4, station 02

8.2.3 Discussion

During event 4 the two rainfall scenarios caused unequal model simulations as well. Comparison of the grids of total rainfall amounts showed that the rainfall quantaties of the rainfall elevation gradient scenario exceeded those of the IDW scenario over a wide area in the central parts of the catchment (Fig. 8.11). Rainfall station 24 is situated on a mountain top in the centre of the watershed. Using the IDW interpolation method the relatively small rainfall amount recorded by this station affected the interpolated rainfall amount in the nearby lower channel area. In contrast, the elevation gradient scenario assumed high rainfall amounts at low elevations close to the main channel. The same phenomenon was reflected by the grids of generated runoff of both scenarios (Figure 8.12). Except for high elevations at the eastern and western margins of the catchment, the rainfall-elevation gradient scenario generally caused more runoff. Summed up over the whole catchment area, rainfall scenario 1 generated roughly 3000 m³ of runoff, whereas the other scenario yielded only 2400 m³. This explains the differences in simulated hydrographs. Because scenario 1 yielded better results at both runoff stations it is concluded that the rainfall-elevation gradient scenario represents catchment rainfall more realistically. At station 02 this scenario reconstructed the measured peak within its uncertainty range. The measured peak discharge of station 04 (1007 l/s) was the second highest peak ever measured at this station. This is noteworthy because stronger rainfalls during events 12, 15 and 16 did not reach this value. The resulting runoff coefficient during event 4 for sub-catchment 04 amounting to 63% is also rather high (Table 9.1). Both rainfall scenarios were not able to reconstruct this extreme value.

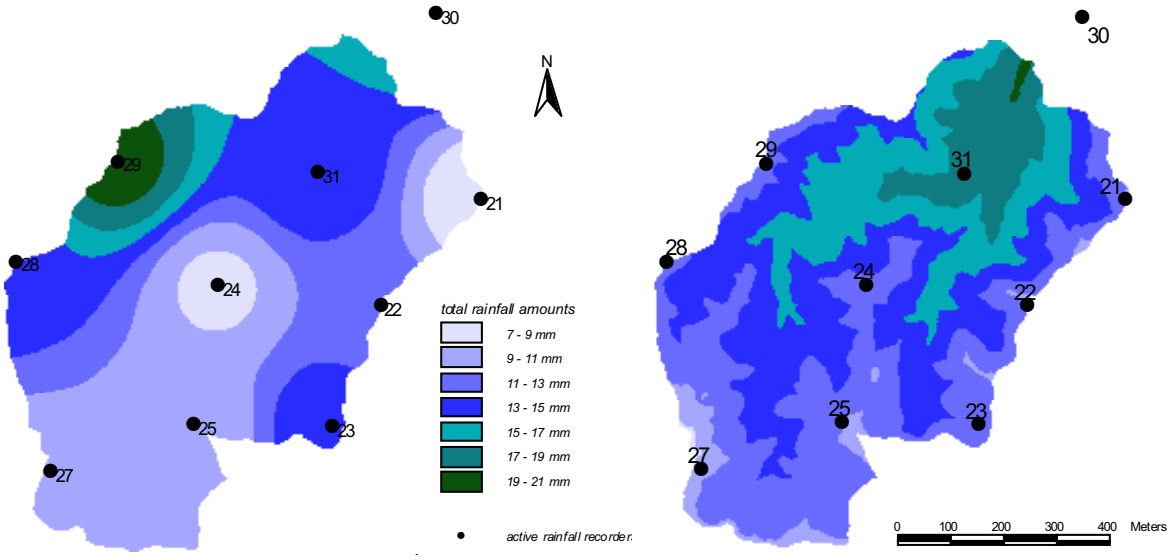

Fig 8.11: Total rainfall amounts of rainfall input scenarios, a: scenario 1, b: scenario 2

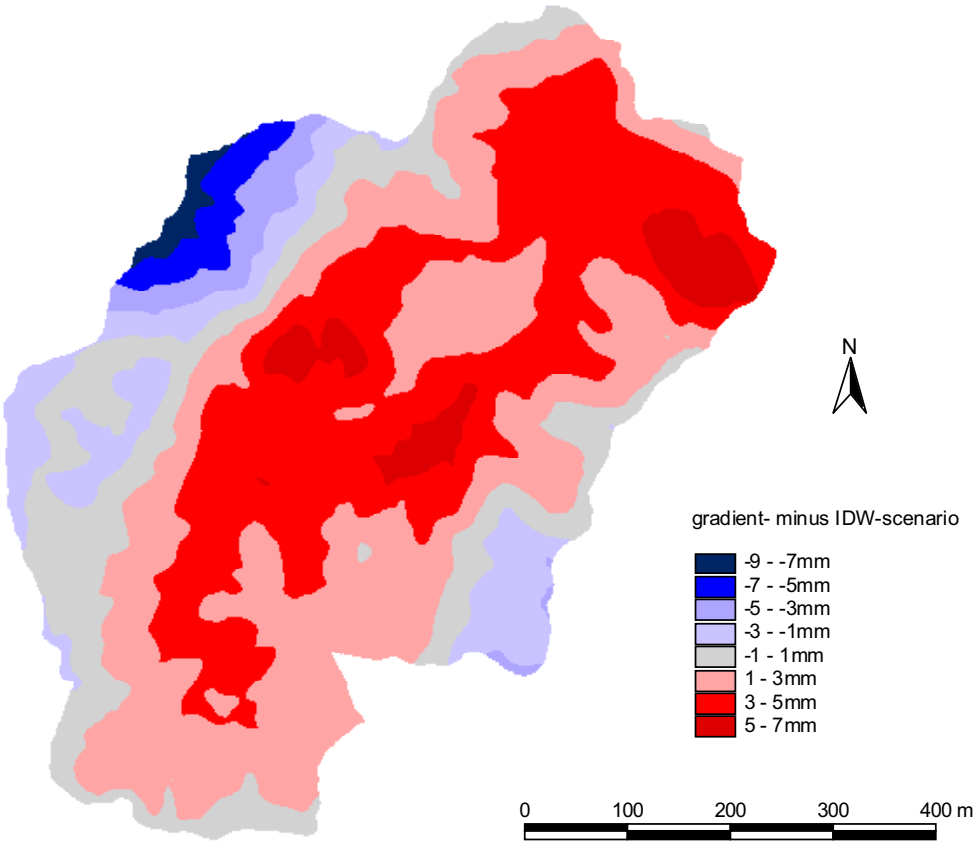

Fig 8.12: Difference in generated runoff by scenario 1 and scenario 2

8.3 Event 6, 25-11-1968

8.3.1 Event characteristics and available data

A few hours before the rainfall that caused event 6 reached Nahal Yael, another storm cell moved over the catchment yielding at least 3.7 mm of precipitation. Because the data records of this pre-event were not complete, this value indicates only a lower limit of the real rainfall amount. The storm of event 6 occurred around 5:00 pm and lasted some 30 minutes during which maximal intensity measured at two stations reached 40 mm/h. Due to pre-wetting of the surface resulting from the preceding rainfall, 4.7 mm were sufficient to initiate surface runoff and channel flow. However, at station 02 only a very small flood wave yielding only 35 l/s peak discharge arrived.

Rainfall was recorded at 10 rain gauges all over the catchment. Runoff data was available from all 4 discharge stations. Station 05 registered a strange shape of the hydrograph and the runoff coefficient comparing measured rainfall and runoff amounted to 1.8 (Table 9.1), i.e. more water was leaving the catchment then entering by precipitation. Sub-catchment 04 showed with 0.95 a very high runoff coefficient as well. Hence, the measured volume is called into question for event 6 at these two stations.

8.3.2 Model results

To account for the pre-rain, the model's runoff generation routine was modified. The time span between the consecutive events was not sufficient to empty the shallow surface storages by evaporation. Because the surface was still moisturised from the preceding rain, depression and detention losses are minimised. Thus, the initial loss was set to zero for all terrain types, resulting in immediate Hortonian runoff generation if rainfall rate exceeded infiltration capacity.

At station 02 simulated peak discharge amounted to just below 40 l/s, which is very close to the measured value of 35 l/s (Figure 8.13). However, the long drawn behaviour of the measured curve could not be simulated. Simulated peak discharges at stations 04 and 05 lie within the uncertainty range of the measured values although the unrealistic measured runoff volumes were underestimated significantly (Figure A.21 and A.22 respectively). At station 03, the model underestimates peak discharge and volume significantly (Figure A.20).

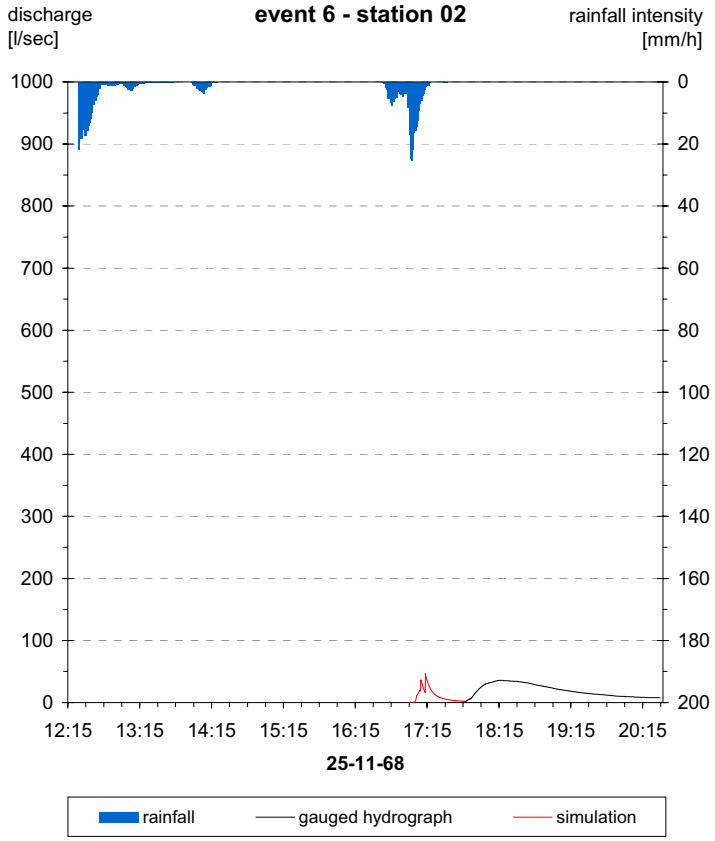

Fig 8.13: Model result event 6, station 02

8.3.3 Discussion

For this event during which the flood was nearly lost into the alluvium on its way downstream, the model's transmission loss routine could be checked. Uncertainty ranges of measured discharges exceeded those of the preceding events because

sedimentation from events 3 and 4 reduced the quality of stage measurement. Furthermore, uncertainty of low stages as measured at station 02 is generally higher. At station 04 the flood wave was reconstructed very well. On its way downstream to station 02 most of the flood water infiltrated into the alluvial fill resulting in a diminished peak of 35 l/s at the basin outlet. The model simulated the peak of this substandard hydrograph very well. Although the volume remained underestimated, it was concluded that the process of transmission losses is represented correctly by the model. Because measured volumes were obviously overestimated at stations 04 and 05 (unrealistic runoff coefficients), it is not remarkable that simulated volumes were much smaller. Significant underestimation occurred at station 03. Based on the good simulations for sub-catchments 04 and 05, it is believed that the runoff generation routine represents natural processes sufficiently. The underestimation at 03 may rather stem from uncertainties in rainfall input, i.e. from neglecting storm cell motion. As shown by model application for event 3, the difference between two rainfall scenarios (instantaneous rainfall onset and moving storm cell) caused strongest differences in simulated runoff at station 03, due to the longish shape of sub-catchment 03.

8.4 Event 7, 21-01-1969

8.4.1 Event characteristics and available data

Two consecutive rain spells were responsible for the double peak event 7 (subdivided into 7A and 7B). One of the nine rainfall gauges that monitored rainfall during this event showed a time shift of 8 hours presumably due to errors of the clockwork. Except for this recording gauge, timing uncertainty amounts to ± 12 minutes for both sub-storms. The first rainfall (event 7A) yielded low to medium intensity rainfall (up to 10 mm/h) for 90 minutes before intensities increased for about 30 minutes with maximum intensity of 47 mm/h measured at rainfall station 24. In total, the first substorm amounted to 8.2 mm and caused a peak of 400 l/s at station 02. The second substorm (event 7B) took place 3 hours after the termination of event 7A. A small intermediate rainfall occurred between the two substorms with intensities not exceeding 6 mm/h. The duration of event 7B was about one hour with maximum intensity amounting to 75 mm/h. 9.2 mm total rainfall were responsible for the second peak that reached 625 l/s at the basin outlet.

Station 02 was the only station with confirmed discharge data. At the other stations, water level data was processed as described in Chapter 6.2.2 resulting in a lower and upper boundary of discharge rating.

8.4.2 Model results

Because of the short time span between the successive storm events and the intermediate rainfall, the model was started and run for both substorms together.

Runoff response at all stations for both substorms was dramatically underestimated by the model. At station 02 the simulated peak for 7A yielded less than 100 l/s, whereas the measured peak amounted to 400 l/s (Figure 8.14). During event 7B the underestimation is not as extreme, but still significant. The shapes of the measured hydrographs at station 02 were not exactly reproduced, for event 7A a little recession was modelled during the rising limb. At stations 03, 04 and 05 estimated peaks even fell below the uncertainty range of runoff measurement (Figures A.23-A.25). Only at station 04 simulated discharge for event 7A somewhat exceeded the minimum uncertainty boundary or discharge measurements.

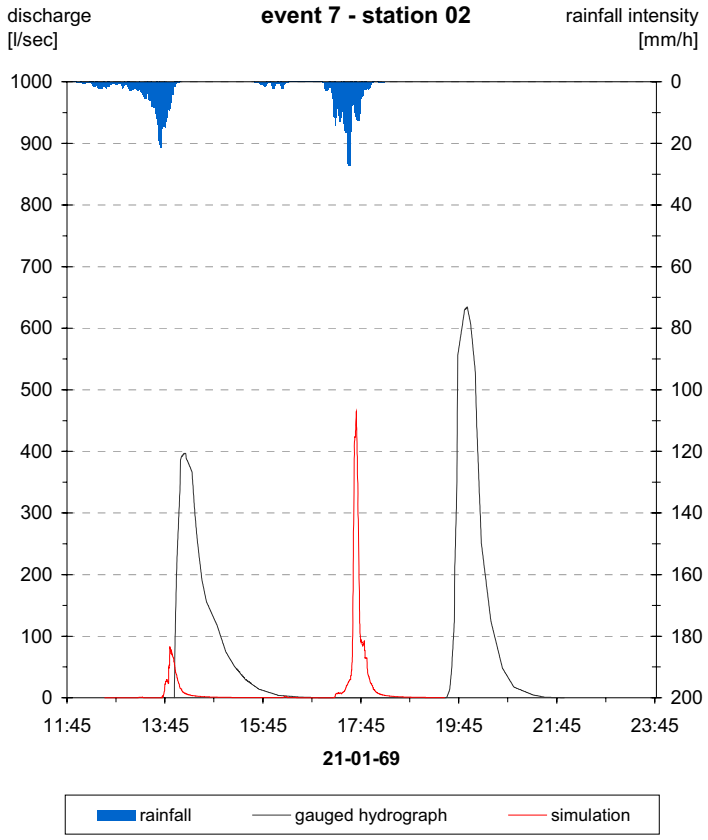

Fig 8.14: Model result event 7, station 02

8.4.3 Discussion

Model application for this event was not successful. Except for the simulation of event 7A at station 04, all peak discharges were significantly underestimated. This is true even for comparison with the minimum rating scenarios of gauged discharge. Errors in model structure, e.g. neglected scale transition of runoff, would rather cause overestimation of

runoff. Errors in the transmission loss routine would cause unequal results at stations 02 and 03 compared to 04 and 05 because the latter are not influenced by transmission losses. An unrecorded pre-event might be a reason for underestimation during event 7A, but this would only affect model results of event 7A and does not explain underestimation during event 7B. Because the model underrates both sub-storms in the same order of magnitude, this explanation is not satisfying. There is evidence, that quality of discharge data was lower during this event than before. Firstly, exact rating was not possible at stations 03, 04 and 05 (a range of discharge rating defined by an upper and a lower limit was determined). The uncertainty of these gauged data is extraordinary high (compare Chapters 6.2.1 and 7.1). Second, low data quality is shown in timing of the measured discharge data. For stations 04 and 02 the second peak arrives very late, for station 03 the peak of event 7B rushed through even before the second spell of rainfall started. A reason for model failure might also be found the particularity of this event. The high intensity period of event 7A started only 90 minutes after the onset of rainfall. By that time, it is possible that surfaces were already saturated and virtually all rainfall was transformed into runoff. If that process occurred during event 7B due to the short drying period and the intermediate rainfall, the model's runoff generation routine is not able to rebuild this phenomenon. Starting the model for both substorms together implied lowest infiltration rate (at the value of the final infiltration rate) during the high intensity period of 7A and during the complete event 7B. By that, highest runoff generation within the limits of the model already took place.

8.5 Event 8, 25-03-71

8.5.1 Event characterstics and available data

This event was a rather small one that yielded only 4.5 mm of rainfall, similar to event 6. No preceding rainfall wetted the surface. Runoff was generated on the slopes and recorded at stations 04 and 05, but did not reach stations 02 and 03. Rainfall records were available from 10 recording stations without any additional information. Thus, calculation of areal precipitation was carried out using synchronised data and inverse distance weighting. Discharge data was recorded at both upper stations (04 and 05). Peak discharges were very low and afflicted with unavoidable uncertainty. Firstly, uncertainty of low stages is per se higher than for high stages and second, discharge measurement was already influenced by accumulated sediment of the preceding event 7. At the uppermost stations with little alluvium upstream this is not as severe as at station 02 but should be kept in mind.

8.5.2 Model results

Except for very small amounts of water, the simulated flood wave did not reach the basin outlet at station 02 (Figure 8.15). At station 03 no discharge at all was simulated (Figure A.26). Compared to the measured data at stations 04 and 05 the model overestimated the measured hydrographs (Figures A.27, A.28). The double peak character recorded at station 04 could not be reconstructed.

8.5.3 Discussion

For this minor event, the model was applied successfully concerning transmission losses as no flow was simulated at stations 02 and 03. Overestimation at the upper stations 04 and 05 was significantly, although the uncertainty ranges of measured discharge are relatively high. The runoff coefficients of measured rainfall and runoff are rather low with 13.6% and 8.4% for station 05 and 04 respectively (Table 9.1). Thus it is difficult to decide whether overestimation arises from inaccurate gauged discharge data (which seems more likely than errors in rainfall measurement) or from errors in model structure. Model structure errors could be related to disregard of runoff losses during scale transition from small runoff plots to the unit of sub-catchments (see Chapter 7.3).

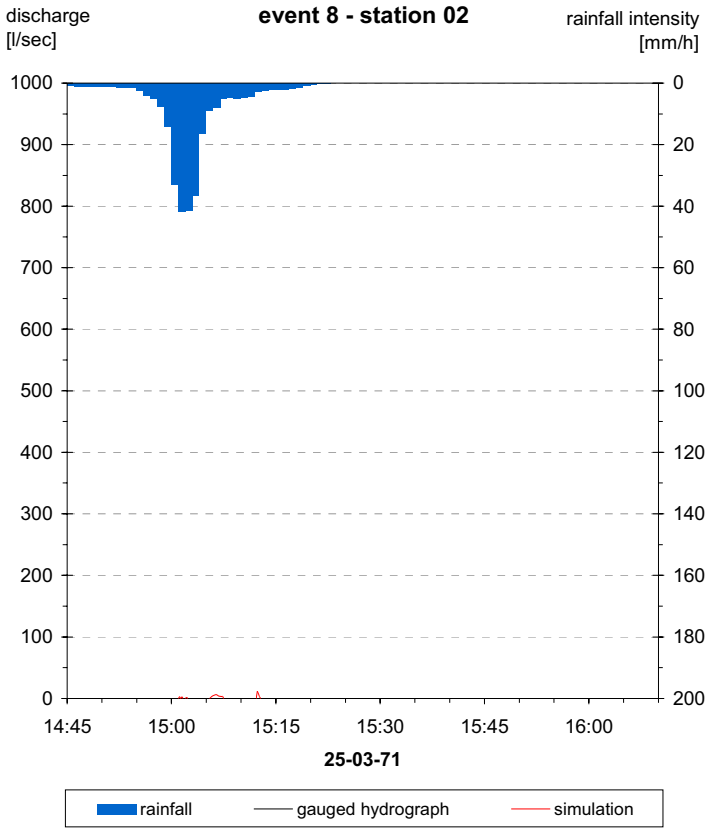

Fig 8.15: Model result event 8, station 02

8.6 Event 12, 20-02-1975

8.6.1 Event characteristics and available data

This was a very special event divided into two sub-events (12A and 12B). It was unique both in the large rainfall amount (for both substorms together 160% of the mean annual rainfall amount were measured) as well as in its duration. During the night of February, 20th, small amounts of rainfall wetted the surface of Nahal Yael. Event 12A was finally caused by 33 mm of rain of light intensity which began in the morning. Rainfall lasted continuously for about 6 hours. Rainfall data was available from stations 24, 26 and 26a. As 26 and 26a represent different measuring devices at the same location (Lambrecht pluviograph and tipping bucket) only station 26 (pluviograph) was considered. Thus, comparability with other events during which only pluviographs were recording is ensured.

The flow of event 12A lasted 6 hours and was the longest flow time ever measured in Nahal Yael. The peak discharge in the upper parts of the watershed was 250 l/s at station 04 and in the lower part at station 02 it reached 750 l/s. The shape of the hydrographs appeared not as usual as a single peak but the long-lasting flow rather showed 4 peaks of different size and shape.

Six hours after the determination of 12A a violent rainstorm that yielded a total amount of 18 mm fell in two high intensity spells. During this substorm the same rainfall gauges were operating as during event 12A. Additionally station 30 was active for 15 minutes during the maximum of event 12B. This data was also incorporated to interpolate catchment rainfall. The peak discharge of event 12B amounted to 1900 l/s at station 02 with a very sharp rise and an equally sharp falling limb. From the other measuring weirs no runoff records were available.

8.6.2 Model results

The model was run separately for both sub-storms. For event 12A the model was started at 3:00 am in order to account for the pre-rain during the night. During the time span between the two substorms surface storages were exposed to evaporation. To what extent surface storages were emptied could not be determined since meteorological conditions (i.e. temperature, wind speed) are not known. Assuming a maximal daily evaporation rate of 10 mm/day (SCHICK 1988), it is possible that during the 5.5 hours between the successive storms all water stored in surface depressions has evaporated. On the other hand, cloudiness, low temperatures and moist air may prevent high values of actual evaporation. Hence, for event 12B two scenarios were run. Scenario 1 used the runoff generation routine with the general values for the initial loss parameter, for scenario 2 the initial loss was reduced to zero.

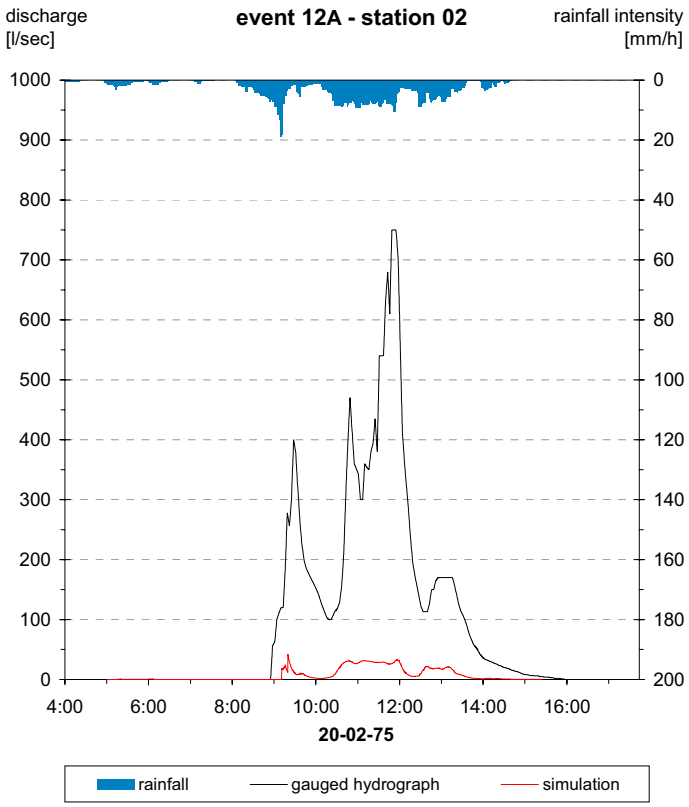

Fig 8.16: Model result event 12A, station 02

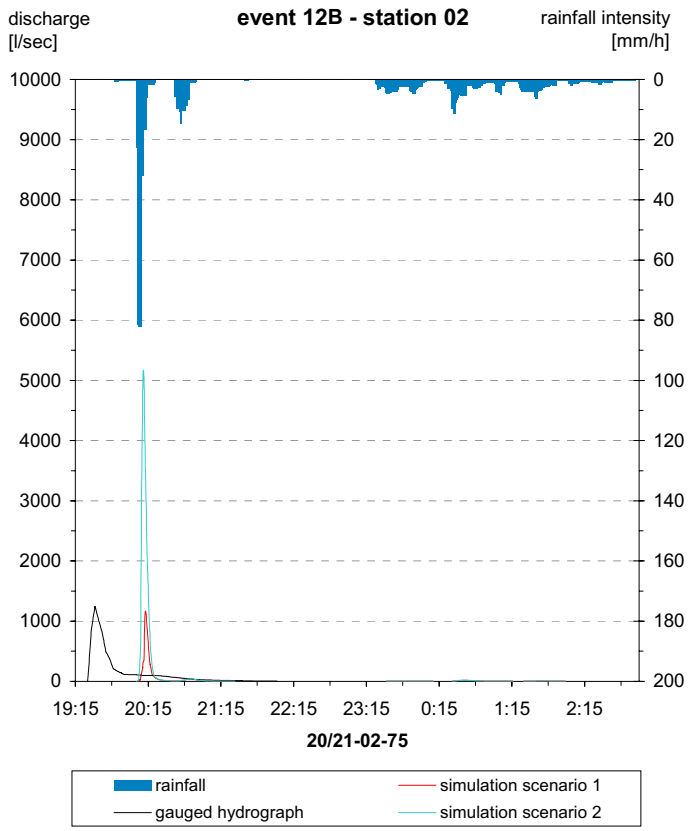

Fig 8.17: Model results event 12B, station 02

For event 12A the model output underestimated measured runoff at both stations with available data although the temporal behaviour resembled the measured hydrographs (Figures 8.16, A.30). At station 02 simulated discharges underestimated measured values by factors of 10 to 20. At station 03 the first peak was not simulated at all, while it was very pronounced at station 05 (Figures A.29 and A.31). Results of the two scenarios for event 12B are considerably different. While scenario 2 (not accounting for initial losses) produced a peak discharge of 5150 l/s and exceeded the measured curve by far, scenario 1 yielded peak discharges within the uncertainty range of the measured discharge (Figure 8.17). The other stations were ungauged during this event, but the simulations for scenario 2 always exceed those for scenario 1 by factors varying between 1.5 and 3.4 (Figures A.32-A.34).

8.6.3 Discussion

The model run of event 12A was started with the first raindrops at 3:26 am. After the initial loss was satisfied, the first surfaces reacted with runoff generation around 5:00 am. Because of very low intensity rainfall, only minor amounts of simulated runoff were produced and reached the gauging stations. The spatial pattern of times at which the initial loss was filled up is presented in Figure 8.18. Ten minutes after the initial loss had been satisfied, final infiltration rates were reached and used to calculat infiltration excess. Thus, infiltration rates of most surfaces had already reached their final values, when the main storm occurred around 8:00 am. Except for 5 minutes of higher rainfall intensities reaching 24 mm/h, rainfall intensities remained below 15 mm/h. During the complete duration of event 12A (6 hours), the model generated runoff exclusively on bare rocky surfaces, which were the only surfaces whose final infiltration rates were exceeded by rainfall intensity. Comparison of simulated and measured discharge gave evidence, that reality was not represented sufficiently by the runoff generation routine for this event. The temporal behaviour of simulated discharge was similar to the measured hydrograph; both mainly reflected the temporal pattern of rainfall intensities. The flood wave measured at stations 04 and 02 could not be explained, if only bare rocky surfaces were active for runoff generation. Seemingly during such a low intensity long duration event, additional processes not incorporated into the model took place, e.g. saturation of surfaces hardly allowing infiltration. Because events like 12A occur only rarely, the special runoff generation processes during such long-lasting rainfall events are not yet understood.

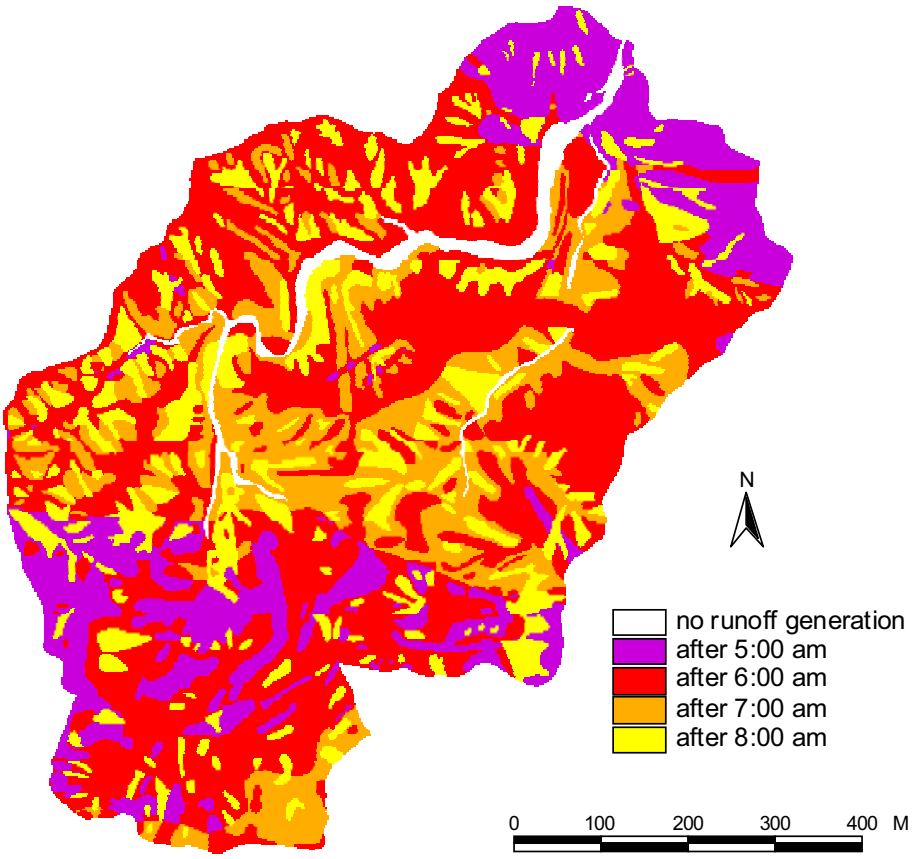

Fig 8.18: Onset of runoff, event 12A

Model results for event 12B suggested that scenario 1 with the general value for the initial loss is closer to reality than scenario 2 (not accounting for initial losses) (Figures 8.16, A.35). Because gauged discharge data was available only for station 02, no assessment of model performance concerning transmission loss behaviour was possible. Thus, it might have happened that effects of different error sources compensated each other, resulting in good model fits only pretending high model accuracy. On the other hand, it is as well possible that the assumptions of scenario 1 were correctly describing natural processes, which might explain good model performance.

8.7 Event 15, 26-12-1980

8.7.1 Event characteristics and available data

Event 15 is another double-peak event divided into two parts, 15A and 15B, which took place in the late afternoon of the day after Christmas 1980. The temporal rainfall pattern was more complex. Around noontime a first storm cell moved across Nahal Yael yielding on average 6.8 mm. No information was available whether this storm caused any runoff.

A second rainfall began three hours later, lasting for one hour and yielding 3.4 mm. The storm that was responsible for events 15A and 15B occurred half an hour after the termination of the preceding storm at 4:30 pm. This storm instantaneously reached very high intensities close to 50 mm/h. During the first 10 minutes of the storm, flow was initiated causing the first peak at the runoff gauges. Altogether, the storm lasted 8 hours, but with very low intensities. Only a second spell with intensities above 20 mm/h generated runoff again and caused the second, smaller discharge peak.

Rainfall was monitored by two stations only (station 26 on the hindermost mountaintop and station 31 close to measuring weir 02, both equipped with Lambrecht pluviograph devices). Because they showed differences in rainfall amount persistently for all sub-storms in the order of 25%, different rainfall scenarios were applied. The first scenario used as model input a simple mean value of both stations applied uniformly all over the area. A second scenario was calculated using synchronised data and IDW interpolation. As third model input, the rainfall-elevation gradient yielded spatially distributed information on rainfall.

During this event, the accuracy of the discharge stations was considerably improved compared to events 6, 7, 8 and 12 because this was the first event that reached the basin outlet after the construction of the dam and the sediment clearing. The rating of discharge was preliminarily accomplished without additional information. Because the runoff volume exceeded the volume accumulated in the reservoir behind the dam, the hydrograph was modified fitting the hydrograph to the volume in the reservoir and accounting for scour during the event.

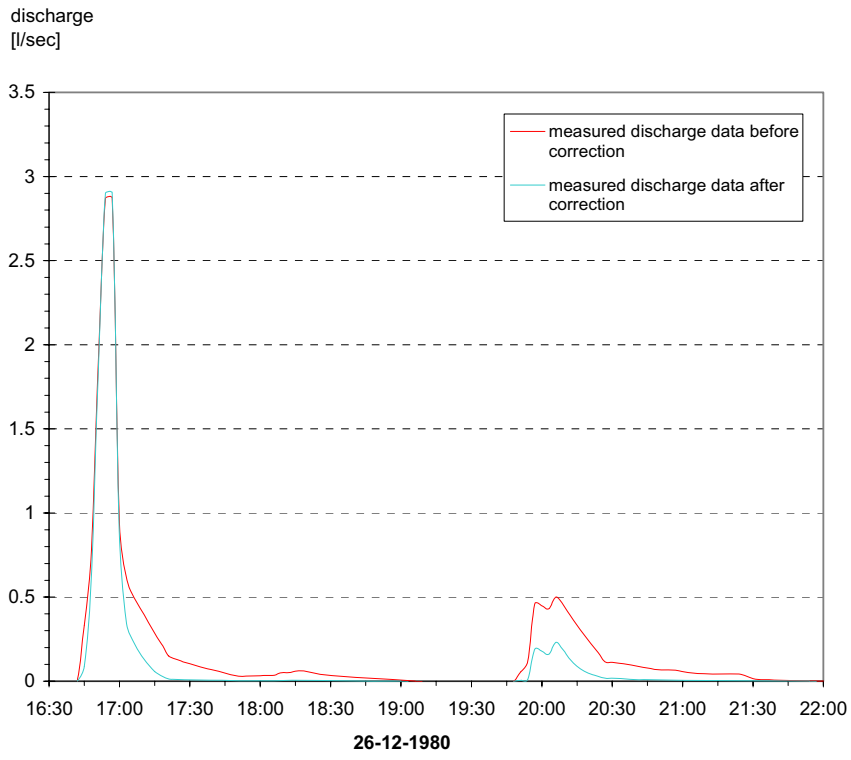

Fig 8.19: Comparison of measured discharge data before and after correction with additional data for station 02

Figure 8.19 compares the resulting hydrographs. The peak of the modified hydrograph lay above the original peak due to scouring during the event whereby more water passed through the enlarged cross-section. The second peak was reduced accounting for the volume measured in the reservoir. Except for station 03 all stations were in operation during event 15A and 15B. The first peak was typical in its very fast rise and nearly equally fast recession at all stations. It amounted to 2900 l/s at station 02, and 722 l/s and 650 l/s at stations 04 and 05 respectively. The second peak was a rather small one reaching 215 l/s at the basin outlet. The shape of the measured hydrograph at station 05 is somewhat suspicious, since flow is not reduced to zero between the subsequent peaks and the recession of the second peak differs from those recorded before. Possibly, this measured hydrograph overestimates real discharge.

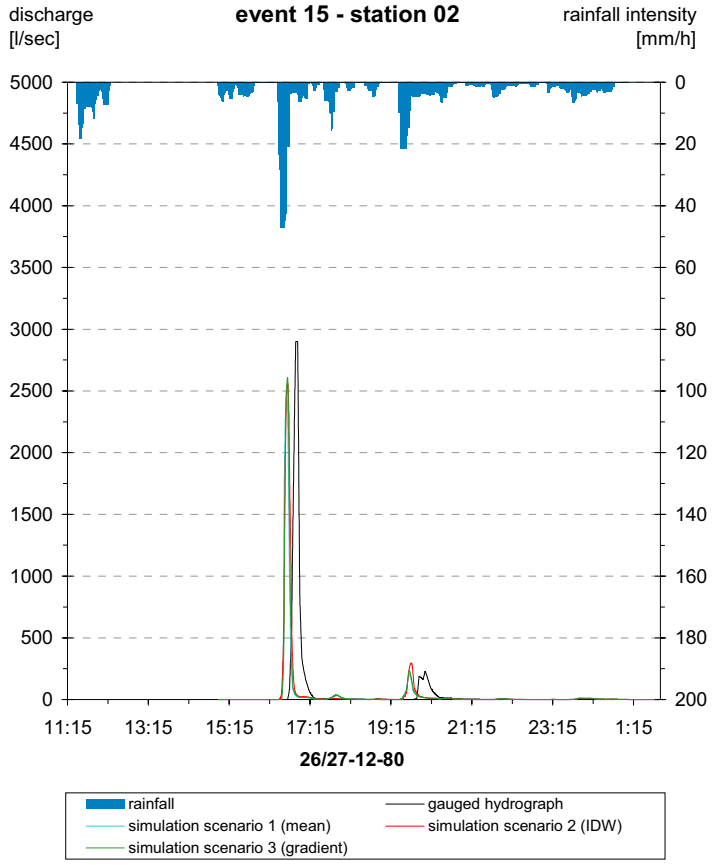

Fig 8.20: Model results event 15, station 02

8.7.2 Model results

Since rainfall did not stop completely after its high intensity period around 4:30 pm, this double peak event was regarded as one event by the model. The model run was initiated at 3:00 pm accounting for the pre-rain that started at that time. Because surfaces were still wetted by the rainfall around noontime, initial loss was set to zero. Compared to events 3 and 4 when different rainfall scenarios produced very different

hydrographs, for this event the three rainfall scenarios generally yielded similar results. All simulated peaks were within the uncertainty range of the measured data except for the first peak at station 05, which was underestimated by all scenarios (Figure A.38). At station 02 the simulations matched the measured hydrograph nearly perfectly, although the double peak character of the second peak was not reconstructed (Figure 8.20). Similar to all other stations, very small flows were simulated between the two main peaks.

8.7.3 Discussion

During this event model simulated measured discharge data very well except for station 05, whose uncertainty was higher compared to the other stations during this event. Good fit of model results indicated that spatial rainfall distribution is represented sufficiently by one station close to the main channel and one mountain top rainfall gauge. Three rainfall scenarios yielded similar results, in which small deviations displayed the characteristics of each scenario (e.g. the rainfall-elevation gradient scenario yielded smallest discharges at the upper stations 04 and 05). A reason for the small difference of the scenarios is found in rainfall input during the high-intensity rainfall period. During this 6 minute spell around 4:40 pm both stations recorded exactly the same rainfall intensity. Thus, the different rainfall scenarios yielded the same uniform rainfall distribution all over the catchment during the time of strongest runoff generation.

Despite the ignoration of the initial loss the small rainfall amounts between 3:00 and 4:00 pm infiltrated completely. Timing uncertainty was especially high during this event. The time shift between both rainfall stations amounted to 43 minutes. The timing of the measuring weirs was also unclear. At station 04 the main peak was recorded at noontime and the time difference between station 05 and 02 amounted to 31 minutes, which is too long to be explained by travel times of the flood wave. Thus rainfall data was synchronised to the mean time of both stations.

8.8 Event 16, 31-10-1981

8.8.1 Event characteristics and available data

Event 16 was the last event before a period of more than 3 years without flow at station 02. It was a rather strong event that yielded 20 mm during one hour with maximum intensity measured at rainfall station 26 of 65 mm/h. Only three of the recording rainfall gauges were in operation. The resulting flow peaked with 2430 l/s at station 02 relatively high. Stations 03 and 05 yielded 1050 l/s and 600 l/s respectively, while flow data from station 04 was not available.

8.8.2 Model results

This event was simulated well by the model. The peak at station 02 was slightly overestimated with 2685 l/s, but still within the uncertainty range of the measured value (Figure 8.21). The recession of the measured hydrograph could not be completely reconstructed. At station 03 the simulated peak matched the measured curve well, although the simulated rise was not as steep as the measured one (Figure A.39). At station 04 a small pre-peak was simulated (Figure A.40). Except for this small first rise, which was found to be even stronger for station 05, the measured hydrograph of station 05 was nicely reconstructed by the model (Figure A.41).

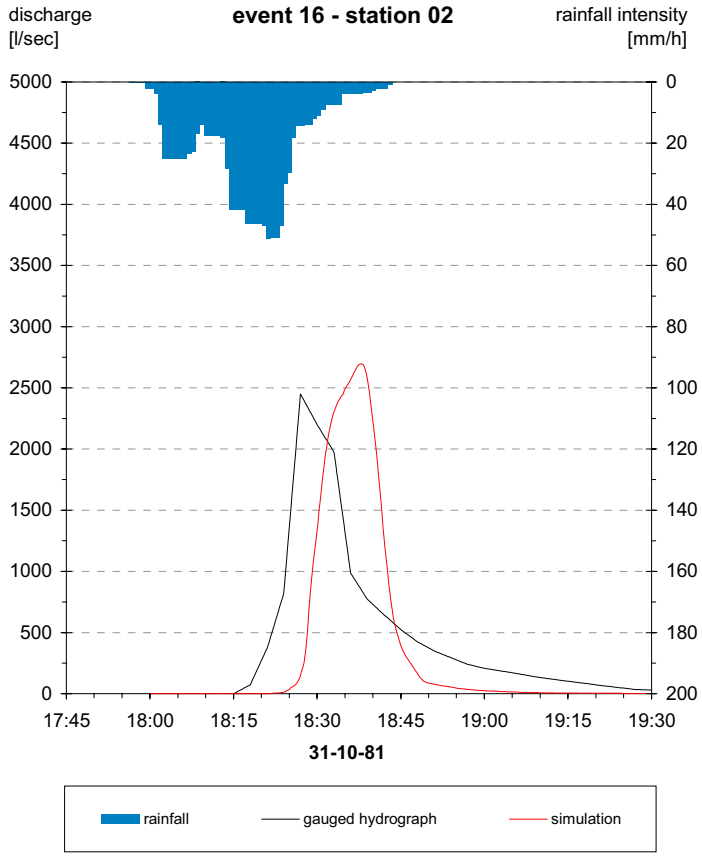

Fig 8.21: Model result event 16, station 02

8.8.3 Discussion

Model application simulated discharge data very close to the measured runoff. The shapes of the hydrographs were not reproduced correctly, but all peak discharges fell within the uncertainty ranges of measured peak discharge. Small peaks preceding the main peak at station 04 and 05 were simulated as answer to the first spell of rainfall around 6:05 pm. Rainfall input differs from other events as this time the smallest rainfall amount and peak intensity was measured at the low lying station 31. However, rainfall input and model assumptions seem to represented real processes correctly. Because a

good model fit was derived at all runoff stations it is unlikely that multiple errors in data, parameters or model structure balance each other.

8.9 Event 27, 18-10-1997

8.9.1 Event characteristics and available data

GRODEK (2002) and GRODEK ET AL. (2000) provide a detailed analysis of this event with respect to impacts of floods to urbanised alluvial fans in desert areas. In the early morning of October 18th a storm cell produced the first rain spell which amounted to 5 mm in Nahal Yael. The centre of this cell was located over the town of Eilat (only 4 kilometres apart), where it yielded a total of 16 mm. A second rain spell occurred around 8:00 am and recorded only 2.5 mm. The flood was caused by the third stormcell, which moved with its centre over Nahal Yael and amounted to 25 mm. This storm was further subdivided into 4 high intensity spells with maximum intensities for each substorm above 40 mm/h and intermissions of 10 to 15 minutes duration. During the second spell of this event, the maximum intensity ever measured in Nahal Yael was reached with 126 mm/h. Rainfall was recorded by two tipping buckets inside the catchment at stations 31 and 33, both located in the main alluvial reach.

Runoff response was as usual very rapid in the small catchment. Due to the rainless intervals between the rain spells discontinuous flow was recorded at station 05. In contrast, at station 02 at the basin outlet continuous flow was recorded that peaked to 3700 l/s, the highest peak discharge ever measured at that station. During this event the spill way of the reservoir was active for the first time (LEKACH & GRODEK, personal communication). Because the storage of the reservoir was not sufficient to store the total flood waters, it was not possible to determine cumulative volume of the event this way. Thus, the gauged hydrograph was not modified and uncertainty ranges of measured data were higher than during events 15 and 16.

The recurrence interval of this event is estimated at a hundred years (GRODEK ET AL. 2000). Discharge was measured at stations 02 and 05 as well as by a flume located in the narrow meander of the main channel, named station 08.

8.9.2 Model results

Because of the short time between the four rain spells, the model was run for all substorms together, similar to the model run of event 7A and 7B. This is the first event, where simulated hydrographs significantly overestimate the measured discharge at all stations. The model simulated more than double the measured values for the first two peaks at station 02. Furthermore, the continuous character of the flow at station 02 could not be reconstructed; the model simulated four distinct peaks. At both other

stations, 08 and 05, the results were similar. At theses stations discontinuous flow was recorded and simulated but peaks were generally overestimated by a factor two or more.

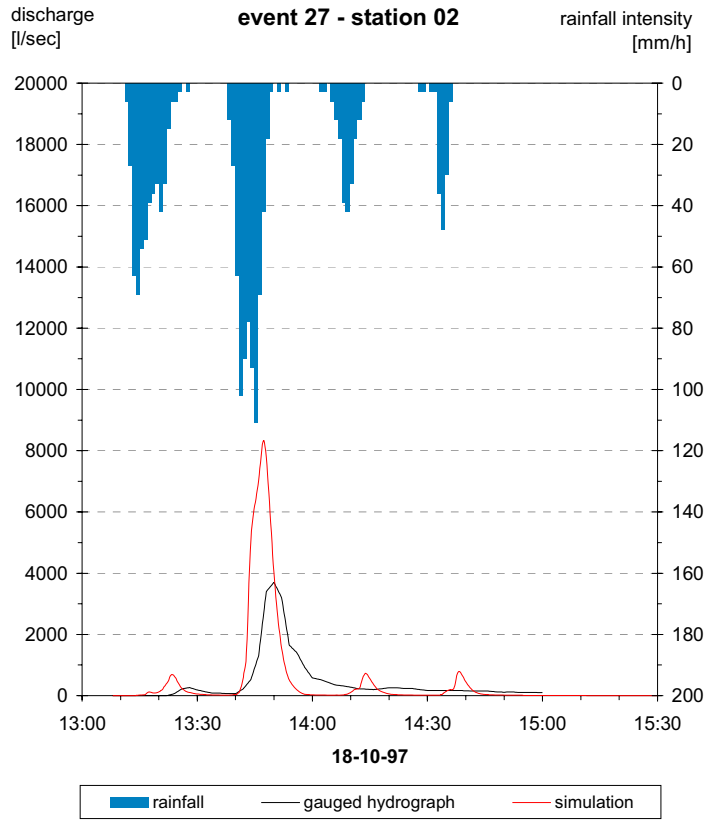

Fig 8.22: Model result event 27, station 02

8.9.3 Discussion

Rainfall intensities of event 27 were extraordinary high, especially during the first two rain spells. As the model reacts very sensitive to rainfall intensity, large amounts of runoff were generated. If a rainfall gradient occurred during this event, it was not detectable as both rainfall stations recorded at relatively low lying locations. Thus it is possible that catchment precipitation was overestimated by these two rainfall gauges causing overestimation in simulated hydrographs as well. Because the simulations yielded similar results at all stations (02, 08 and 05) it is unlikely that the transmission loss routine is responsible for model overestimation. A wrong representation of transmission losses would cause different results at stations influenced by alluvium compared to stations with bare rock channels upstream. Transmission losses were only active until the wetting front reached the bottom of the alluvial fill. The wetting front reached the maximal depths of the alluvium of 1.8 meter shortly after the third peak had been measured. After that time, no infiltration into the alluvium occurred in the model. Because mean depth of alluvium amounts only to 0.8 meters, transmission losses

stopped much earlier at most segments. The wetting front reached a depth of 80 centimetres during the rising limb of the second, main peak. Overestimation of peak discharge occurred already at the first peak during which transmission losses took place at every location. Thus an incorrect representation of transmission losses due to the stopping wetting front is not very likely.

During this event rainfall intensities in the order of the intensity used the during sprinkler experiments (~ 70 mm/h) on which the runoff generation routine is based were reached and exceeded for several minutes. It could well be that infiltration rates increased with increasing rainfall intensity (SALMON & SCHICK 1980) to values above the rates assumed in the model. This would explain overestimated runoff generation. Assuming correct rainfall input and runoff generation, overestimation of discharge may stem from the neglected losses during scale transition (compare Chapter 7.3). The uncertainty of discharge measurement is relatively high during this event. Sedimentation from the preceding events influenced water level measurements. Furthermore, the records of the flume are per se not as accurately as those of the installed measuring weirs. Additionally, under extreme flow conditions (extremely low or high water level) uncertainty is generally increased. Especially during the second, main peak, underestimation of true discharge by the stream flow stations is possible. The continuous character of the hydrograph at station 02 is somewhat surprisingly as both other stations 05 and 08 recorded 4 distinct peaks. GRODEK ET AL. (2000) interprets the flow continuum as the sequential addition of the flow from small subcatchments along the main water course. During previous events measurement problems during the recession were evident. This might also be a reason for the long falling limb of the hydrograph at station 02.

8.10 Conclusion

Nine events were incorporated into model application. For each of these events, the characteristics of rainfall and resulting flows as well as data availability are summarised. The performance of the model is described for all events independently. Results of model runs were compared to measured discharge data with greatly differing results. For some events, discharge was strongly underestimated (events 3, 4, 7, 12A), whereas the model overestimated runoff during event 27 considerably. The remaining events were simulated reasonably well. A semi-quantitative overview of model performance is given in Table 8.1.

9 Discussion

9.1 Data analysis

Even though the database of Nahal Yael comprises extraordinary long data records which have been collected by elaborate equipment, this data is not error-free. Each rainfall-runoff event in the desert is unique and responsible for extreme operating conditions of the instruments. Under the severe climatic conditions with long non-operating periods between subsequent events mechanical constraints and extreme rainfall properties may cause data quality problems. To examine the quality of the rainfall and runoff data, the ratio of rainfall volume to runoff volume (runoff coefficient) was determined (Table 9.1). In some cases (event 6, station 04 and 05; event 7, station 02 and event 12A, station 04) where the runoff coefficient is close or above 100% the measured rainfall can not be responsible for the measured discharge volume. Unrealistic runoff coefficients may either stem from inaccurate rainfall or runoff measurements or from a combination of both. The obvious errors may be responsible for some of the model failures (event 7A+B; 12A, station 04).

Generally, rainfall coefficients increase with increasing rainfall amount (CHOW ET AL. 1988). This tendency was also found in the Nahal Yael data. The small rainfall quantity of event 6 only caused a runoff amounting to about the tenth part of the rainfall amount (runoff coefficient 9%), while 27% of the 33 mm of the rainfall event 12A left the catchment as runoff at station 02. Event 15B showed very low rainfall-runoff ratios, but this event was exceptional concerning the temporal distribution. The runoff generating part of this event fell within the first hour of the five hours lasting rainfall. During the last 4 hours the rainfall intensity did not exceed 10 mm/h. As a result, low runoff coefficients of 3% at station 02 and 5% at station 04 were measured.

In the context of runoff coefficients, the rainfall-runoff ratios of events 3 and 4 seem exceptionally high. Unfortunately, during event 3 the volume was not recorded at station 02 but only peak discharge was measured. Thus the runoff coefficient could not be determined but the peak of 1100 l/s is relatively high. Direct comparison with events that yielded the same amount of rainfall (event 7A and 7B) was not possible, because these runoff measurements were particularly questionable. Event 12 A showed a similar peak discharge like event 3 but the shape of the hydrographs was not comparable due to the long-lasting flow during event 12A. The rainfall-runoff ratios for event 3, stations 03 and 04 also seem very high compared to the other reliable runoff coefficients (excluding runoff coefficients of event 7A, 7B and unrealistic values of events 6 and 12A).

Tab 9.1: Rainfall-runoff ratios for simulated events determined from measured data

	mean max. intensity [mm/h]	rainfall amount [mm]	peak discharge at station 02 [l/s]	station 02	station 03	station 04	station 05
E3	34.5	9.2	1100				
rainfall amount [m³]				4630	1170	846	503
measured runoff volume [m³]				-	511	322	-
runoff coefficient				-	44%	38%	-
E4	49.5	14.0	2100				
rainfall amount [m³]				7577	1902	1344	792
measured runoff volume [m³]				3977	-	843	-
runoff coefficient				52%	-	63%	-
E6	31.6	4.7	30				
rainfall amount [m³]				2391	575	426	244
measured runoff volume [m³]				213	187	407	445
runoff coefficient				9%	33%	96%	182%
E7-A	27.1	8.2	850				
rainfall amount [m³]				4088	891	734	441
measured runoff volume [m³] *				3593	153	87	147
runoff coefficient				88%	17%	12%	33%
E7-B	41.6	9.2	1900				
rainfall amount [m³]				4593	1166	904	542
measured runoff volume [m³] *				7466	443	406	105
runoff coefficient				163%	38%	45%	19%
E8	42.0	4.5	0				
rainfall amount [m³]				2426	556	472	274
measured runoff volume [m³]				0	-	40	37
runoff coefficient				0%	-	8%	14%
E12-A	18.7	33.3	1080				
rainfall amount [m³]				16954	4313	2985	1757
measured runoff volume [m³]				4571	-	3038	-
runoff coefficient				27%	-	102%	-
E12-B	87.8	18.3	2050				
rainfall amount [m³]				9429	2400	1636	961
measured runoff volume [m³]				1312	-	-	-
runoff coefficient				14%	-	-	-
E15-A	47.3	19.3	2750				
rainfall amount [m³]				9831	2591	1424	817
measured runoff volume [m³]				1853	-	418	461
runoff coefficient				19%	-	29%	56%
E15-B		18	470				
rainfall amount [m³]				9154	2363	1493	871
measured runoff volume [m³]				267	-	75	239
runoff coefficient				3%	-	5%	27%
E16	51.7	20.0	2350				
rainfall amount [m³]				10042	2480	1914	1095
measured runoff volume [m³]				2411	744	-	536
runoff coefficient				24%	30%	-	49%
E27	117	25.4	3700				
rainfall amount [m³]				12912	-	-	1338
measured runoff volume [m³]				2910	-	677	253
runoff coefficient				23%	-	-	19%

* : for stations 03, 04 and 05 comparison with gauged minimum scenario

Runoff coefficients of event 4 were even higher than those of event 3. The value of 52% at station 02 was nearly double as high as the second highest runoff coefficient determined for event 12A. The runoff coefficient of 63% at station 04 was also very high compared e.g. to that of event 15A which amounted to only 29%.

Thus it is concluded that events 3 and 4 indicate some sort of *data inconsistency*. The measured runoff coefficients differed significantly from those determined for the majority of events. A sufficient explanation for this inconsistency was not found. It might be related to uncertainties in data collection, either of rainfall or of runoff measurements. Rainfall measurements may be negatively influenced by wind influence or sloping ground, problems of discharge measurements were mostly related to sedimentation.

Model results reflected the data inconsistency. While for the majority of events model performance could be interpreted sufficiently, reasons for the underestimation of hydrographs during event 3 and 4 were not clear. For example, underestimation of events 7A and 7B were related to highly uncertain discharge measurements and model failure of event 12A was associated to additional processes during runoff generation not incorporated into the model. Similar explanations could not be found for events 3 and 4.

9.2 Rainfall input

The present study emphasises the strong influence of rainfall input on quality of model output. Model application with different rainfall scenarios yielded considerably different results depending on spatial (event 4) and temporal (event 3) rainfall distribution.

Rainfall intensity as model input plays a key role in model application, since it determines directly the amount of generated runoff. Over- or underestimation of real rainfall intensity results immediately in errors in the amount of generated runoff, which is propagated throughout the model resulting in over- or underestimation of hydrographs. Unfortunately, the rainfall data base did not allow quantitative estimates of precipitation uncertainty ranges for each event.

MELCHING (1995) reports of two investigations where timing errors due to clock malfunctions and lack of synchronisation were the most common cause of rain gauge unreliability. Especially in the small watershed Nahal Yael synchronisation of rainfall data played an important role. In the present study, an instantaneous onset of rainfall all over the catchment had to be assumed, neglecting trajectories of the storm cells. The consequent impact was illustrated by event 3. For this event, model results from rainfall input following true storm trajectories and from synchronised rainfall data were compared, whereby the former scenario yielded much better model results.

A decisive part in the determination of catchment rainfall is the interpolation from point data. The spatial pattern of rainfall distribution measured by the gauge network at distinct points is transferred to the whole area to determine catchment rainfall. In this

study, the IDW-method was used for all events. Model applications of event 4 indicate that a rainfall recording station is not always representative for a larger area. Using the IDW method errors occurred, because small rainfall amounts recorded on a mountain top in the centre of the watershed had unrealistic strong influence on calculated rainfall amounts in the adjoining channel area. Rainfall input derived from the rainfall-elevation gradient seemed to represent the natural processes more closely.

Quality of model output did not increase with increasing number of rainfall gauges. It would have been expected that the greater the number of recording stations the greater the accuracy of catchment rainfall determination. In contrast, model results rather suggest, that rainfall input is even better represented by a smaller number of rain gauges at representative sites. In Nahal Yael, 9 of 13 stations were located on mountain tops. During events with a high number of active Lambrecht recorders, most were located at high elevations. It seems that this rain gauge set-up overvalues the influence of high elevations. This is underlined by the fact that during the first events with many operating stations (events 3, 4, 6, 7) discharge and volumes are generally underestimated. For events 8 and 12 no statement on the influence of rainfall on model output can be given, as other problems (uncertain discharge measurement, errors in model structure) prevail. Event 15 and 16 approve the theory as catchment rainfall is well represented by 2 or 3 stations, at least one in the main channel and one on a mountain top. Model overestimation of event 27 is partly related to the same phenomenon. In this case, rainfall input was provided by two valley stations only, possibly not being representative for the entire watershed, but largely overestimating rainfall.

9.3 Runoff generation

Parameters during runoff generation are initial loss and infiltration rates at every minute time step down to a final infiltration rate. Model results from event 12B indicate that the initial loss is a decisive parameter for runoff generation. Runoff generation is retarded by the initial loss parameter varying according to terrain type. During model runs without initial loss (event 6, event 12B (scenario 2) and event 15), infiltration and runoff generation started immediately after the onset of rain on all terrain types except for alluvium. After the initial loss has been satisfied, the ratio of infiltration rate and rainfall intensity decides how much runoff is generated. Although infiltration rates directly influence the amount of generated runoff, a primary role is played by the rainfall intensity as rainfall rates usually exceed infiltration rates and vary over much larger ranges than the uncertainty of infiltration rates.

Infiltration behaviour of the surfaces had been determined in the field under rainfall simulator conditions using constant rainfall intensities in the order of 70 mm/h. In the strict sense, infiltration rates are only valid for similar rainfall intensities. SALMON &

SCHICK (1980) found a positive linear relationship between rainfall intensity and final infiltration rate, meaning that during highly intense rainfall more water infiltrates as during lower intensity rainfall. Thus during events of intensities lower than 70 mm/h the model may rather underestimate runoff generation. This might also deliver an explanation for the overestimation of event 27. Maybe during rainfall of intensities greater 70 mm/h more water infiltrates as assumed by the model and less runoff is generated.

The model structure was kept as simple as possible, accounting only for the main process (Hortonian overland flow) during runoff generation. Despite one exception, the dominance of Hortonian overland flow is confirmed by good model results. Only if additional processes take place as during event 12A, during which presumably saturation might have played a role due to exceptional prolonged rainfall, the model was not able to reconstruct a plausible flood hydrograph.

9.4 Runoff concentration

Runoff concentration is a critical part in model conception. By using a simple, constant time delay as runoff concentration mechanism, continuous overland flow is discretised assuming that all runoff generated anywhere on the slope needs the same travel time to reach the adjoining channel segment. The decisive parameter of the concept is the travel time (= time-lag), it was determined for each slope independently from literature studies (see Chapter 5.2.2). The time-lag was not very sensitive during model application when varied by a factor of 2. The direct response of subcatchments causes steepening of the flood wave but has no influence on flood volume. An alternative concept of runoff concentration, e.g. time distribution of runoff, would probably attenuate and broaden the hydrograph. Because of steep slopes, small model units and very short travel times it seemed reasonable to apply the simplified time delayed impulse model. It was further validated by model application which yielded generally good results in reconstruction of the rising limbs of the hydrograph. During some events (3, 4 and 7) the measured hydrograph was even steeper than the reconstructed one. However, gauged recession was usually more pronounced than reconstructed by the model.

An additional critical point is the assumption that after the initial loss has been filled and rainfall excess generates overland flow, no water is lost on its way downslope to the channel. At a much larger scale LANGE (1999) introduced a scale transition factor accounting for the transfer of runoff from the plot to sub-catchment scale. Good model performances and underestimation of runoff indicate, that scale transition losses may be neglected, although model results of events 8 and 27 would improve when applying an additional loss component. It seems more likely, that during these events, measurement errors prevailed.

9.5 Channel flow and transmission losses

9.5.1 Channel flow

As already noticed by LANGE (1999) and WAGNER (2002), mass conservation in the channel routing and transmission loss component of the model was incomplete during this model application as well. Water balance calculations were carried out for sub-catchment 05 and for the entire catchment. The amount of generated runoff (which serves as input to the channel routing routine) was compared with the simulated discharge for stations 02 and 05. To assure a complete water balance for station 02 transmission losses were neglected. The results of these calculations are summarised in Table 9.2. Generally, a water excess was noted for most events, i.e. more water was leaving the channel routing routine than entering. For the majority of events the deviation between input and output volume was around 5% or less, which is acceptable for a comparison of volumes. Flood volumes are generally less predictable and the uncertainty ranges of measured discharge volume are much higher than 5%. Especially during the events with low flows (events 6 and 8), the mass balance was not stable. This might be due to the fact, that small values of discharge are much more affected by rounding errors during routing calculations. Besides events with low volume, mass balance problems were evident for events 3 (scenario 2 only) and 12B. For these two events model results should be treated with more caution. On the other hand, numerical errors may be responsible for more than complete mass conservation, if the time step and distance step of the model were not selected correctly (FREAD 1993). Because the Courant-condition (see Chapter 5.3.1) is satisfied for 256 out of 258 channel segments this is not very likely.

The channel routing routine is responsible for flood wave propagation, i.e. the displacement of the wave throughout the channel course. For channel routing, the channel geometry is the dominant factor. LANGE (1999) showed that routing parameters had much more influence on flood arrival than on peak discharge or volume. Of all channel parameters, the Manning coefficient was the most sensitive (LANGE 1999). Unfortunately, wave celerity and timing of hydrographs could not be validated due to inaccurate time measurements of both rainfall and runoff stations. The time span of wave translation from station 05 or 04 to the basin outlet (about 2 minutes) was much shorter than timing uncertainty (at least 15 minutes). However, the routing component of the model yielded good estimates of measured hydrographs for steep waves of short duration as well as during more prolonged events. Despite large underestimation of peak and volume for event 12A, the shape of the simulated hydrograph was close to the measured one even for this long-lasting event.

Tab 9.2: Mass balance of channel routing, input vs. output

	station 02	station 05
E3 (scenario 1)		
water amount from runoff generation routine [m³]	1371.1	125.9
runoff volume not considering transmission losses [m³]	1409.6	127.4
deviation	2.8%	1.2%
E3 (scenario 2)		
water amount from runoff generation routine [m³]	1240.7	140.5
runoff volume not considering transmission losses [m³]	1497.8	148.0
deviation	20.7%	5.3%
E4 (scenario1)		
water amount from runoff generation routine [m³]	2937.3	191.8
runoff volume not considering transmission losses [m³]	2974.5	193.2
deviation	1.3%	0.7%
E4 (scenario 2)		
water amount from runoff generation routine [m³]	2399.9	140.6
runoff volume not considering transmission losses [m³]	2468.6	141.8
deviation	2.9%	0.9%
E6		
water amount from runoff generation routine [m³]	796.8	62.3
runoff volume not considering transmission losses [m³]	857.6	71.6
deviation	7.6%	14.9%
E7 A+B		
water amount from runoff generation routine [m³]	2610.4	191.3
runoff volume not considering transmission losses [m³]	2739.5	203.4
deviation	4.9%	6.3%
E8		
water amount from runoff generation routine [m³]	269.0	30.4
runoff volume not considering transmission losses [m³]	343.4	43.0
deviation	27.7%	41.4%
E12-A		
water amount from runoff generation routine [m³]	2488.8	82.8
runoff volume not considering transmission losses [m³]	2478.4	89.5
deviation	-0.4%	8.1%
E12-B		
water amount from runoff generation routine [m³]	1842.5	157.6
runoff volume not considering transmission losses [m³]	2143.7	185.0
deviation	16.3%	17.4%
E15 A+B		
water amount from runoff generation routine [m³]	5398.6	333.8
runoff volume not considering transmission losses [m³]	5534.7	344.3
deviation	2.5%	3.1%
E16		
water amount from runoff generation routine [m³]	4951.3	502.3
runoff volume not considering transmission losses [m³]	4758.8	479.6
deviation	-3.9%	-4.5%
E27		
water amount from runoff generation routine [m³]	7714.7	753.2
runoff volume not considering transmission losses [m³]	7981.2	765.3
deviation	3.5%	1.6%

9.5.2 Transmission losses

In general, infiltration of flood waters into the alluvial fill may reduce peak discharges and volume of desert floods. In Nahal Yael, this may occur only in the main channel reach between 02 and 04 and in small parts of sub-catchment 03 that are filled with thin alluvium. Transmission loss parameters were responsible for a high portion of parameter uncertainty during application of the model inside the Zin-catchment (LANGE 1999). In Nahal Yael, the extent of the alluvial fill is relatively well known, which reduces the uncertainty to reproduce transmission losses considerably. A higher portion of uncertainty was caused by the unknown behaviour of infiltration rates during flood events.

Transmission losses were validated comparing model results at stations not influenced by transmission losses (04 and 05) to those at station 02. Model application of event 6 suggested that the transmission losses routine represents natural processes sufficiently. Even during the multi-peak event 15 transmission losses were simulated correctly by the model. After the first peak, the wetting front had reached the base of the alluvium and the second flood rushed over a saturated channel fill without any transmission losses.

The model sets a threshold discharge (*qrobeg*) above which transmission losses occur. The infiltration into the alluvium is stopped if the discharge falls below the value of this parameter or if the base of the alluvial fill is reached. Sensitivity tests of qrobeg proved that this parameter is not very sensitive if varied only over a range of small absolute values (e.g. between 0 l/s and 20 l/s) (Fig. 9.1). Because of generally fast rising limbs of the hydrograph, the time difference is very short between the points of time at which transmission losses start for different scenarios. During this small time span the wetting front advances only a few millimetres, thus the effect of qrobeg is rather small.

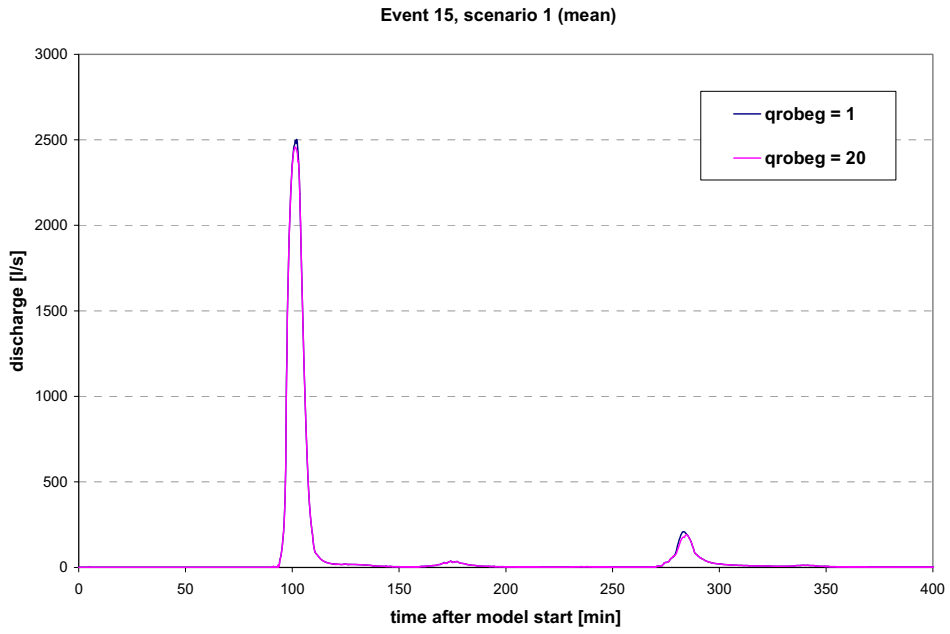

Fig 9.1: Sensitivity of model output to variation of parameter qrobeg

Influence of “red layer”:

The red-layer unit below the surficial grey alluvium is considered as a buffer to transmission losses. Due to its compacted nature, infiltration rates of the red layer are much lower than those of the alluvium above (LEKACH ET AL. 1998). To analyse the impact of the red layer, it was incorporated into the model as a barrier for infiltration at its average depth of 0.5 metres below the surface. After the wetting front had reached this depth, transmission losses into the alluvium were completely stopped by the model.

Tab 9.3: Time spans between onset of transmission losses and peak discharge

	A	B	C
E3 (scenario 1)	29.0	32	3.0
E3 (scenario 2)	26.5	35.5	9.0
E4 (scenario 1)	24.5	36.6	12.1
E4 (scenario 2)	25.5	38.3	12.8
E6	42.0	46	4.0
E7 A	71.0	80	9.0
E12-A	251.0	256	5.0
E12-B	21.5	26.83	5.3
E15 A	91.5	103	11.5
E16	21.8	38	16.2
E27	5.0	14.5	9.5

A: onset of transmission losses [min after model start]
B: time till peak [min after model start]
C: time difference [min]

The depth of the wetting front was depending on the infiltration rate and porosity of the alluvial fill as well as on the time since infiltration into the alluvium had started (defined by the threshold parameter qrobeg). Because porosity and infiltration rate were kept constant in the model, the advancement of the wetting front was only determined by the time after the initiation of transmission losses. With assumed values of 0.3 for the porosity and 480 mm/h as infiltration rate, the wetting front needed around 19 minutes to reach the depth of the red layer (0.5 metres). Table 9.3 shows that the time spans from onset of infiltration (qrobeg = 1 l/s) to peak discharges of simulated floods were always below 19 minutes for station 02.

Event 16 was chosen to illustrate influence of the red layer on flood hydrographs. Fig. 9.2 illustrates a comparison of simulated discharges with and without the red layer. Peak discharge of the red-layer scenario is higher than without stopping wetting front at 0.5 metres depth. Because of earlier onset of flow in the upper channel segments, here the wetting front reached the depth of 0.5 meter earlier. The alluvium of these segments was obviously saturated before the main peak rushed through, stopping transmission losses and causing a higher peak discharge. Another effect was noted in the falling limb

of the hydrograph. Here, a secondary peak occurred due to reduced transmission losses. Out of 38 channel segments with alluvial fill, only 24 segments are deeper than 0.5 meters and contribute to the change in infiltration properties. Because event 16 simulated a rather long rising time, it is assumed that the influence of the red layer on peak discharge is not very strong for the majority of events. Additionally, the assumption used by the model that the red layer is completely impermeable, is simplifying and results in overestimation of the red layer's impact. Infiltration rates of the red layer as determined by infiltrometer tests were considerably lower than those of the coarse alluvium but not negligible (LEKACH ET AL. 1998). Thus, the effect of the red layer on most flood hydrographs in Nahal Yael is not very strong and most pronounced for the falling limb, where it may cause secondary peaks.

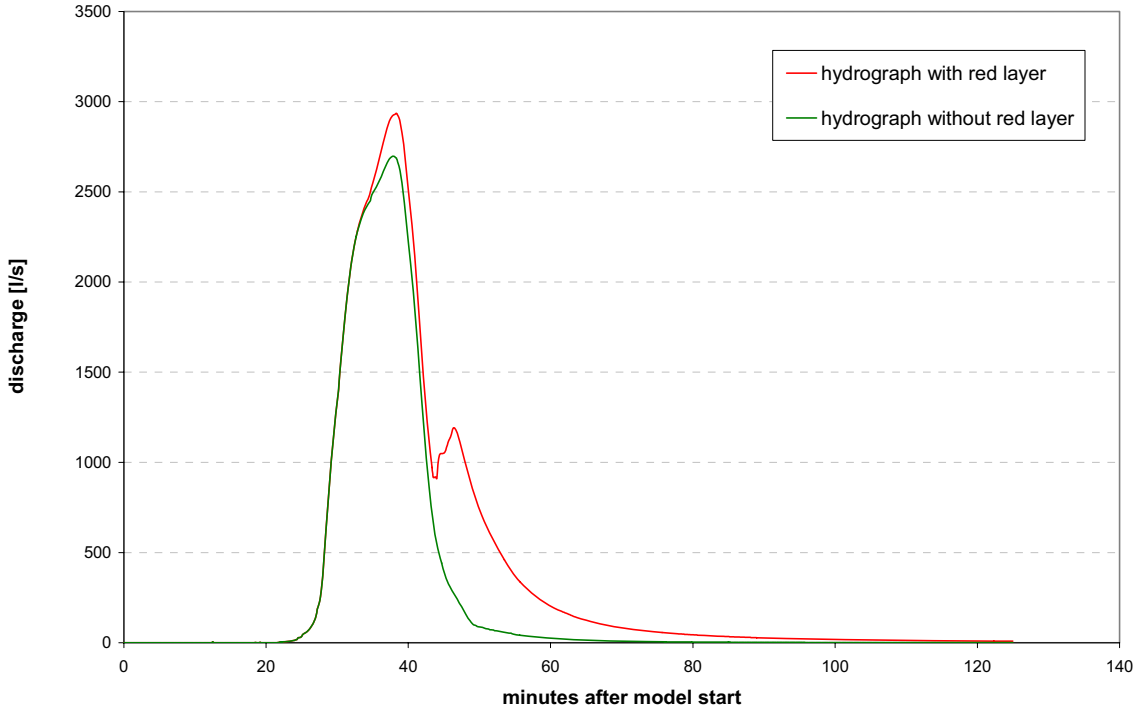

Fig 9.2: Comparison of simulated hydrographs accounting and not accounting for red layer at station 02, event 16

9.6 Conclusion

The application of the ZIN-Model in Nahal Yael emphasises the importance of rainfall input for hydrologic modelling. Data inconsistencies were detected in the rainfall and runoff data of two events which were also reflected in rather poor model results for these events. This confirms that crucial factor in rainfall runoff modelling is the determination of catchment precipitation. Despite demonstrable small scale variations (SHARON 1970A;

SHARON 1970B; SHARON 1972A; SHARON 1972B; SHARON 1980; SHARON & ARAZI 1997) catchment rainfall seems to be represented sufficiently by one valley and one mountain top rainfall gauge. In contrast, the accurate determination of catchment rainfall from a denser rain gauge network without additional information on storm cell trajectories or rainfall elevation gradient was not always successful. The multitude of rainfall recorders located at high elevations rather seemed to be not representative for catchment rainfall.

Another important factor for the successful application of the ZIN-Model is the knowledge on antecedent conditions. A pre-event may play a significant role for catchment response on a storm as it influences both hillslope runoff (reduced initial loss) and main channel hydrograph propagation (reduced transmission losses).

With accurate rainfall data the model application was mostly successful. The rather simple structure of the ZIN-Model accounting solely for the main processes Hortonian overland flow and transmission losses is able to rebuilt natural processes sufficiently. Limitations arise if additional processes (e.g. saturation overland flow) that are not incorporated into the model take place. Only one example (event 12A) during 30 years of research was found where the storm lasted exceptionally long and runoff generation mechanisms seemed to be more complex than purely Hortonian.

Flood volume is governed by rainfall input and the runoff generation routine with the main emphasis on rainfall. From the plot, generated runoff is transferred by runoff concentration to the adjoining channel segment. This module was mainly responsible for timing and temporal distribution of generated runoff. Because of small sub-catchments, extreme slopes and high flow velocities, the simplified concept of runoff concentration was applied successfully. The channel flow routine determined the timing and shape of the final hydrograph, while transmission losses reduced flood volume considerably.

The impact of the red layer, a partial buffer to transmission losses at a depth of 0.5 meter below the channel surface, was studied for event 16. Flood volumes increased due to the red layer unit as transmission losses were stopped by the model when the wetting front had reached the depth of the red layer. Because of generally fast rising limbs of the hydrographs, the red layer mainly influenced the recession of flood hydrographs. Its main impacts were longer lasting recessions and secondary peaks.

Generally, very good results were found for the rising limbs of the hydrographs, while partially long-lasting recessions were not reconstructed. Obvious and assumed uncertainties in discharge measurement certainly contributed to differences in gauged and simulated volumes, while for most events good fits of peak discharge were found.

10 Concluding remarks and outlook

The ZIN-Model was one of the first approaches in arid zone hydrological modelling that totally refrained from calibration. Rainfall characteristics in the hyperarid zone differ from one event to another and are highly variable in space and time. Each runoff event can be compared with an extraordinary flood in humid catchments. In Nahal Yael the recurrence interval of an event reaching the basin outlet is estimated to 2-2.5 years, while flow at the uppermost station 05 occurs every 1-1.5 years (LEKACH ET AL. 1998). This study validated the non-calibrated approach and showed that in general the ZIN-Model is able to reproduce flood hydrographs of diverse extreme storm events in the desert.

The unique data base of Nahal Yael parallels from the point of view of observed events a record of one or two years duration only in a non-arid watershed. On the other hand, considering the difficulties of extreme arid hydrology, which suffers from unattended instrumentation operating under adverse environmental conditions, a data base including more than 30 years of data records is very valuable. Still, modelling problems were mostly related to uncertainties in rainfall or runoff data. Inconsistencies in data records were revealed by analysing the runoff coefficients derived from measured rainfall and runoff data. Two out of nine event showed exceptional high rainfall-runoff ratios and could not be simulated successfully. The decisive factor for the quality of model output was the quality of the pattern of catchment-wide rainfall input. The fact that two rainfall stations at representative sites seemed to represent catchment rainfall sufficiently and even better than eight or more stations was one of the rather astonishing findings of this investigation. Further investigations, e.g. comparison of catchment rainfall derived from these two stations only with the rainfall input interpolated from more than eight stations, are required to approve this thesis.

Each of the model's sub-systems runoff generation, runoff concentration and channel flow represented natural processes satisfactorily. Limitations of the model only arise, if additional processes not incorporated into the conceptual structure of the model occur. This was the case when during long-lasting rainfall events runoff generation processes more complex than purely Hortonian overland flow occurred. In the small catchment of Nahal Yael it was possible to simplify runoff concentration by using a constant time delay. For future applications in larger areas, the original approach of a response function used in the Zin-catchment or a storage approach might be more capable. The flexible model structure consisting of sub-routines allows incorporation of catchment specific features like the red layer. After successful simulation of transmission losses, the model could be modified to analyse the impact of a fluvio-pedogenic unit (red layer), which obstructs channel bed infiltration. Nahal Yael is the first arid catchment, in which calibration of the ZIN-Model would have been possible due to extensive data records on both rainfall and runoff. However, it was refrained from calibration as calibrating single

events would not improve the model for future applications but only embellish the model performance of this study.

To facilitate future applications of the model, a challenge is to develop a more user-friendly interface of the model, e.g. incorporating all model sub-systems into one computer program.

Model results indicated that a scale transition factor accounting for processes active during the transition from the plot scale (0.5 m²) to the larger scale of sub-catchments (about 1000 m²) may be disregarded. This surprising finding is in contradiction to results of YAIR (1992). It implies that obviously all generated runoff reaches the channel network, and no water is lost into the colluvial base of a slope. On the other hand, good model results might have been obtained due to the wrong reasons. If for instance, the rainfall intensities were underestimated, the amount of generated runoff is underestimated as well. Due to this effect neglected scale transition factors might be compensated. However, in this study it was found that underestimation of precipitation is one order of magnitude too small to balance scale transition losses completely. It is therefore unlikely that mistakes in process understanding are responsible for satisfactory model results.

To obtain reliable statements for water resource management with classical hydrologic standard methods (flood frequency analysis, estimations of extreme discharges and volumes) long data records are required. The experience from Nahal Yael confirms that several decades of observation are needed to supply a reasonable data basis for such purposes. This study demonstrates that the non-calibrated modelling approach of the ZIN-Model provides an appropriate alternative. Although a considerable amount of field-based parameters has to be determined, it is worth the effort if no data records are available, a common situation in arid catchments. Thus, the ZIN-Model is a convenient tool to simulate high magnitude floods in ungauged arid catchments. Compared to model application in the Zin-catchment, decreasing simulation uncertainty was obtained due to more detailed field information on infiltration properties and extent of alluvium.

References

ABDULRAZZAK, M. J., SORMAN, A. U. & ALHAMAS, A. S. (1989): Water balance approach under extreme arid conditions - a case study of Tabalah Basin, Saudi Arabia. *Hydrological Processes* **3**: 107-122.

ABRAHAMS, A. D., PARSONS, A. J. & LUK, S.-H. (1986A): Field measurement of the velocity of overland flow using dye tracing. *Earth Surface Processes and Landforms* **11**: 653 - 657.

ABRAHAMS, A. D., PARSONS, A. J. & LUK, S.-H. (1986B): Resistance to overland flow on desert hillslopes. *Journal of Hydrology* **88**: 343-363.

ABRAHAMS, A. D., PARSONS, A. J. & WAINWRIGHT, J. (1994): Resistance to overland flow on semiarid grassland and shrubland hillslopes, Walnut Gulch, southern Arizona. *Journal of Hydrology* **156**: 431-46.

ADAMI, A. & DA DEPPO, L. (1986): On the systematic errors of tipping bucket recording rain gauges. In: B. Sevruk (Ed.), *Correction of precipitation measurements*. Züricher Geographische Schriften, Zürich, 27-30.

AGNEW, C. & ANDERSON, E. (1992): Water resources in the arid realm. *Physical environments series*. Routledge, London, 329 pp.

ANDERSON, M. G. & BURT, T. P. (1990): Process studies in hillslope hydrology. Wiley, Chichester, 539 pp.

BENDAVID-NOVAK, H. & SCHICK, A. P. (1997): The response of Acacia tree populations on small alluvial fans to changes in the hydrological regime: southern Negev Desert, Israel. *Catena* **29**: 343-351.

BEVEN, K. J. (2001): Rainfall-runoff modelling - the primer. Wiley, Chichester.

BOGDANOVA, E. G. (1966): Investigation of precipitation measurement losses due to the wind (in Russian). *Trans. Voyeykov Main Geophys. Observ.* **195**: 40-62.

BULL, L. J. & KIRKBY, M. J. (EDITORS) (2002): Dryland rivers - hydrology and geomorphology of semi-arid channels. Wiley, New York.

BULL, L. J. ET AL. (2000): The impact of rainstorms on floods in ephemeral channels in southeast Spain. *Catena* **38**(3): 191-209.

BULL, W. B. & SCHICK, A. P. (1979): Impact of Climate Change on an Arid Watershed: Nahal Yael, Southern Israel. *Quarternary Research* **11**: 153-171.

BWG (2001): Rauheiten in ausgesuchten schweizerischen Fließgewässern. *Berichte des BWG - Serie Wasser*, **1**. Bundesamt für Wasser und Geologie, Bern.

CHOW, V. T., MAIDMENT, D. R. & MAYS, L. W. (1988): Applied Hydrology. McGraw-Hill, New York.

CLAPP, E. M. ET AL. (2000): Sediment yield exceeds sediment production in arid region drainage basins. *Geology* **28**(11): 995-998.

CUNGE, P. A. (1969): On the subject of a flood propagation computation method (Muskingum Method). *Journal of Hydraulic Research* **7**(2): 205-230.

DEICHMANN, U. & EKLUNDH, L. (1991): Global digital data sets for land degradation studies: a GIS approach, *GRID Case Study Series*. UNEP/GEMS and GRID, Nairobi, Kenya, 29-32. Internet source: http://www.grid.unep.ch/data/grid/gnv172.php (as of December, 12th 2003)

DEVRIES, J. J. & HROMADKA, T. V. (1993): Computer models for surface water. In: D.R. Maidment (Ed.), *Handbook of Hydrology*. McGraw-Hill, New York, 21.1-21.39.

DVWK (1991): Starkniederschläge in der Bundesrepublik Deutschland. *Schriftenreihe des DVWK*, **97**. Parey, Hamburg, Berlin, 190 pp.

DYCK, S. & PESCHKE, G. (1995): Grundlagen der Hydrologie. Verlag für Bauwesen, Berlin.

EL-HAMES, A. S. & RICHARDS, K. S. (1994): Progress in arid-lands rainfall-runoff modelling. *Progress in Physical Geography* **18**(3): 343-365.

EMMETT, W. W. (1970): The hydraulics of overland flow on hillslopes. *U.S. Geological Survey Professional Paper*, **662-A**, 68 pp.

FAURES, J.-M. ET AL. (1995): Impact of small-scale spatial rainfall variability on runoff modelling. *Journal of Hydrology* **173**: 309-326.

FREAD, D. L. (1993): Flow Routing. In: D.R. Maidment (Ed.), *Handbook of Hydrology*. McGraw-Hill, New York, 10.1- 10.36.

GOODRICH, D. C. ET AL. (1997): Linearity of basin response as a function of scale in a semiarid watershed. *Water Resources Research* **33**(12): 2951-2965.

GRAF, W. L. (1988): Fluvial Processes in dryland rivers. *Springer Series in Physical Environment*. Springer, Heidelberg, 342 pp.

GREENBAUM, N. (1986): Point runoff in an extremly arid region. Infiltration-runoff test on small plots in the southern Arava and their hydrological and pedological implications. MSc Thesis , The Hebrew University of Jerusalem.

GREENBAUM, N., SCHICK, A. P. & BAKER, V. R. (2000): The paleoflood record of a hyperarid catchment, Nahal Zin, Negev Desert, Israel. *Earth Surface Processes and Landforms* **25**: 1-21.

GRODEK, T. (2002): Impact of urbanization on arid alluvial fans, the town of Eilat (in hebrew & engl. abstract). PhD-Thesis , The Hebrew University, Jerusalem, 140pp.

GRODEK, T., LEKACH, J. & SCHICK, A. P. (2000): Urbanizing alluvial fans as flood-conveying and flood-reducing systems: lessons from the October 1997 Eilat flood. In: M. Hassan et al. (Eds.), *The Hydrology-Geomorphology Interface:*

Rainfall, Floods, Sedimentation, Land Use. IAHS-publ. **no. 261**, Wallingford, 229-250.

HOOKE, J. & MANT, J. (2002): Morpho-dynamics of ephemeral streams. In: L.J. Bull & M.J. Kirkby (Eds.), *Dryland rivers: hydrology and geomorphology of semi-arid channels*. Wiley, Chichester, 173-204.

HORTON, R. E. (1933): The role of infiltration in the hydrological cycle. *American Geophysical Union Transactions* **14**: 446-460.

HUGHES, D. A. & SAMI, K. (1994): A semi-distributed, variable time interval model of catchment hydrology - structure and parameter estimation procedures. *Journal of Hydrology* **155**: 265-291.

JARRETT, R. D. (1985): Determination of roughness coefficients for streams in Colorado. *Water Resources Investigations Report*, **85-4004**, Lakewood, Colorado.

KIRBY, W. (1985): Statistical error analysis of the slope-area method of indirect discharge determination. *EOS* **66**(18): 267.

KIRKBY, M. J. & CHORLEY, R. J. (1967): Throughflow, overland flow and erosion. *Bulletin of the International Association of Scientific Hydrology* **12**(3): 5-21.

KOCHEL, R. C. & BAKER, V. R. (1988): Paleoflood analysis using slackwater deposits. In: V.R. Baker et al. (Eds.), *Flood geomorphology*. Wiley, New York, 357-376.

KREUELS, R. K. & BREUER, L. J. (1986): Wind influenced rain gauge errors in heavy rain. In: B. Sevruk (Ed.), *Correction of precipitation measurements*. Züricher Geographische Schriften, Zürich, 105-107.

KÜLLS, C. ET AL. (1995): Channel infiltration study using dye tracers, *Application of Tracers in Arid Zone Hydrology*. IAHS-publ. **no. 232**, 429-436.

LANGE, J. (1999): A non-calibrated rainfall-runoff model for large arid catchments, Nahal Zin, Israel. *Freiburger Schriften zur Hydrologie*, **9**, Freiburg, 130 pp.

LANGE, J. (submitted): Dynamics of transmission losses in a large arid stream channel. *Hydrological Processes*

LANGE, J. & LEIBUNDGUT, C. (1997): Using artificial tracers to study water losses of ephemeral floods in small arid streams. In: C. Leibundgut et al. (Eds.), *Proceedings of the International Workshop W2 held in Rabat, Morocco*. IAHS-publ. **no. 247**, 31-40.

LANGE, J. ET AL. (1999): A noncalibrated rainfall-runoff model for large, arid catchments. *Water Resources Research* **35**(7): 2161-2172

LANGE, J. ET AL. (2001): A field-based hydrological model to study the impacts of urbanization on regional water resources. In: A.H. Schumann et al. (Eds.), *Regional management of water resources*. IAHS-publ. **no. 268**, Wallingford, 255-262.

LANGE, J. & LEIBUNDGUT, C. (2003A): Surface runoff and sediment dynamics in arid and semi-arid regions. In: I. Simmers (Ed.), *Understanding water in a dry environment*. International Contributions to Hydrogeology. Balkema, Lisse, 115-150.

LANGE, J., WAGNER, A. & TETZLAFF, D. (2003B): Hochwassersimulation in kleinen Einzugsgebieten: Eignung von Niederschlagsradar und Auswirkung versiegelter Flächen. In: Kleeberg (Ed.), *Tagungsband zum Tag der Hydrologie, 20. -21. 03. 2003: Klima - Wasser - Flussgebietsmanagement - in Lichte der Flut*. Forum für Hydrologie und Wasserbewirtschaftung, 123-130.

LARSON, L. W. (1986): Experiences, investigations and recommendations concerning wind induced precipitation measurement errors. In: B. Sevruk (Ed.), *Correction of precipitation measurement*. Zürcher Geographische Schriften. **Heft 23**, Zurich, 49-56.

LEKACH, J. & GRODEK, T. (2003): personal communication

LEKACH, J. ET AL. (1998): Fluvio-pedogenic processes in an ephemeral stream channel, Nahal Yael, Southern Negev, Israel. *Geomorphology* **23**: 353-369.

LEKACH, J. & SCHICK, A. P. (1982): Suspended Sediment in Desert Floods in Small Catchments. *Israel Journal of Earth-Sciences* **31**: 144-156.

MAIDMENT, D. R. (EDITOR) (1992): Handbook of hydrology. McGraw-Hill, New York.

MAINGUET, M. (1999): Aridity. Springer, Berlin, 302 pp.

MARCUS, W. A. ET AL. (1992): An evaluation of methods for estimating Manning's n in small mountain streams. *Mountain Research and Development* **12**(3): 227-239

MELCHING, C. S. (1995): Reliability estimation. In: V.P. Singh (Ed.), *Computer models of watershed hydrology*. Water Resources Publications, Highlands Ranch, CO, 69-118.

ORNI, E. & EFRAT, E. (1966): Geographie Israels. Israel University Press, Jerusalem.

OSBORN, H. B., LANE, L. J. & HUNDLEY, J. F. (1972): Optimum gaging of thunderstorm rainfall in the southwestern United States. *Water Resources Research* **8**(1): 259-265.

PHILLIPS, J. V. & INGERSOLL, T. L. (1998): Verification of roughness coefficients for selected natural and constructed stream channels in Arizona. *U.S. Geological Survey Profession Paper* **1584.**

PORATH, A. & SCHICK, A. P. (1974): The use of remote sensing systems in monitoring desert floods, *Proceedings of Symposium on Flash Floods*. IAHS-publ. **no. 112**, Paris, 133-139.

RENARD, K. G. ET AL. (1993): Agricultural impacts in an arid environment: Walnut Gulch case study. *Hydrological Science and Technology* **9**: 145-190.

ROELS, J. M. (1984): Flow resistance in concentrated overland flow on rough slope surfaces. *Earth Surface Processes and Landforms* **9**: 541-551.

SALMON, O. & SCHICK, A. P. (1980): Infiltration Tests. In: A.P. Schick (Ed.), *Arid zone Geosystems*. Physical Geography, Institut of Earth Science, The Hebrew University, Jerusalem, 55-115.

SCHICK, A. P. (1977): A tentative sediment budget for an extremely arid watershed in the Southern Negev. In: D.O. Doehring (Ed.), *Geomorphology in arid regions*. Publications in Geomorphology. State University of New York, New York, 139-163.

SCHICK, A. P. (1980A): Arid Zone Geosystems. Division of Physical Geography, Institute of Earth Sciences, The Hebrew University of Jerusalem, Jerusalem, 170 pp.

SCHICK, A. P. (1980B): Geophysical survey of Nahal Yael channel bed. In: A.P. Schick (Ed.), *Arid Zone Geosystems*. Physical Geography, Institut of Earth Science, The Hebrew University, Jerusalem, 50-54.

SCHICK, A. P. (1988): Hydrological aspects of floods in extreme arid environments. In: V.R. Baker (Ed.), *Flood Geomophology*. Wiley, New York, 189-203.

SCHICK, A. P. (2000): A brief summary of a third of a century: Nahal Yael in retrospect, with some ideas for the future of catchment research. In: M. Hassan et al. (Eds.), *The Hydrology-Geomorphology Interface: Rainfall, Floods, Sedimentation, Land Use*. IAHS-publ. **no. 261**, Wallingford, 5-9.

SCHICK, A. P., GRODEK, T. & LEKACH, J. (1997): Sediment management and flood protection of desert towns: effects of small catchments. In: D.E. Walling (Ed.), *Human Impact on erosion and sedimentation*. IAHS-publ. **no. 245**, Wallingford.

SCHICK, A. P. & LEKACH, J. (1993): An evaluation of two ten-year sediment budgets, Nahal Yael, Israel. *Physical Geography* **14**(3): 225-238.

SCHICK, A. P. & SHARON, D. (1974): Geomorphology and climatology of arid watersheds. Department of Geography, The Hebrew University of Jerusalem, Jerusalem, 162 pp.

SCHWARTZ, U. (1986): Water in the alluvial fill of stream channels in arid environments - availability, distribution and fluctuations. (in Hebrew). MSc Thesis, Hebrew University, Jerusalem, 100.

SEVRUK, B. (1974): The use of stereo, horizontal and ground level orifice gages to determine a rainfall-elevation relationship. *Water Resources Research* **10**(6): 1138-1141.

SEVRUK, B. (1981): Methodische Untersuchung des systematischen Messfehlers der Hellmann-Regenmesser im Sommerhalbjahr in der Schweiz. PhD-Thesis, ETH Zurich, Zurich, 297.

SEVRUK, B. (1982): Methods of correction for systematic errors in point precipitation measurements for operational use. *Operational Hydrology Report*, **No. 21**, Geneva.

SEVRUK, B. (1983): Genauigkeit der konventionellen Regenmessung. In: F. Sieker (Ed.), *Die Bedeutung der räumlichen Niederschlagsverteilung für den Abflussprozess in kleinen Einzugsgebieten*. Mitteilungen des Instituts für Wasserwirtschaft, Hydrologie und landwirtschaftlichen Wasserbau der Universität Hannover. **Heft 52**, Hannover, 27-41.

SEVRUK, B. (1986): Summary report. In: B. Sevruk (Ed.), *Correction of precipitation measurements*. Züricher Geographische Schriften, Zürich, 13-23.

SEVRUK, B. & GEIGER, H. (1981): Selection of distribution types for extremes of precipitation. *Operational Hydrology Report*, **15**. World Meteorological Organisation (WMO), Geneva, 64 pp.

SHANAN, L. & SCHICK, A. P. (1980): A hydrological model for the Negev Desert Highlands: effects of infiltration, runoff and ancient agriculture. *Hydrological Science Bulletin* **25**(3): 269-282.

SHANNON, J., RICHARDSON, R. & THORNES, J. (2002): Modelling event-based fluxes in ephemeral streams. In: L.J. Bull & M.J. Kirkby (Eds.), *Dryland rivers: hydrology and geomorphology of semi-arid channels*. Wiley, Chichester, 129-172.

SHARMA, K. D. & MURTHY, J. S. R. (1998): A pratical approach to rainfall-runoff modelling in arid zone drainage basins. *Hydrological Science Journal* **43**: 331-348.

SHARON, D. (1970A): Areal patterns of rainfall in a small watershed as affected by wind and meteorological conditions, *Symposium of Results of Research on Representative and Experimental Basins*. IAHS-publ. **no. 96**, Wellington, 3-11.

SHARON, D. (1970B): Topography-conditioned variations in rainfall as related to the runoff-contributing areas in a small watershed. *Israel Journal of Earth-Sciences* **19**: 85-89.

SHARON, D. (1972A): Spatial analysis of rainfall data from dense networks. *Bulletin of the International Association of Hydrological Sciences* **17**(3): 291-300.

SHARON, D. (1972B): The spotiness of rainfall in a desert area. *Journal of Hydrology* **17**: 161-175.

SHARON, D. (1980): The distribution of hydrologically effective rainfall incident on sloping ground. *Journal of Hydrology* **46**: 165-188.

SHARON, D. & ARAZI, A. (1997): The distribution of wind-driven rainfall in a small valley; an empirical basis for numerical model verification. *Journal of Hydrology* **201**: 21-48.

SHARON, G. & SCHICK, A. P. (1980): The areal framework of the Nahal Yael Model. In: A.P. Schick (Ed.), *Arid Zone Geosystems*. Physical Geography, Institut of Earth Science, The Hebrew University, Jerusalem, 116-164.

SHERMAN, L. K. (1932): Streamflow from rainfall by the unit hydrograph method. *Eng. News Record* **108**: 501-505.

SHIMRON, A. (1974): The geology of Nahal Yael Watershed; a preliminary report. In: A.P. Schick & D. Sharon (Eds.), *Geomorphology and climatology of arid watersheds*. Department of Geography, The Hebrew University of Jerusalem, Jerusalem, 103-122.

SIMMERS, I. (2003): Hydrological processes and water resource management. In: I. Simmers (Ed.), *Understanding water in a dry environment*. International Contributions to Hydrogeology. Balkema, Lisse, 1-14.

SMITH, R. E. ET AL. (1995): KINEROS - A kinematic runoff and erosion model. In: V.P. Singh (Ed.), *Computer Models of watershed hydrology*. Water Resources Publications, Colorado, 697-732.

SORMAN, A. U. & ABDULRAZZAK, M. J. (1993): Flood hydrograph estimation for ungauged wadis in Saudi Arabia. *Journal of Water Resource Planning and Management* **119**(1): 45-63.

THOMAS, D. S. G. (1997): Arid zone geomorphology - process, form and change in drylands. Wiley, Chichester, 713 pp.

TODINI, E. (1988): Rainfall-runoff modeling - past, present and future. *Journal of Hydrology* **100**: 341-352.

TROSTLER, Y. (1975): unpublished data

UNESCO (1977): Map of the world distribution of arid regions. *MAB Technical Note* **7.**

WAGNER, A. (2002): Anwendung eines nicht-kalibrierten Niederschlags-Abfluss-Modells in den hydrologischen Versuchsgebieten des Ostkaiserstuhls. Diplomarbeit, Albert-Ludwigs Universität, Freiburg.

WALTER, H. & LIETH, M. (1979): Vegetationen und Klimazonen, Stuttgart.

WARD, R. C. & ROBINSON, M. (2000): Principles of Hydrology. McGraw-Hill, Berkshire, England, 450 pp.

WEISCHET, W. (1995): Einführung in die Allgemeine Klimatologie. *Teubner Studienbücher der Geographie*. B.G. Teubner, Stuttgart, 276 pp.

WOHL, E. E. & GRODEK, T. (1994): Channel bed-steps along Nahal Yael, Negev desert, Israel. *Geomorphology* **9**: 117-126.

WOOLHISER, D. A. (1986): Sensitivity of calculated peak runoff rates to rainfall sampling frequency. In: M.E. Moss (Ed.). IAHS-publ. **no. 158**, Wallingford, 161-171.

YAIR, A. (1992): The control of headwater area on channel runoff in a small arid watershed. In: A.J. Parsons & A.D. Abrahams (Eds.), *Overland Flow - Hydraulics and erosion mechanics*. UCL Press, London, 53-68.

YAIR, A. & KLEIN, M. (1973): The influence of surface properties on flow and erosion processes on debris covered slopes in an arid area. *Catena* **1**: 1-18.

Acknowledgements

It is a great pleasure to complete my degree with this study. Without the support of many people I would not have reached this state and this study would not have become what it is today. Thus, I would like to express my gratitude to all people who accompanied me on the way.

First, I would like to thank Prof. Dr. Leibundgut for assigning the topic to me, which has not been taken for granted.

Dr. Jens Lange initiated, supported and coordinated this project from the very first beginning. Without his ideas and suggestions for my research it would not have been possible to fulfil the task. He investigated much time in discussions, was open for various questions and problems and always helped out with valuable advice.

Dr. Tamir Grodek, Dr. Judith Lekach and Yovav Zakai from the Department of Physical Geography at the Hebrew University in Jerusalem welcomed me with open hearts and provided a very warm working atmosphere in Israel. Their hospitality is greatly acknowledged. Judith and Tamir spent hours introducing me to arid zone hydrology and illustrating particular processes in Nahal Yael. Special thanks to Tamir for solving all technical problems concerning GIS, printers and field equipment. Thanks to Judith for taking the time for valuable talks, for searching for old data files in the tremendous archive and the best apple strudel I ever ate. Yovav and his friends gave insights to everyday live in Israel and showed me Jerusalem by day and night.

Many thanks to Dr. Noam Greenbaum for spending two hot days with me in the field. Guiding a greenhorn through the desert, he shared his vast field experience and general knowledge with me. He contributed decisively to this study by introducing me to infiltration properties of the surfaces and discussing runoff processes in general.

Only a scholarship of the DAAD (German Academic Exchange Service) provided the financial base for my inspiring stay in Israel.

Special thanks to Tessa Alke, Jan-Henning Ross, Margret Johst and Beatrice Guwang and Tim aus der Beek for their valuable reviews of my drafts.

Thanks as well to all fellow students in the Computerraum for their moral support and readiness to think about my arid zone specific problems.

Last but not least it was the unconditional support of Boris which brought this study to conclusion. With his assistance in Israel as well as in Freiburg he gave the maximum possible guidance at all stages of the work and kept me on the right track.

Annex

A. 1: Measuring weir at station 05

A. 2: Measuring weir at station 04

A. 3: Measuring weir at station 03

A. 4: Measuring weir at the basin outlet, station 02

A. 5: Water level gauging station in the reservoir, dam in left foreground

A. 6: Main alluvial reach - channel type 3

A. 7: Middle reach of sub-catchment 03 - channel type 2

A. 8: Steep headwater - channel type 1

A. 9: Detail of the alluvial fill

A. 10: Steep colluvial slope – terrain type sc

A. 11: Moderate colluvium – terrain type mc

A. 12: Bare rocky slope partly covered with colluvium with Lambrecht rainfall recording station on the right and tipping bucket rain gauge more uphill – terrain type bcGg

A. 13: Mixted terrain type in close up view – terrain type bcS

A. 14: Bare rocky slope – terrain type brS, alluvial terrace with incised gullies on the left

A. 15: Overview over parts of sub-catchment 05, bare rock outcrops at the mountain tops, below steep, moderate colluvial and mixed surfaces

A. 16: Looking downstream sub-reach 03 that joins the main channel on its way towards Nahal Roded (large wadi from left to right in background)

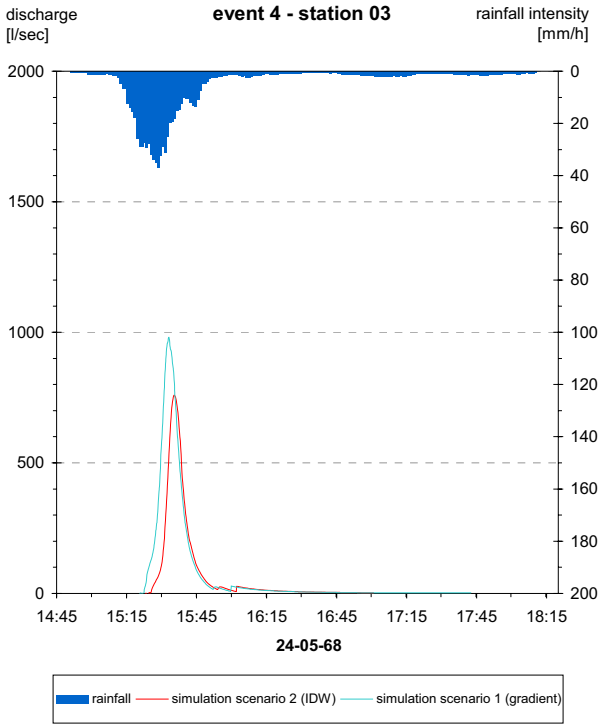

A. 17: Model results event 4, station 03

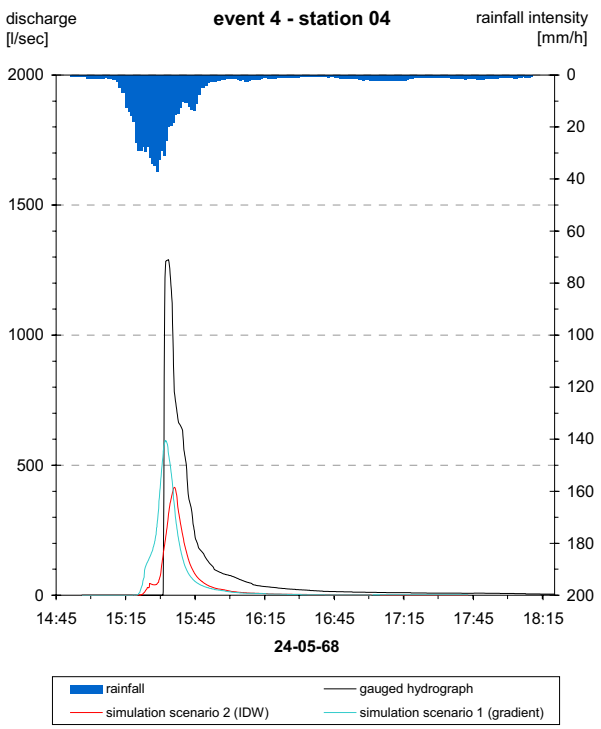

A. 18: Model results event 4, station 04

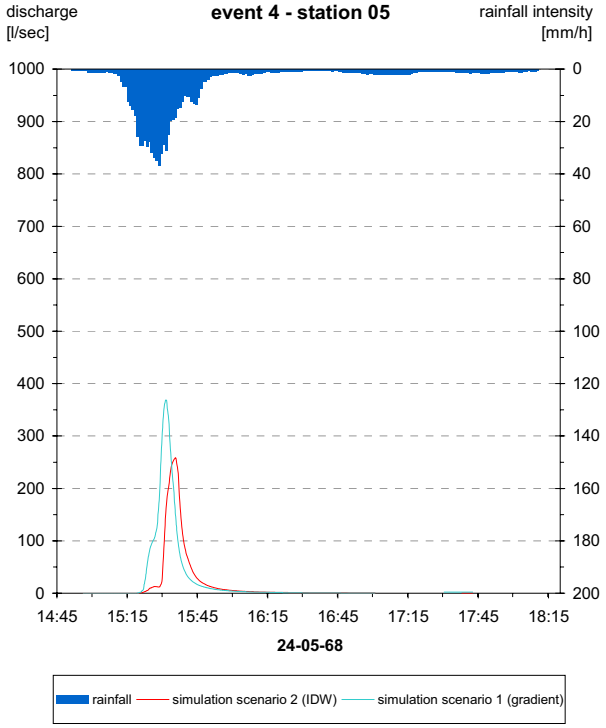

A. 19: Model results event 4, station 05

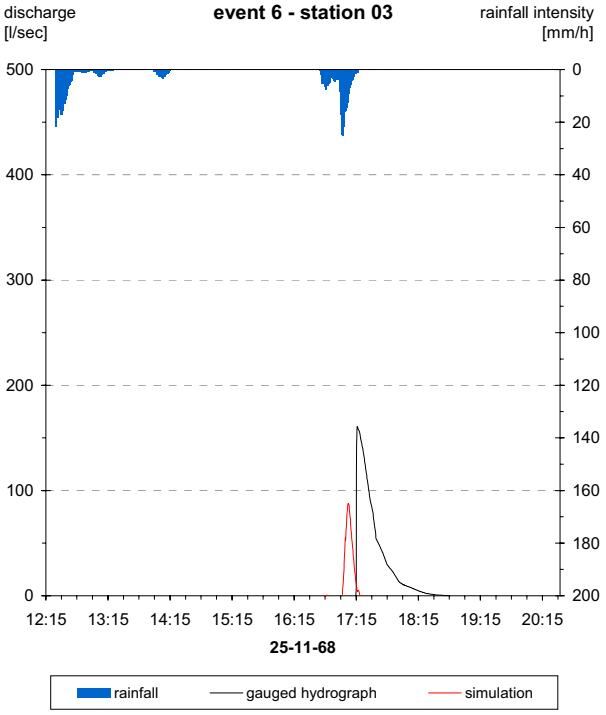

A. 20: Model results event 6, station 03

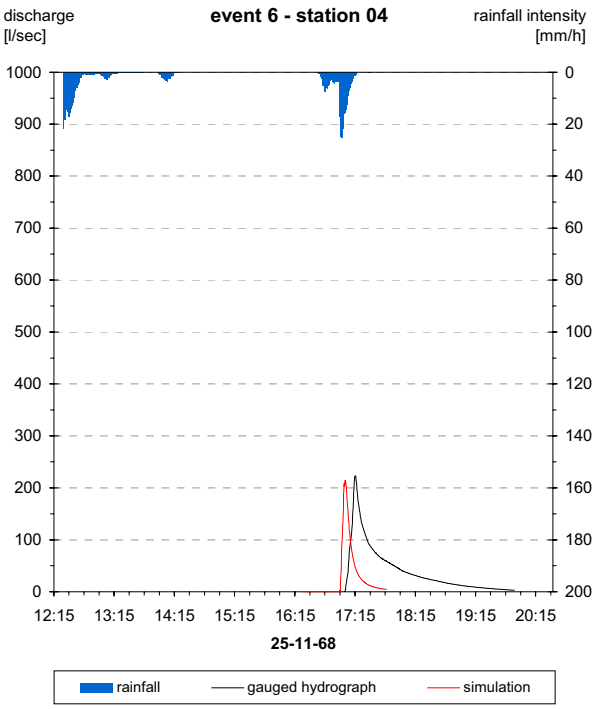

A. 21: Model results event 6, station 04

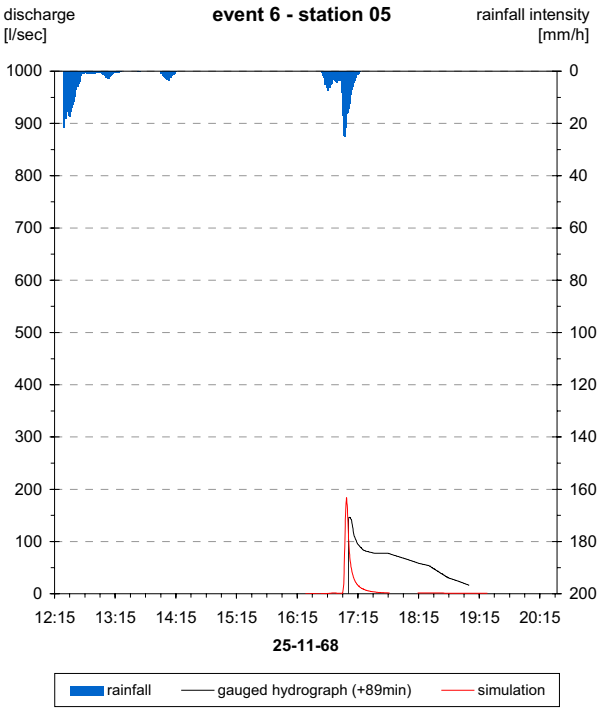

A. 22: Model results event 6, station 05

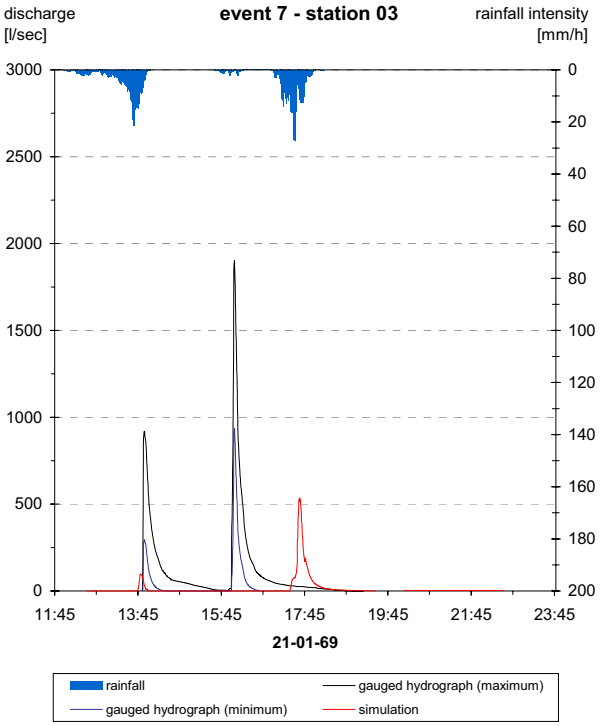

A. 23: Model results event 7, station 03

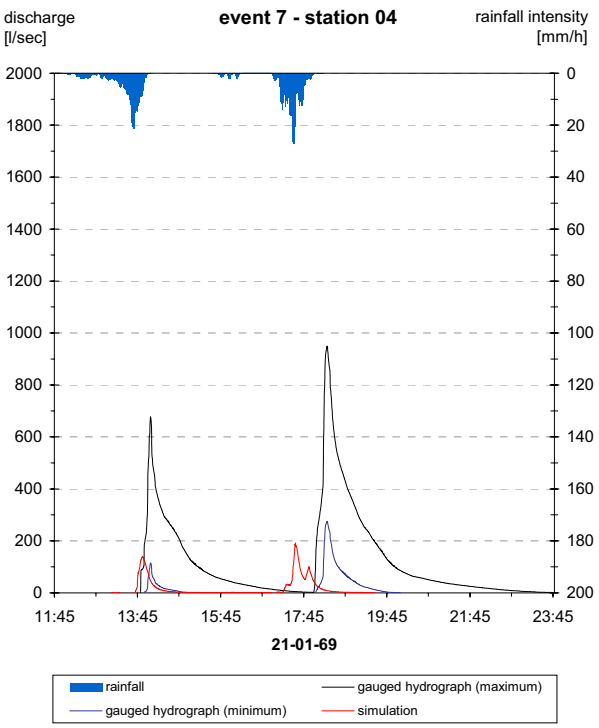

A. 24: Model results event 7, station 04

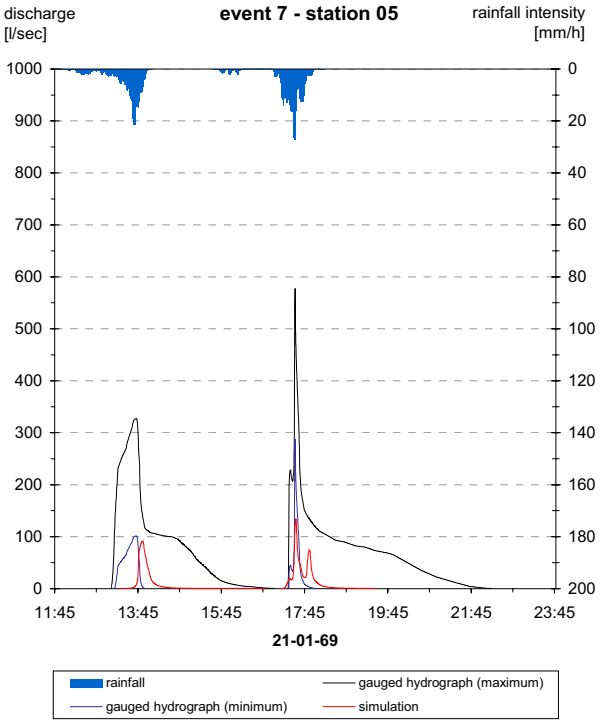

A. 25: Model results event 7, station 05

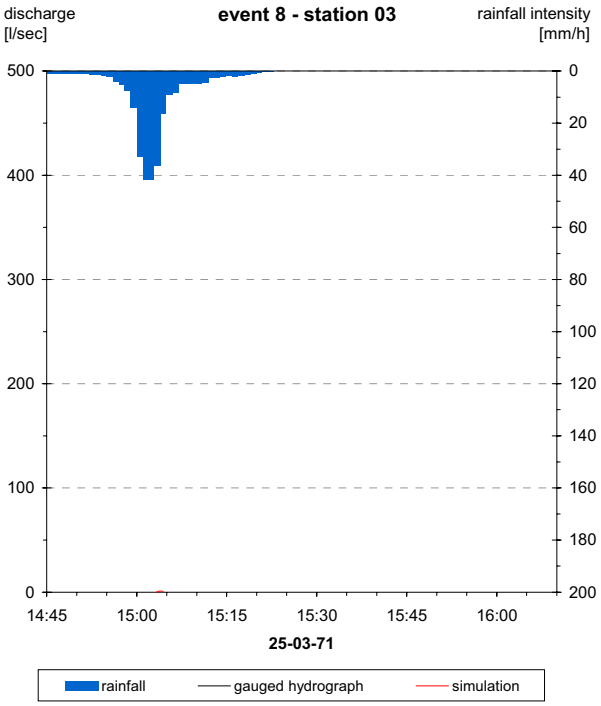

A. 26: Model results event 8, station 03

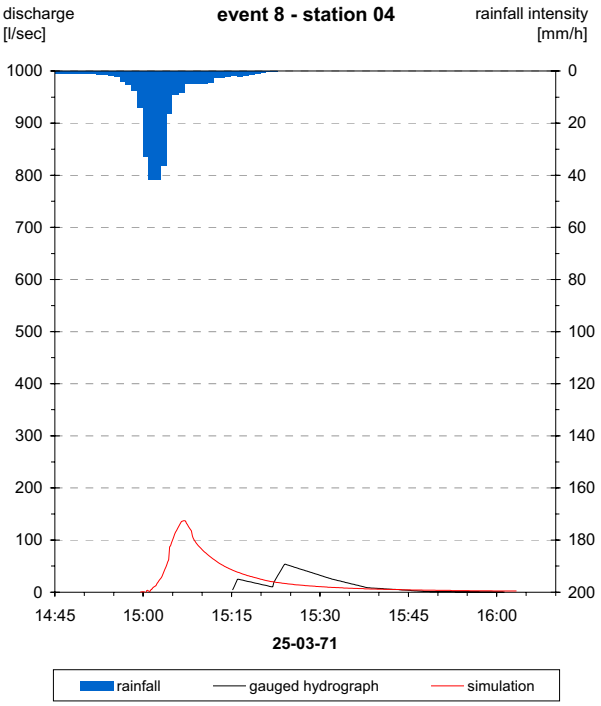

A. 27 : Model results event 8, station 04

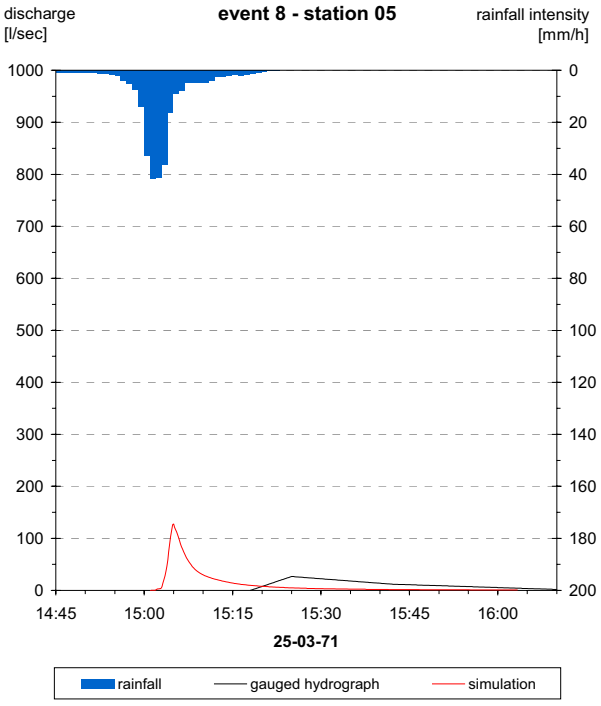

A. 28: Model results event 8, station 05

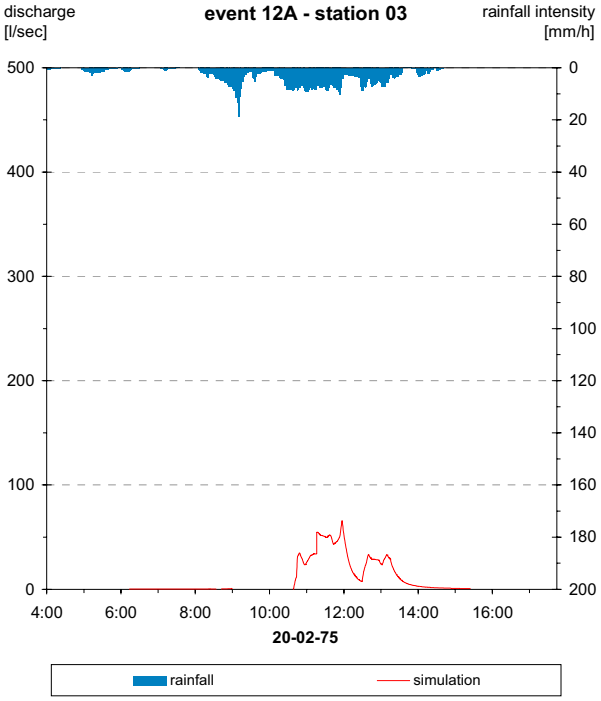

A. 29: Model results event 12A, station 03

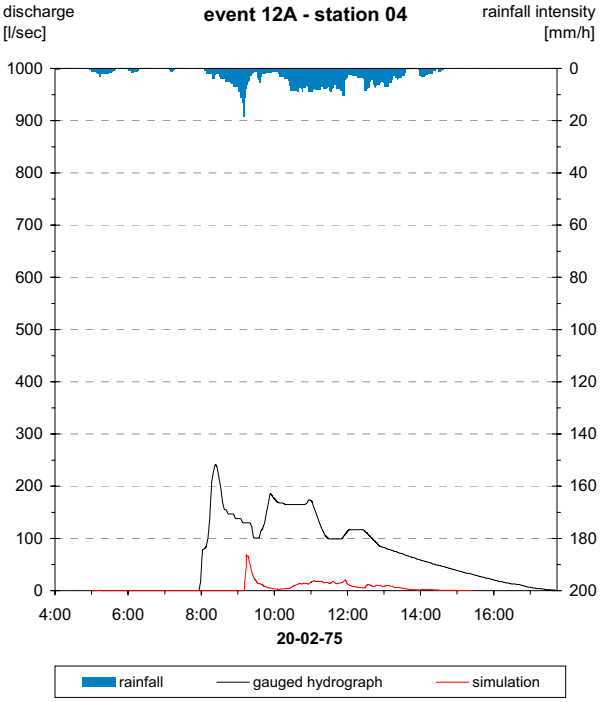

A. 30: Model results event 12A, station 04

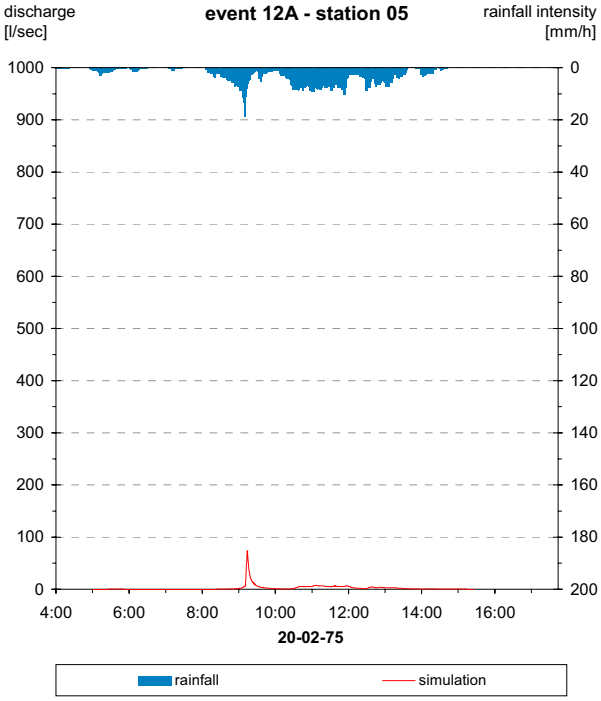

A. 31: Model results event 12A, station 05

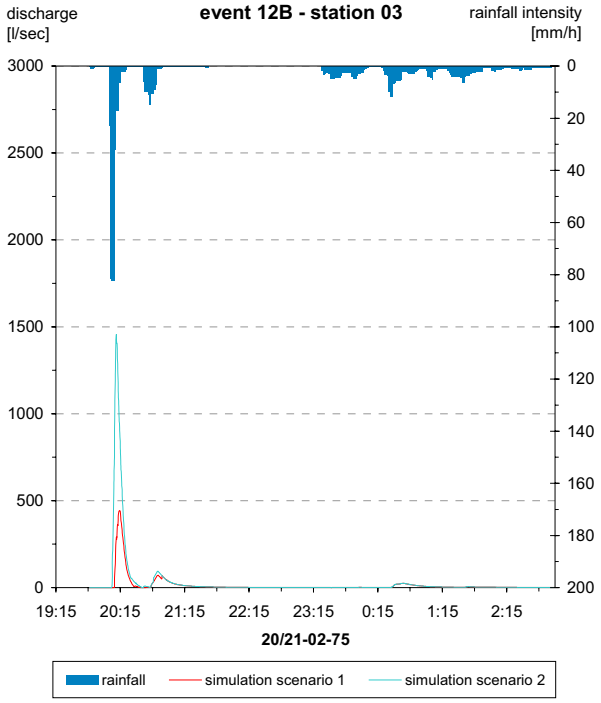

A. 32: Model results event 12B, station 03

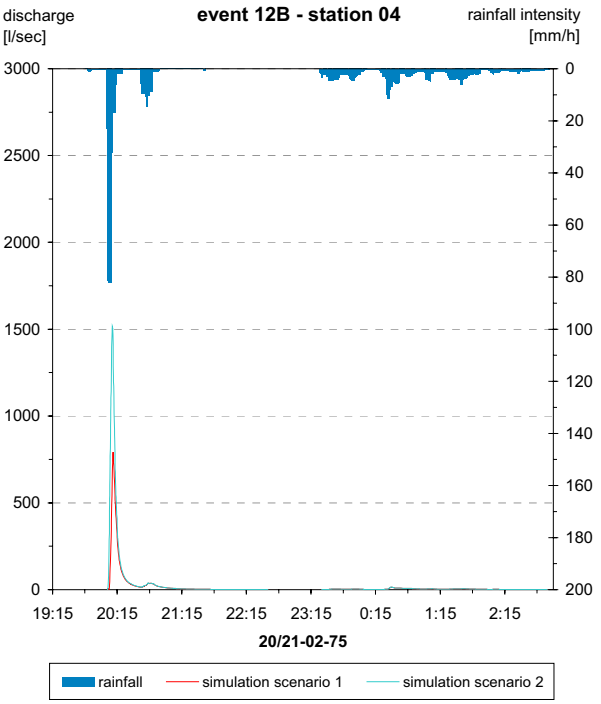

A. 33: Model results event 12B, station 04

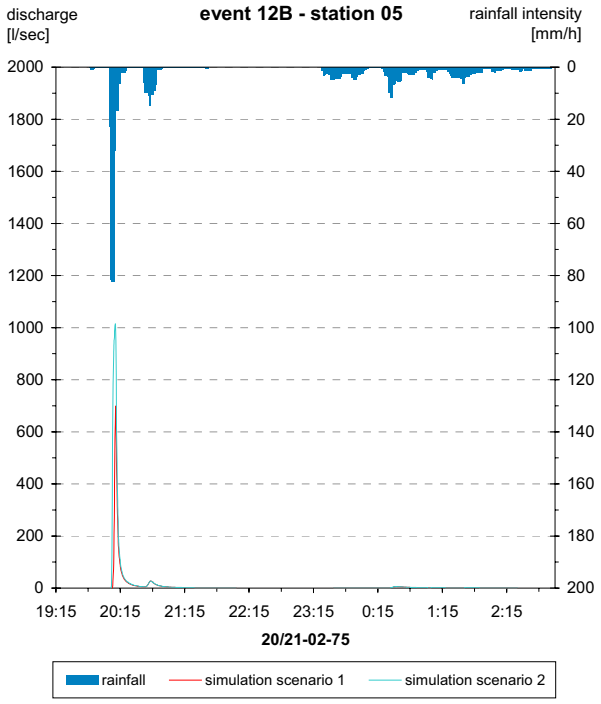

A. 34: Model results event 12B, station 05

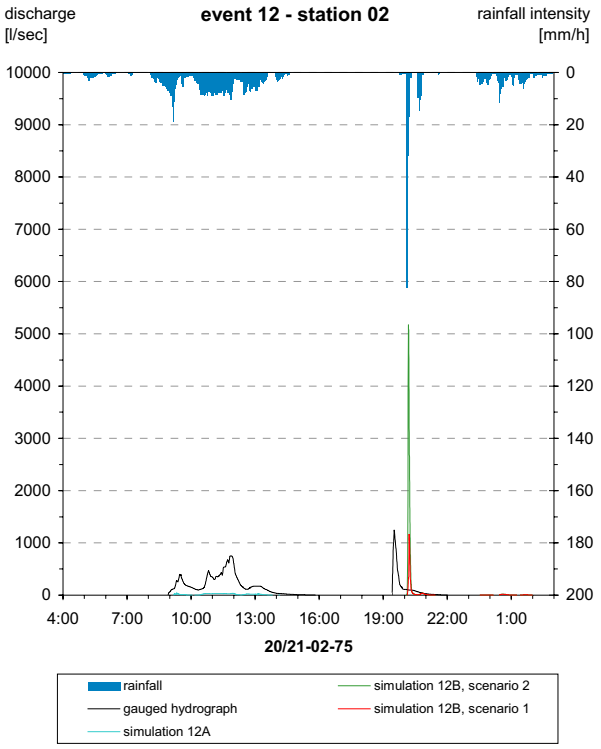

A. 35: Model results events 12, station 02

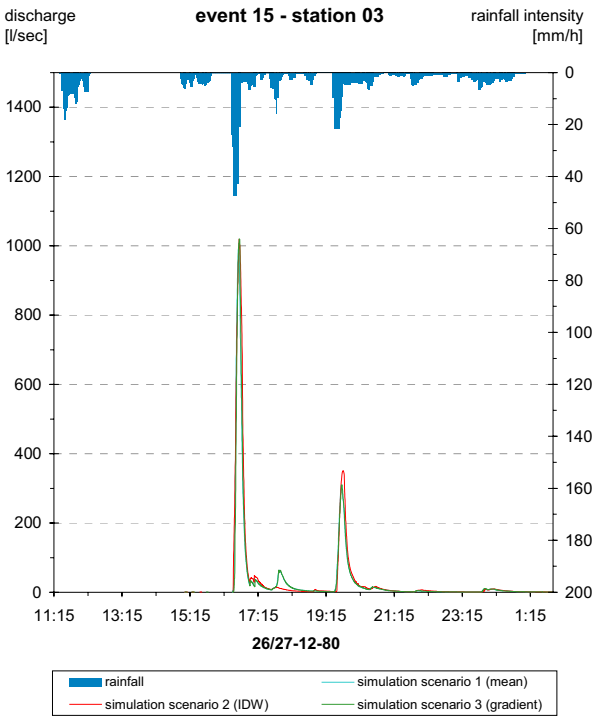

A. 36: Model results event 15, station 03

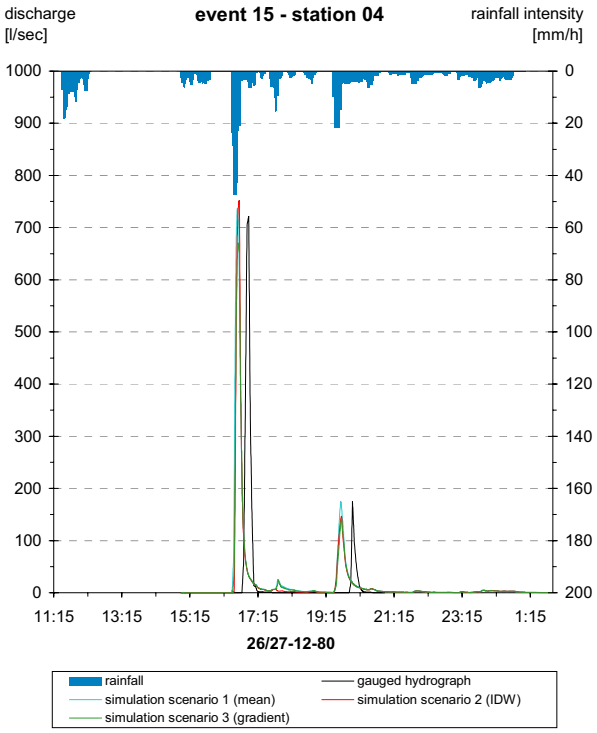

A. 37: Model results event 15, station 04

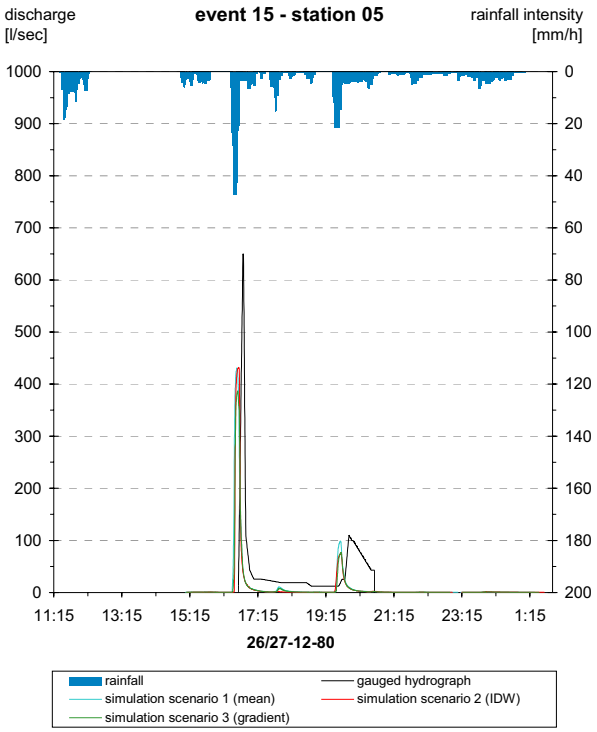

A. 38: Model results event 15, station 05

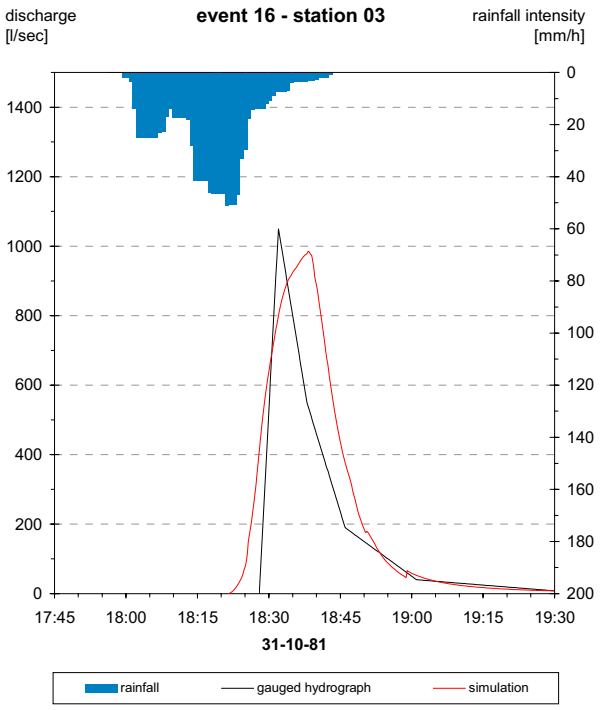

A. 39: Model results event 16, station 03

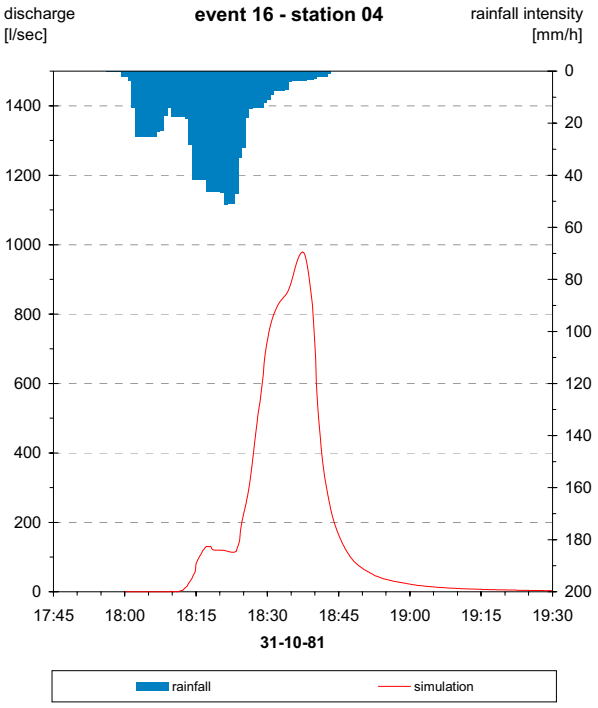

A. 40: Model results event 16, station 04

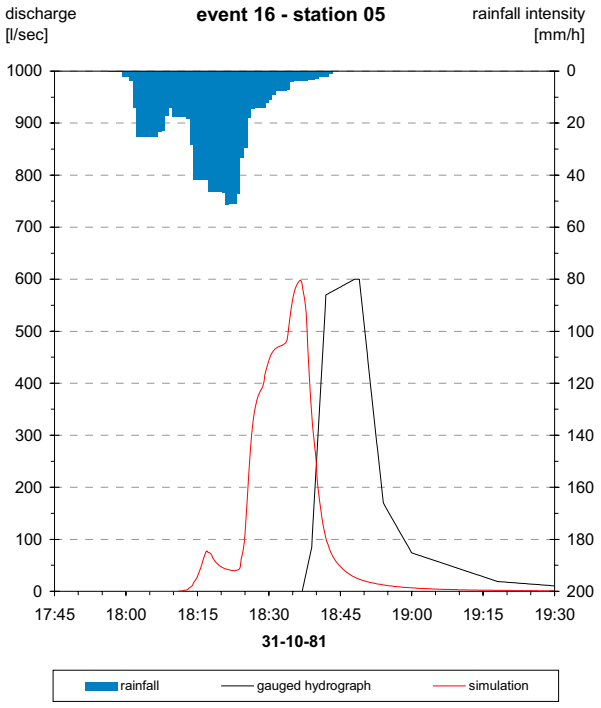

A. 41: Model results event 16, station 05

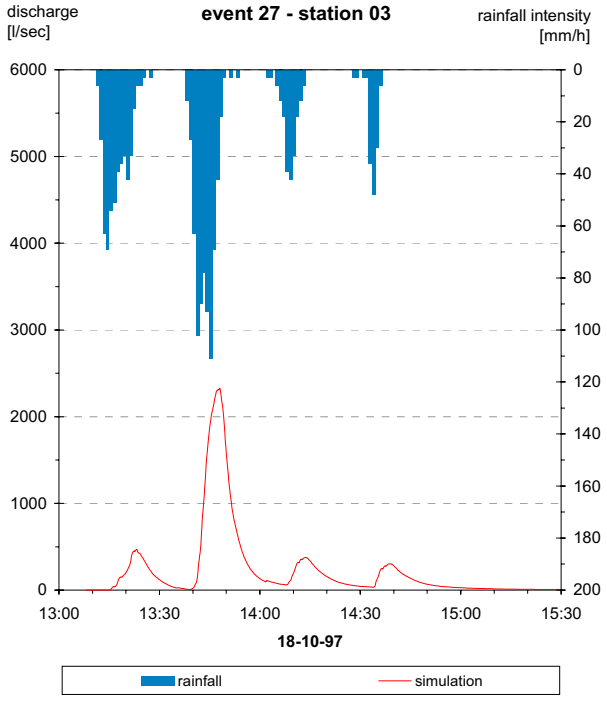

A. 42: Model results event 27, station 03

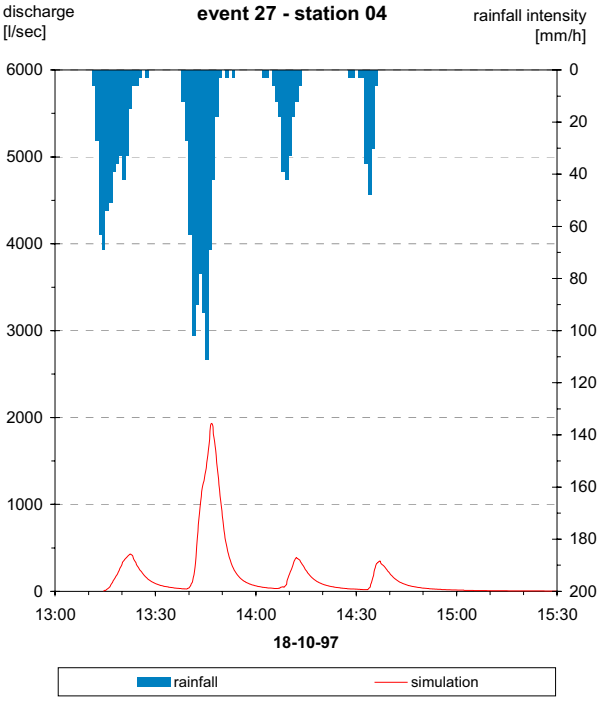

A. 43: Model results event 27, station 04

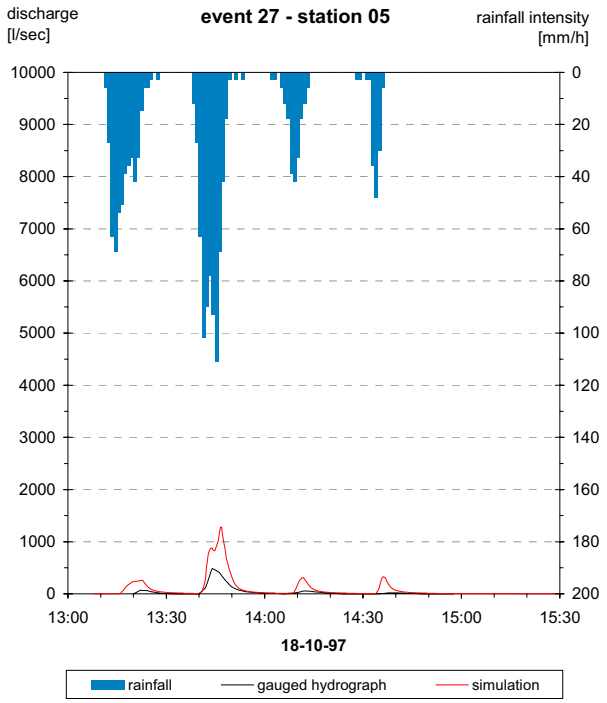

A. 44: Model results event 27, station 05

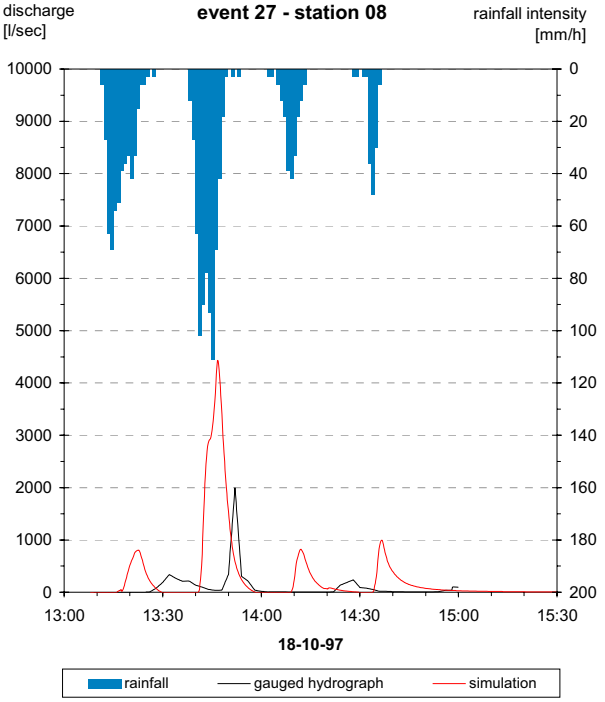

A. 45: Model results event 27, station 08

A. 46: Example of an ArcInfo AML-routine performing runoff generation for time step 26

```
grid
setwindow surface
setcell surface
DOCELL
IF(ev26grid > 0)
BEGIN
raintot26 = raintot25 + (ev26grid / 60)
IF(raintot26 >= surface.loss)
BEGIN
rbe26 = CON(rbe25 > 0, rbe25, 26)
IF(rbe26 >= 26 - 9)
r26 := CON(rbe26 == 26, raintot26 - surface.loss - surface.inf1,~
rbe26 == 26 - 1, (ev26grid / 60) - surface.inf2,~
rbe26 == 26 - 2, (ev26grid / 60) - surface.inf3,~
rbe26 == 26 - 3, (ev26grid / 60) - surface.inf4,~
rbe26 == 26 - 4, (ev26grid / 60) - surface.inf5,~
rbe26 == 26 - 5, (ev26grid / 60) - surface.inf6,~
rbe26 == 26 - 6, (ev26grid / 60) - surface.inf7,~
rbe26 == 26 - 7, (ev26grid / 60) - surface.inf8,~
rbe26 == 26 - 8, (ev26grid / 60) - surface.inf9,~
rbe26 == 26 - 9, (ev26grid / 60) - surface.inf10, 0)
IF(rbe26 < 26 - 9)
r26 := CON(rbe26 >= 0, (ev26grid / 60) - surface.inf10, 0)
ros26 = CON(r26 > 0, r26 + ros25, ros25)
END
ELSE
BEGIN
ros26 = ros25
rbe26 = rbe25
END
END
ELSE
BEGIN
raintot26 = raintot25
ros26 = ros25
rbe26 = rbe25
END
IF(ISNULL(ev26grid / 60))
BEGIN
raintot26 = raintot25
ros26 = ros25
rbe26 = rbe25
END
END
zor26 = zonalsum(seggrid, (ros26 - ros25), DATA)
zoros26 = CON(ISNULL(zor26), 0, INT(zor26 + .5))
kill zor26 all
roex26 = COMBINE(seggrid, zoros26)
kill zoros26 all
kill raintot25 all
kill rbe25 all
q
tables
sel roex26.vat
unload roex26.txt seggrid zoros26 columnar #
q
kill roex26 all
```

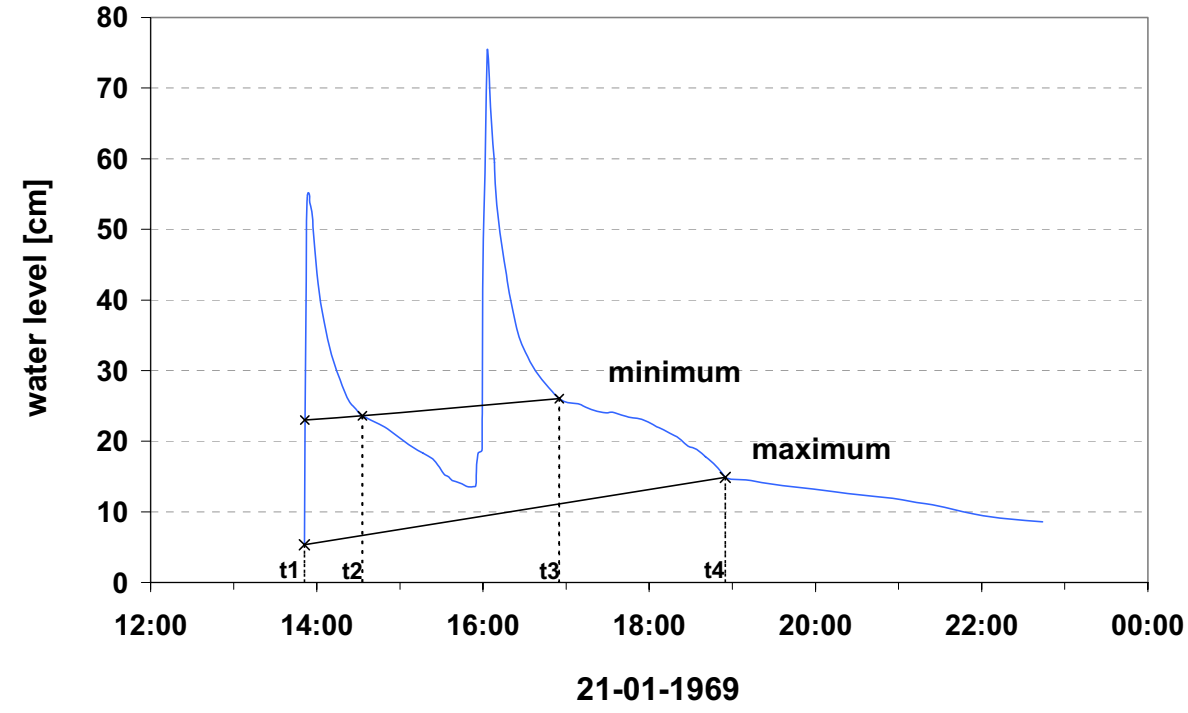

A. 47: Measured water level at station 04, event 7

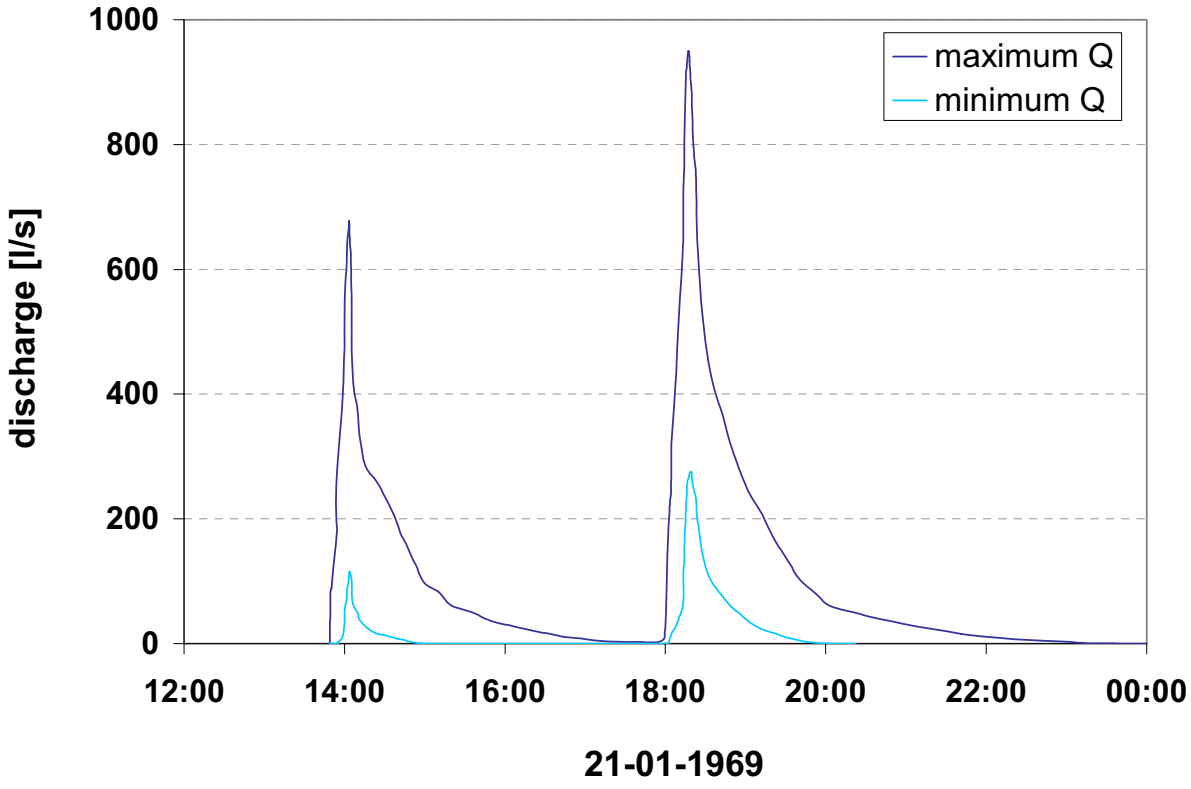

A. 48: Determined range of discharge rating at station 04, event 7

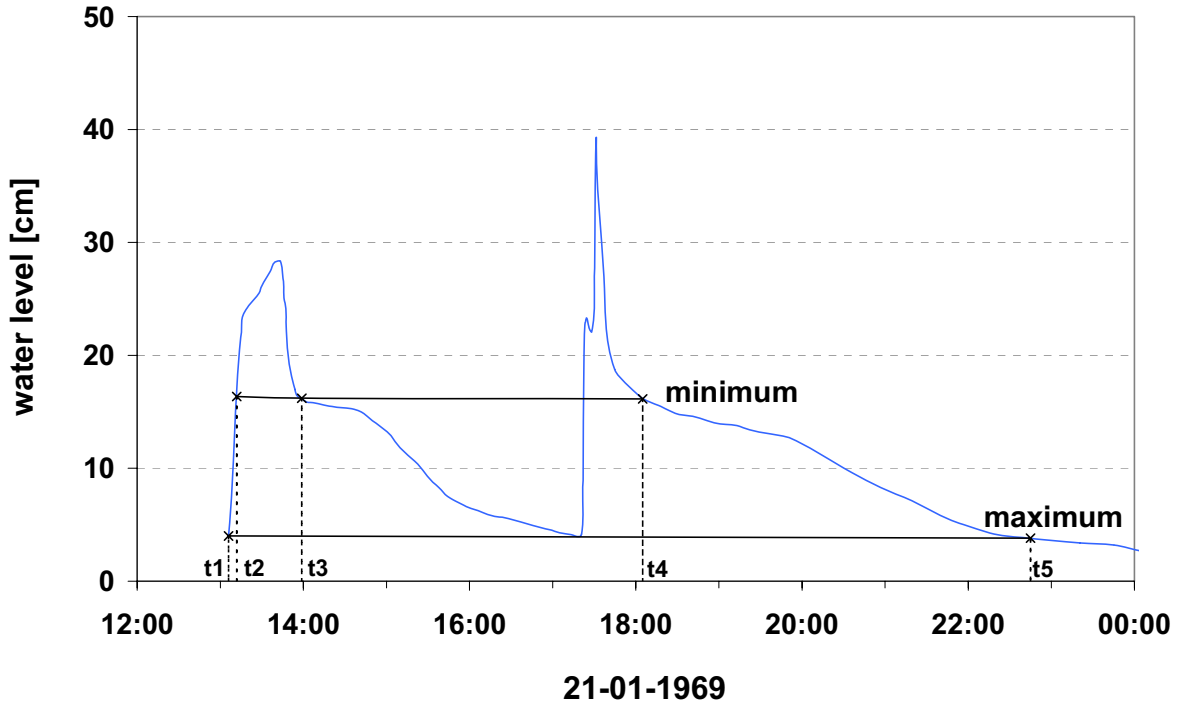

A. 49: Measured water level at station 05, event 7

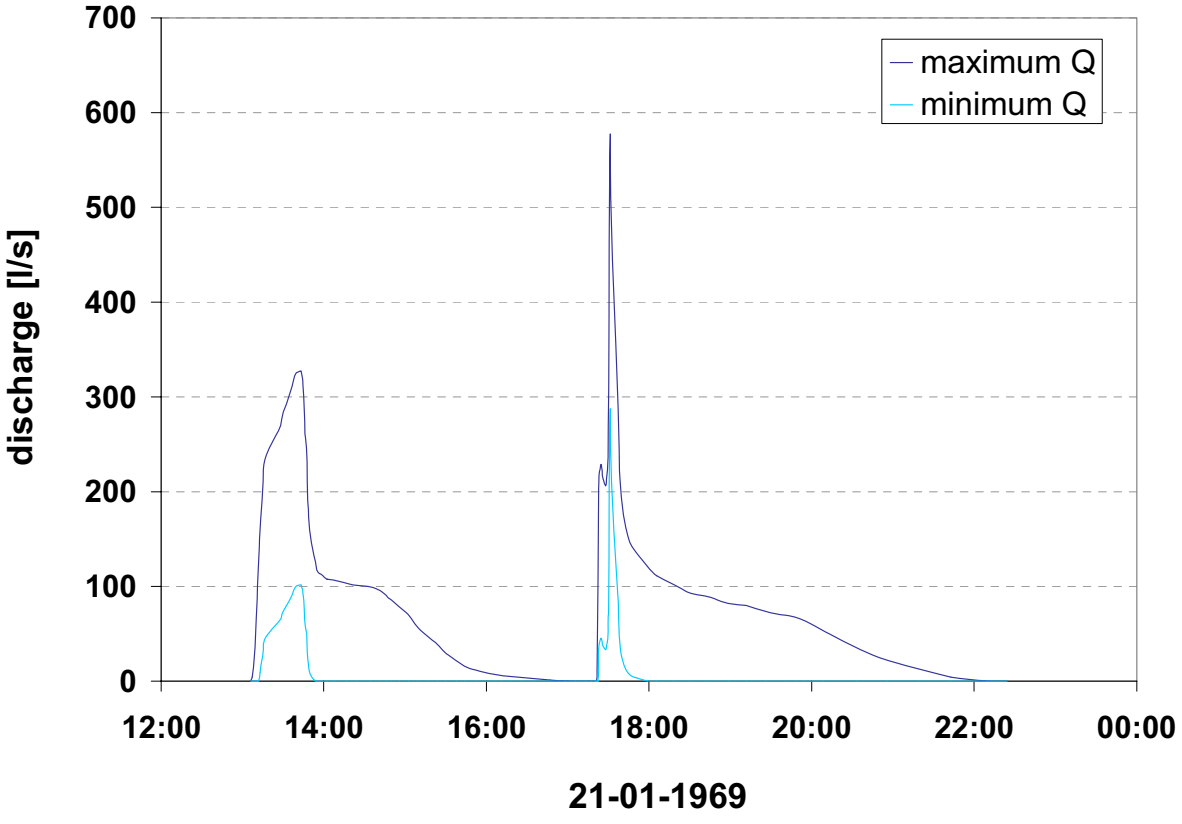

A. 50: Determined range of discharge rating at station 05, event 7

A. 51: Channel segments with corrresponding sub-catchments (poly) and associated time-lag

secment no.	left poly	right poly	timelag [min:sec]	secment no.	left poly	right poly	timelag [min:sec]
1	1001	2001	1 : 55	51	1051	2051	1 : 05
2	1002	2002	0 : 25	52	1052	2052	0 : 25
3	1003	2003	1 : 40	53	1053	2053	0 : 20
4	1004	2004	0 : 40	54	1054	2054	0 : 25
5	1005	2005	1 : 00	55	1055	2055	0 : 30
6	1006	2006	0 : 55	56	1056	2056	1 : 35
7	1007	2007	0 : 15	57	1057	2057	1 : 00
8	1008	2008	0 : 25	58	1058	2058	0 : 30
9	1009	2009	1 : 20	59	1059	2059	0 : 20
10	1010	2010	0 : 25	60	1060	2060	0 : 25
11	1011	2011	0 : 25	61	1061	2061	0 : 30
12	1012	2012	0 : 30	62	1062	2062	0 : 30
13	1013	2013	0 : 35	63	1063	2063	0 : 12
14	1014	2014	0 : 35	64	1064	2064	1 : 15
15	1015	2015	0 : 50	65	1065	2065	0 : 55
16	1016	2016	0 : 50	66	1066	2066	0 : 50
17	1017	2017	0 : 45	67	1067	2067	1 : 20
18	1018	2018	0 : 45	68	1068	2068	0 : 45
19	1019	2019	0 : 40	69	1069	2069	0 : 30
20	1020	2020	0 : 45	70	1070	2070	0 : 50
21	1021	2021	1 : 40	71	1071	2071	1 : 00
22	1022	2022	0 : 40	72	1072	2072	0 : 35
23	1023	2023	0 : 55	73	1073	2073	0 : 40
24	1024	2024	0 : 30	74	1074	2074	0 : 50
25	1025	2025	0 : 45	75	1075	2075	0 : 35
26	1026	2026	0 : 55	76	1076	2076	1 : 10
27	1027	2027	0 : 50	77	1077	2077	0 : 25
28	1028	2028	0 : 30	78	1078	2078	0 : 50
29	1029	2029	1 : 05	79	1079	2079	0 : 30
30	1030	2030	1 : 20	80	1080	2080	0 : 20
31	1031	2031	1 : 30	81	1081	2081	0 : 40
32	1032	2032	0 : 35	82	1082	2082	1 : 00
33	1033	2033	0 : 15	83	1083	2083	0 : 20
34	1034	2034	0 : 25	84	1084	2084	0 : 10
35	1035	2035	1 : 10	85	1085	2085	0 : 30
36	1036	2036	0 : 25	86	1086	2086	0 : 20
37	1037	2037	0 : 30	87	1087	2087	1 : 55
38	1038	2038	0 : 45	88	1088	2088	0 : 40
39	1039	2039	0 : 55	89	1089	2089	0 : 40
40	1040	2040	0 : 35	90	1090	2090	0 : 30
41	1041	2041	0 : 30	91	1091	2091	0 : 35
42	1042	2042	0 : 55	92	1092	2092	0 : 20
43	1043	2043	0 : 45	93	1093	2093	1 : 10
44	1044	2044	0 : 40	94	1094	2094	0 : 30
45	1045	2045	0 : 35	95	1095	2095	0 : 30
46	1046	2046	0 : 40	96	1096	2096	0 : 60
47	1047	2047	1 : 15	97	1097	2097	0 : 20
48	1048	2048	0 : 35	98	1098	2098	0 : 25
49	1049	2049	1 : 10	99	1099	2099	0 : 45
50	1050	2050	0 : 25	100	1100	2100	0 : 30

secment no.	left poly	right poly	timelag [min:sec]	secment no.	left poly	right poly	timelag [min:sec]
101	1101	2101	0 : 30	152	1152	2152	1 : 30
102	1102	2102	1 : 20	153	1153	2153	0 : 20
103	1103	2103	0 : 20	154	1154	2154	0 : 35
104	1104	2104	0 : 20	155	1155	2155	0 : 55
105	1105	2105	0 : 45	156	1156	2156	0 : 45
106	1106	2106	0 : 20	157	1157	2157	1 : 15
107	1107	2107	1 : 20	158	1158	2158	0 : 45
108	1108	2108	0 : 40	159	1159	2159	1 : 10
109	1109	2109	0 : 25	160	1160	2160	1 : 05
110	1110	2110	0 : 45	161	1161	2161	0 : 25
111	1111	2111	0 : 25	162	1162	2162	1 : 00
112	1112	2112	0 : 40	163	1163	2163	1 : 10
113	1113	2113	0 : 40	164	1164	2164	1 : 40
114	1114	2114	1 : 10	165	1165	2165	0 : 25
115	1115	2115	0 : 40	166	1166	2166	0 : 45
116	1116	2116	0 : 50	167	1167	2167	0 : 35
117	1117	2117	1 : 10	168	1168	2168	0 : 25
118	1118	2118	1 : 00	169	1169	2169	0 : 30
119	1119	2119	0 : 25	170	1170	2170	2 : 20
120	1120	2120	0 : 55	171	1171	2171	0 : 30
121	1121	2121	0 : 40	172	1172	2172	1 : 05
122	1122	2122	0 : 50	173	1173	2173	0 : 40
123	1123	2123	0 : 55	174	1174	2174	1 : 30
124	1124	2124	1 : 15	175	1175	2175	1 : 15
125	1125	2125	0 : 55	176	1176	2176	0 : 40
126	1126	2126	0 : 50	177	1177	2177	0 : 35
127	1127	2127	3 : 05	178	1178	2178	0 : 35
128	1128	2128	0 : 20	179	1179	2179	1 : 00
129	1129	2129	1 : 10	180	1180	2180	0 : 30
130	1130	2130	0 : 55	181	1181	2181	0 : 45
131	1131	2131	1 : 20	182	1182	2182	0 : 35
132	1132	2132	0 : 50	183	1183	2183	0 : 40
133	1133	2133	0 : 15	184	1184	2184	0 : 20
134	1134	2134	1 : 10	185	1185	2185	0 : 25
135	1135	2135	1 : 10	186	1186	2186	3 : 55
136	1136	2136	0 : 20	187	1187	2187	0 : 55
137	1137	2137	0 : 40	188	1188	2188	1 : 05
138	1138	2138	0 : 35	189	1189	2189	5 : 15
139	1139	2139	1 : 20	190	1190	2190	1 : 20
140	1140	2140	0 : 30	191	1191	2191	0 : 40
141	1141	2141	0 : 40	192	1192	2192	2 : 40
142	1142	2142	0 : 55	193	1193	2193	2 : 10
143	1143	2143	0 : 20	194	1194	2194	2 : 10
144	1144	2144	0 : 25	195	1195	2195	0 : 55
145	1145	2145	0 : 25	196	1196	2196	0 : 25
146	1146	2146	0 : 45	197	1197	2197	0 : 25
147	1147	2147	0 : 30	198	1198	2198	3 : 45
148	1148	2148	0 : 50	199	1199	2199	0 : 55
149	1149	2149	0 : 40	200	1200	2200	2 : 05
150	1150	2150	0 : 25	201	1201	2201	0 : 30
151	1151	2151	0 : 40	202	1202	2202	1 : 00

secment no.	left poly	right poly	timelag [min:sec]	secment no.	left poly	right poly	timelag [min:sec]
203	1203	2203	0 : 30	254	1254	2254	5 : 30
204	1204	2204	0 : 50	255	1255	2255	3 : 30
205	1205	2205	0 : 25	256	1256	2256	1 : 05
206	1206	2206	0 : 50	257	1257	2257	0 : 25
207	1207	2207	1 : 20	258	1258	2258	0 : 20
208	1208	2208	1 : 05				
209	1209	2209	0 : 90				
210	1210	2210	0 : 55				
211	1211	2211	0 : 20				
212	1212	2212	2 : 00				
213	1213	2213	0 : 35				
214	1214	2214	0 : 40				
215	1215	2215	3 : 05				
216	1216	2216	0 : 50				
217	1217	2217	0 : 40				
218	1218	2218	1 : 35				
219	1219	2219	0 : 35				
220	1220	2220	1 : 40				
221	1221	2221	1 : 30				
222	1222	2222	0 : 15				
223	1223	2223	0 : 40				
224	1224	2224	2 : 10				
225	1225	2225	1 : 00				
226	1226	2226	1 : 15				
227	1227	2227	1 : 20				
228	1228	2228	1 : 05				
229	1229	2229	1 : 30				
230	1230	2230	0 : 55				
231	1231	2231	0 : 20				
232	1232	2232	0 : 45				
233	1233	2233	0 : 10				
234	1234	2234	0 : 15				
235	1235	2235	0 : 30				
236	1236	2236	0 : 15				
237	1237	2237	0 : 30				
238	1238	2238	0 : 45				
239	1239	2239	0 : 20				
240	1240	2240	0 : 30				
241	1241	2241	0 : 55				
242	1242	2242	0 : 50				
243	1243	2243	0 : 15				
244	1244	2244	0 : 25				
245	1245	2245	0 : 15				
246	1246	2246	0 : 25				
247	1247	2247	1 : 10				
248	1248	2248	0 : 35				
249	1249	2249	0 : 30				
250	1250	2250	2 : 20				
251	1251	2251	0 : 20				
252	1252	2252	1 : 35				
253	1253	2253	2 : 25				